

## Supporting Information

### Spontaneous macrocyclization through multiple dynamic cyclic amination formation

#### Table of Contents

<b>Experimental</b>	<b>S1</b>
General	S1
Nuclear Magnetic Resonance	S1
Matrix-Assisted Laser Desorption/Ionization Mass Spectrometry (MALDI-TOF/TOF)	S1
<b>General procedure for the synthesis of di/tetra-amines</b>	<b>S2</b>
<b>Computational details</b>	<b>S2</b>
<b>Characterization of compounds</b>	<b>S9</b>
<b>General procedure to macrocyclization</b>	<b>S19</b>
<b>References</b>	<b>S56</b>

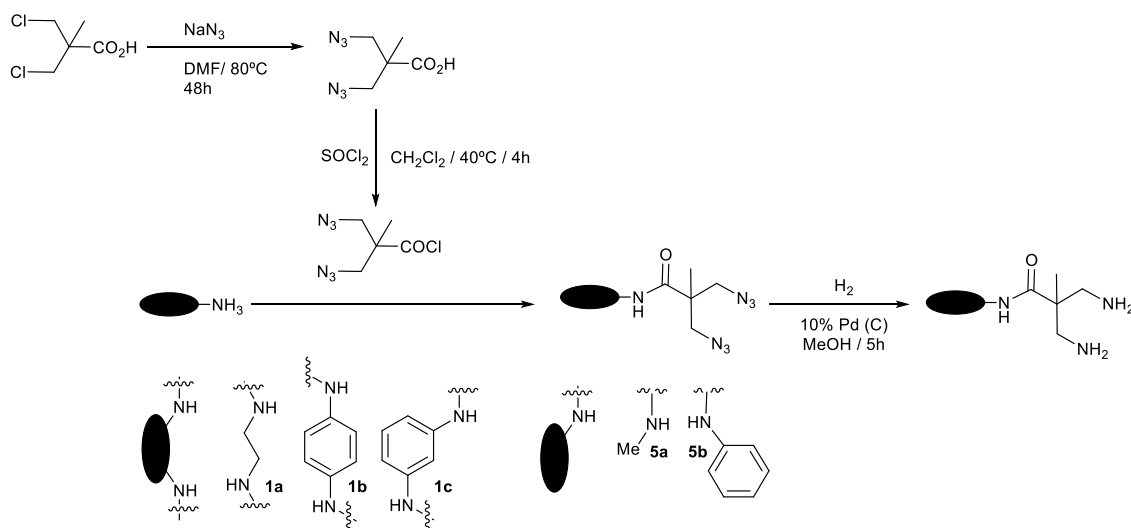
#### Experimental

**General:** Reagents and solvents were purchased from commercial suppliers (Aldrich, Fluka or Merck) and were used without further purification. TLCs were performed using 6x3 cm SiO<sub>2</sub> pre-coated aluminium plates (ALUGRAM® SIL G/UV<sub>254</sub>).

**Nuclear Magnetic Resonance (NMR):** Spectroscopic experiments for the characterization of compounds were carried out on a Varian Mercury 400 and a Bruker ARX-400 instruments (400 MHz for <sup>1</sup>H and 101 MHz for <sup>13</sup>C). Chemical shifts (δH) are quoted in parts per million (ppm) and referenced to the appropriate NMR solvent peak(s). 2D-NMR experiments COSY, HSQC and HMBC were used where necessary in assigning NMR spectra.

**Matrix-Assisted Laser Desorption/Ionization Mass Spectrometry (MALDI-TOF/TOF):** A MALDI-TOF/TOF mass spectrometer (AutoFLEX III, Bruker Daltonics, Bremen, Germany) equipped with a pulsed N<sub>2</sub> laser (337 nm) controlled by the Flexcontrol 3.4 software package was used to obtain MS and MS/MS data. The accelerating voltage was 19 kV and the reflectron voltage 21 kV. Spectra are the sum of 200 shots with a frequency of 200 Hz. The MS/MS spectra were obtained in the collision induced dissociation (CID) mode using argon as the collision gas. Trihydroxyacetophenone was used as a matrix, as a non-acidic matrix was required for the stability of the cycles.

## General procedure for the synthesis of di/tetra-amines



**Scheme S1:** Synthetic procedure for the synthesis of **1a-c** and **5a-b**.

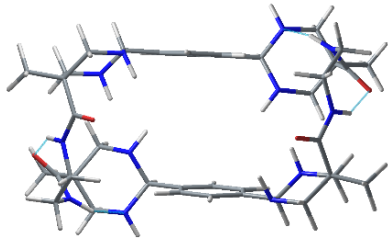
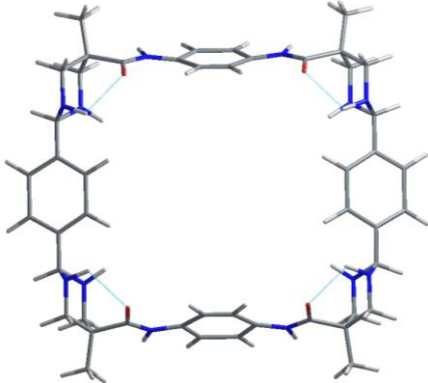
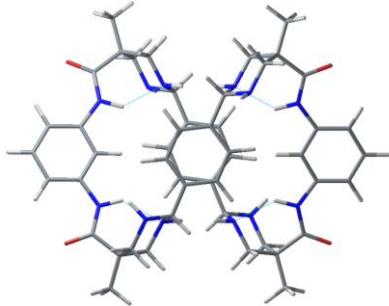
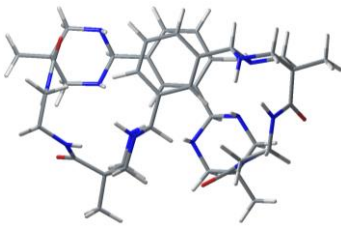
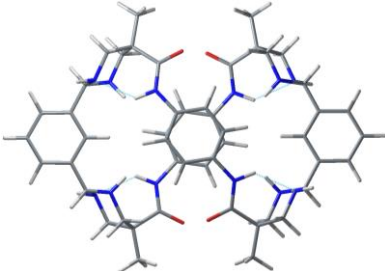
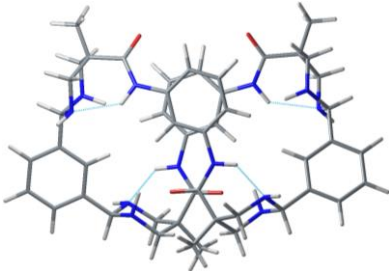
15 mmol of freshly prepared 3,3'-diazidopivaloyl chloride as described in the bibliography<sup>[1]</sup>, is dissolved in 20 mL of dichloromethane and added dropwise over a cooled to  $0^\circ\text{C}$  (ice bath) mixture of 18 mmol of monoamine (methylamine or aniline) or 6 mmol of diamine (ethylenediamine, *m*-phenylenediamine or *p*-phenylenediamine), 20 mL of dichloromethane and 20 mL of 10% aqueous sodium hydroxide using a pressure-equalizing dropping funnel keeping temperature at  $0^\circ\text{C}$ . After that, the reaction was stirred at  $23^\circ\text{C}$  for 12 h. The organic layer was then separated, washed with 10% aqueous sodium hydroxide (3 x 10 mL), 1 M aqueous HCl (3 x 10 mL) and water (10 mL), dried over anhydrous  $\text{MgSO}_4$  and the solvent was removed under reduced pressure. Purification by silica gel column chromatography (EtOAc/Hexane = 1/1) gave the corresponding desired azide compound as white solids with a yield around 80% in all the cases. The corresponding azide derivative, 200 mg, was dissolved in MeOH (10 mL) and the solution shaken under a hydrogen atmosphere (20bar) in the presence of 10% Pd/C, 20 mg, for 5 hours. The catalyst was filtered off through Celite<sup>®</sup> and washed with methanol. The filtrate was concentrated under reduced pressure to yield the desired di/tetra-amine compounds as colourless oil in almost quantitative yield.

## Computational details

All molecules were constructed according the NOE effects observed in the aminor ring. Then, a conformational search was performed using the scan program of the TINKER molecular modeling package,<sup>[2]</sup> and using the force field amber99. The missing bonds, angle torsions, or van der Waals parameters not included in this force field were transferred from the general AMBER force field (GAFF).<sup>[3]</sup> The parameters used in the conformational analysis were: a dielectric constant ( $\epsilon$ ) of 32.6, a number of search directions of 10, the energy threshold for local minima of 50 kcal/mol and a convergence criterion for local geometry optimizations of 0.1 kcal/mol Å.

The conformation of minimum energy obtained for each compound was submitted to density-functional theory (DFT) calculation. In all cases, the Gaussian 16.A.03 package<sup>[4]</sup> employing the B3LYP functional with the 6-31G(d,p) basis set was used. The solvent effect (methanol) was considered including the polarizable continuum model (PCM).<sup>[5]</sup> When possible, the minimization was carried out imposing the corresponding group symmetry (see Table S1). The absence of negative frequency in analytical Hessian calculations corroborated the nature of all minima. To study the intramolecular hydrogens bonds in **3a**, a topological analysis has been done using the Bader's atoms in molecules (AIM) theory<sup>[6]</sup> and the Multiwfn 3.6 program.<sup>[7]</sup>

**Table S1:** Geometries from the conformational search of the macrocycles **3a-f** and the energies obtained after DFT calculation at PCM(MeOH)/B3LYP/6-31G(d,p) level.

Compound <b>3a</b> (symmetry C2) <sup>a</sup>	Compound <b>3b</b> (symmetry C2v) <sup>a</sup>	Compound <b>3c</b> (symmetry C2) <sup>a</sup>
		
Energy: -1580389.01 kcal/mol	Energy: -1771675.63 kcal/mol	Energy: -1771690.03 kcal/mol
Compound <b>3d</b>	Compound <b>3e</b> (symmetry D2) <sup>a</sup>	Compound <b>3f</b> (symmetry C2) <sup>a</sup>
		
Energy: -1580379.87 kcal/mol	Energy: -1771688.54 kcal/mol	Energy: -1771691.20 kcal/mol

<sup>a</sup> Hydrogen bonds are represented in cyan.

To further study the compound **3a** and the hydrogen bonds between the amides and the NH moieties, all combinations between the configurations of the hydrogens in the NH aminal group were constructed and minimized at PCM(MeOH)/B3LYP/6-311G(2d,p) level. Then, fine-tuned the energies were obtained with the 6-311++G(2d,p) basis set. The energy of structures with their corresponding symmetry are collected in Table S2 and their geometries in Table S3.

**Table S2:** Energies of selected symmetries for **3a** calculated at PCM(MeOH)/6-311++G(2d,p)//PCM(MeOH)/6-311G(2d,p) level.

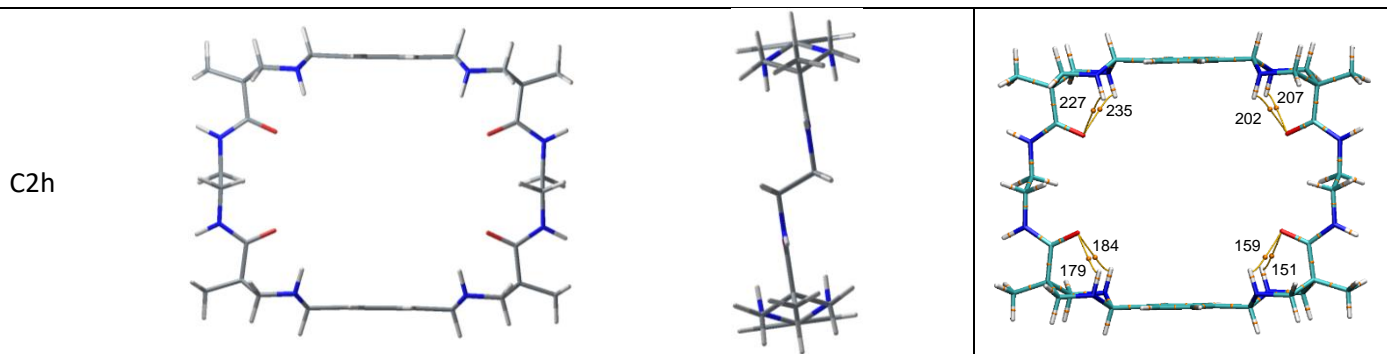
Symmetry	D2	C2	Cs	Ci	C2h
Energy (kcal/mol)	-1580799.73	-1580797.88	-1580797.67	-1580794.15	-1580790.30
Relative Energy (kcal/mol)	0.00	1.85	2.06	5.58	9.43

One of the most useful tools to study atomic and molecular interactions, mainly hydrogen bonds, is the topological analysis based in the Bader theory of AIM.<sup>[6]</sup> The main topological parameters for the different geometries of **3a** can be found in Table S4 to Table S8. According to this theory, the chemical bonds are characterized by the presence of bond critical points (BCP). This theory uses the value of electron density at the bond critical point and the electron density paths as criteria for the existence of the hydrogen bond. According the AIM analysis, a hydrogen bond occurs if the electron density ( $\rho$ ) at the bond critical point should be between 0.002 and 0.035 au and the Laplacian of electron density ( $\nabla^2\rho$ ) should be within 0.024-0.139 au.<sup>[8]</sup> For hydrogens bond critical points (hBCP),  $\rho$  usually has small values and  $\nabla^2\rho > 0$ , both characteristic of closed-shell interactions.<sup>[9]</sup> Likewise, it is also convenient to consider the energetic properties of electron density at the hBCP (Tables S4-S8). In closed-shell interactions, as hydrogen bonds, the potential electron energy density (V) has a negative value and its absolute value should be similar to the kinetic electron energy density (G). In the different geometries found for **3a**, the electron energy density (H = G + V) has low values, indicating weak hydrogen bonds and mainly of electrostatic nature.<sup>[10]</sup> With respect to the Eigenvalues of Hessian matrix, two of

them ( $\lambda_1$  and  $\lambda_2$ ) usually have negative values confirming that all the hBCP correspond to true hydrogen bonds. The hydrogen bonds energy can also be evaluated from the potential energy density at each.<sup>[11]</sup>

**Table S3:** Geometries and AIM analysis for the conformations of **3a**.

Symmetry	Front view <sup>a</sup>	Side View <sup>a</sup>	AIM analysis <sup>b</sup>
D2			
C2			
Cs			
Ci			



<sup>a</sup> Hydrogen bonds are represented in cyan. <sup>b</sup> The Bond Critical Points (BCP) are numbered and represented in orange. The path connecting the (3,-3) and (3,-1) CP in the hydrogen bonds are represented in yellow.

**Table S4:** Energetic properties obtained from AIM analysis for **3a** with symmetry D2.

Symmetry D2		BCP 157 / BCP 173 / BCP 197 / BCP 198 NH...N
Hydrogen Bond Critical Point (BCP)	$\rho^{\text{BCP}}_{\text{N}\cdots\text{HN}}$	0.0305
	$\nabla^2\rho^{\text{BCP}}_{\text{N}\cdots\text{HN}}$	0.0922
Energetic properties of electron density at BCP	G	0.0221
	V	-0.0211
	H	0.0010
	$ V /G$	0.9571
Eigenvalues of the Hessian matrix	$\lambda_1$	-0.0118
	$\lambda_2$	-0.0382
	$\lambda_3$	0.0777
	$ (\lambda_1+\lambda_2) /\lambda_3$	0.3386
Hydrogen Bond Energy	$E_{\text{HB}}$	-6.62
	$E_{\text{HB total}}$	-26.48

$\rho$ : Electron density in  $e/a_0^3$ ;  $\nabla^2\rho$ : Laplacian of electron density in  $e/a_0^5$ ; G: Lagrangian kinetic energy in  $e/a_0^3$ ; V: Potential energy density in  $e/a_0^3$ ; H: Energy density in  $e/a_0^3$ ;  $\lambda_1, \lambda_2, \lambda_3$ : Eigenvalues of Hessian matrix in  $e/a_0^5$ ;  $E_{\text{HB}}$ : Hydrogen Bond Energy in kcal/mol.

**Table S5:** Energetic properties obtained from AIM analysis for **3a** with symmetry C2.

Symmetry C2		BCP 174 / BCP 212 $\text{N}_{\text{aminal}}\cdots\text{HNCO}$	BCP 129 / BCP 260 $\text{NCO}\cdots\text{HNCO}$	BCP 162 / BCP 225 $\text{aminalN}\cdots\text{HN}_{\text{aminal}}$
Hydrogen Bond Critical Point (BCP)	$\rho^{\text{BCP}}$	0.0280	0.0211	0.0042
	$\nabla^2\rho^{\text{BCP}}$	0.0871	0.0742	0.0126
Energetic properties of electron density at BCP	G	0.0203	0.0164	0.0027
	V	-0.0187	-0.0143	-0.0022
	H	0.0015	0.0021	0.0005
	$ V /G$	0.9212	0.8719	0.8148
Eigenvalues of the Hessian matrix	$\lambda_1$	-0.0334	-0.0244	-0.0027
	$\lambda_2$	-0.0362	-0.0252	-0.0029
	$\lambda_3$	0.1567	0.1238	0.0182
	$ (\lambda_1+\lambda_2) /\lambda_3$	0.4442	0.4006	0.3077
Hydrogen Bond Energy	$E_{\text{HB}}$	-5.87	-4.49	-0.69
	$E_{\text{HB total}}$		-22.10	

$\rho$ : Electron density in  $e/a_0^3$ ;  $\nabla^2\rho$ : Laplacian of electron density in  $e/a_0^5$ ; G: Lagrangian kinetic energy in  $e/a_0^3$ ; V: Potential energy density in  $e/a_0^3$ ; H: Energy density in  $e/a_0^3$ ;  $\lambda_1, \lambda_2, \lambda_3$ : Eigenvalues of Hessian matrix in  $e/a_0^5$ ;  $E_{\text{HB}}$ : Hydrogen Bond Energy in kcal/mol.

**Table S6:** Energetic properties obtained from AIM analysis for **3a** with symmetry Cs.

Symmetry Cs		BCP 125 / BCP 146	BCP 175 / BCP 206
		NH...N	NH...N
Hydrogen Bond Critical Point (BCP)	$\rho^{\text{BCP}}_{\text{N}\cdots\text{HN}}$	0.0267	0.0288
	$\nabla^2\rho^{\text{BCP}}_{\text{N}\cdots\text{HN}}$	0.0832	0.0884
Energetic properties of electron density at BCP	G	0.0191	0.0207
	V	-0.0174	-0.0194
	H	0.0017	0.0014
	$ V /G$	0.9105	0.9351
Eigenvalues of the Hessian matrix	$\lambda_1$	-0.0313	-0.0350
	$\lambda_2$	-0.0336	-0.0372
	$\lambda_3$	0.1481	0.1605
	$ (\lambda_1+\lambda_2) / \lambda_3 $	0.4381	0.4495
Hydrogen Bond Energy	$E_{\text{HB}}$	-5.46	-6.09
	$E_{\text{HB total}}$		-23.10

$\rho$ : Electron density in  $e/a_0^3$ ;  $\nabla^2\rho$ : Laplacian of electron density in  $e/a_0^5$ ; G: Lagrangian kinetic energy in  $e/a_0^3$ ; V: Potential energy density in  $e/a_0^3$ ; H: Energy density in  $e/a_0^3$ ;  $\lambda_1, \lambda_2, \lambda_3$ : Eigenvalues of Hessian matrix in  $e/a_0^5$ ;  $E_{\text{HB}}$ : Hydrogen Bond Energy in kcal/mol.

**Table S7:** Energetic properties obtained from AIM analysis for **3a** with symmetry Ci.

Symmetry Ci		BCP 165 / BCP 227	BCP 174 / BCP 218
		NH...N	NH...N
Hydrogen Bond Critical Point (BCP)	$\rho^{\text{BCP}}_{\text{N}\cdots\text{HN}}$	0.0280	0.0279
	$\nabla^2\rho^{\text{BCP}}_{\text{N}\cdots\text{HN}}$	0.0854	0.0853
Energetic properties of electron density at BCP	G	0.0199	0.0198
	V	-0.0184	-0.0184
	H	0.0015	0.0015
	$ V /G$	0.9246	0.9293
Eigenvalues of the Hessian matrix	$\lambda_1$	-0.0337	-0.0336
	$\lambda_2$	-0.0359	-0.0358
	$\lambda_3$	0.1550	0.1546
	$ (\lambda_1+\lambda_2) / \lambda_3 $	0.4490	0.4489
Hydrogen Bond Energy	$E_{\text{HB}}$	-5.77	-5.77
	$E_{\text{HB total}}$		23.08

$\rho$ : Electron density in  $e/a_0^3$ ;  $\nabla^2\rho$ : Laplacian of electron density in  $e/a_0^5$ ; G: Lagrangian kinetic energy in  $e/a_0^3$ ; V: Potential energy density in  $e/a_0^3$ ; H: Energy density in  $e/a_0^3$ ;  $\lambda_1, \lambda_2, \lambda_3$ : Eigenvalues of Hessian matrix in  $e/a_0^5$ ;  $E_{\text{HB}}$ : Hydrogen Bond Energy in kcal/mol.

**Table S8:** Energetic properties obtained from AIM analysis for **3a** with symmetry C2h.

Symmetry C2h		BCP 151 / BCP 207	BCP 159 / BCP 202
		BCP 179 / BCP 235	BCP 184 / BCP 227
		NH...OC	NH...OC
hydrogen Bond Critical Point (BCP)	$\rho^{\text{BCP}}_{\text{O}\cdots\text{H}}$	0.0151	0.0146
	$\nabla^2\rho^{\text{BCP}}_{\text{O}\cdots\text{H}}$	0.0514	0.0495
Energetic properties of electron density at BCP	G	0.0114	0.0110
	V	-0.0100	-0.0096
	H	0.0014	0.0014
	$ V /G$	0.8752	0.8736
Eigenvalues of the Hessian matrix	$\lambda_1$	-0.0118	-0.0111
	$\lambda_2$	-0.0145	-0.0137
	$\lambda_3$	0.0777	0.0743
	$ (\lambda_1+\lambda_2) / \lambda_3 $	0.3386	0.3332
Hydrogen Bond Energy	$E_{\text{HB}}$	-3.14	-3.01
	$E_{\text{HB total}}$		-24.60

$\rho$ : Electron density in  $e/a_0^3$ ;  $\nabla^2\rho$ : Laplacian of electron density in  $e/a_0^5$ ; G: Lagrangian kinetic energy in  $e/a_0^3$ ; V: Potential energy density in  $e/a_0^3$ ; H: Energy density in  $e/a_0^3$ ;  $\lambda_1, \lambda_2, \lambda_3$ : Eigenvalues of Hessian matrix in  $e/a_0^5$ ;  $E_{HB}$ : Hydrogen Bond Energy in kcal/mol.

In order to obtain further insights in the relationship between the experimental  $^1\text{H}$  and  $^{13}\text{C}$ -NMR spectra (figures S11 and S12) and the structures proposed for **3a** (Tables S2 and S3), we accomplished a single-point calculation of  $^{13}\text{C}$  and  $^1\text{H}$  chemical shielding tensors. We used the keyword (nmr = giao) at the PCM(MeOH)/B3LYP/6-311++G(2d,p) level of theory for the optimized structures of **3a**. All chemical shifts were determined with respect to tetramethylsilane as computational reference.

**Table S9:** Experimental and computed values of the  $^{13}\text{C}$ -NMR chemical shifts for compound **3a** in different geometries.

$^{13}\text{C}$ -NMR	Symm. D2		Symm. C2		Symm. Cs		Symm. Ci		Symm. C2h		Average <sup>a</sup>		
	$\delta_{\text{exp}}^b$	$\delta_{\text{calc}}^c$	$\Delta^d$	$\delta_{\text{calc}}^c$	$\Delta^d$	$\delta_{\text{calc}}^c$	$\Delta^d$	$\delta_{\text{calc}}^c$	$\Delta^d$	$\delta_{\text{calc}}^c$	$\Delta^d$	$\delta_{\text{calc}}^c$	$\Delta^d$
CO	179.1	183.6	-4.5	187.3	-8.2	184.4	-5.3	185.8	-6.7	185.5	-6.4	185.3	-6.2
C_ arom	142.7	150.7	-8.0	151.0	-8.3	150.1	-7.4	149.8	-7.1	150.2	-7.5	150.4	-7.7
CH_ arom	128.0	132.9	-4.9	133.1	-5.1	132.3	-4.3	132.4	-4.4	131.2	-3.2	132.4	-4.4
CH_ aminal	74.8	79.9	-5.1	80.3	-5.5	79.7	-4.9	79.9	-5.1	77.1	-2.3	79.4	-4.6
CH <sub>2</sub> _ ring	55.6	59.7	-4.1	58.9	-3.3	60.2	-4.6	59.9	-4.3	60.7	-5.1	59.9	-4.3
CH <sub>2</sub> _ eda	40.6	41.7	-1.1	46.0	-5.4	42.4	-1.8	42.9	-2.3	41.6	-1.0	42.9	-2.3
C_ quat	40.4	45.8	-5.4	48.1	-7.7	45.9	-5.5	45.1	-4.7	42.8	-2.4	45.5	-5.1
CH <sub>3</sub>	22.0	23.1	-1.1	24.0	-2.0	23.1	-1.1	22.8	-0.8	21.3	0.7	22.9	-0.9
<b>MAE<sup>e</sup></b>			4.28		5.69		4.36		4.43		3.58		4.43

<sup>a</sup>Values are reported as an average over a Boltzmann-weighted population of conformers. <sup>b</sup>Experimental chemical shift ( $\delta_{\text{exp}}$ ) in ppm obtained in CD<sub>3</sub>OD. <sup>c</sup>Calculated chemical shift ( $\delta_{\text{calc}}$ ) in ppm at PCM(MeOH)/6-311++G(2d,p)//PCM(MeOH)/6-311G(2d,p) level. <sup>d</sup>Difference ( $\Delta$ ) between  $\delta_{\text{exp}}$  and  $\delta_{\text{calc}}$ . <sup>e</sup>Mean absolute error.

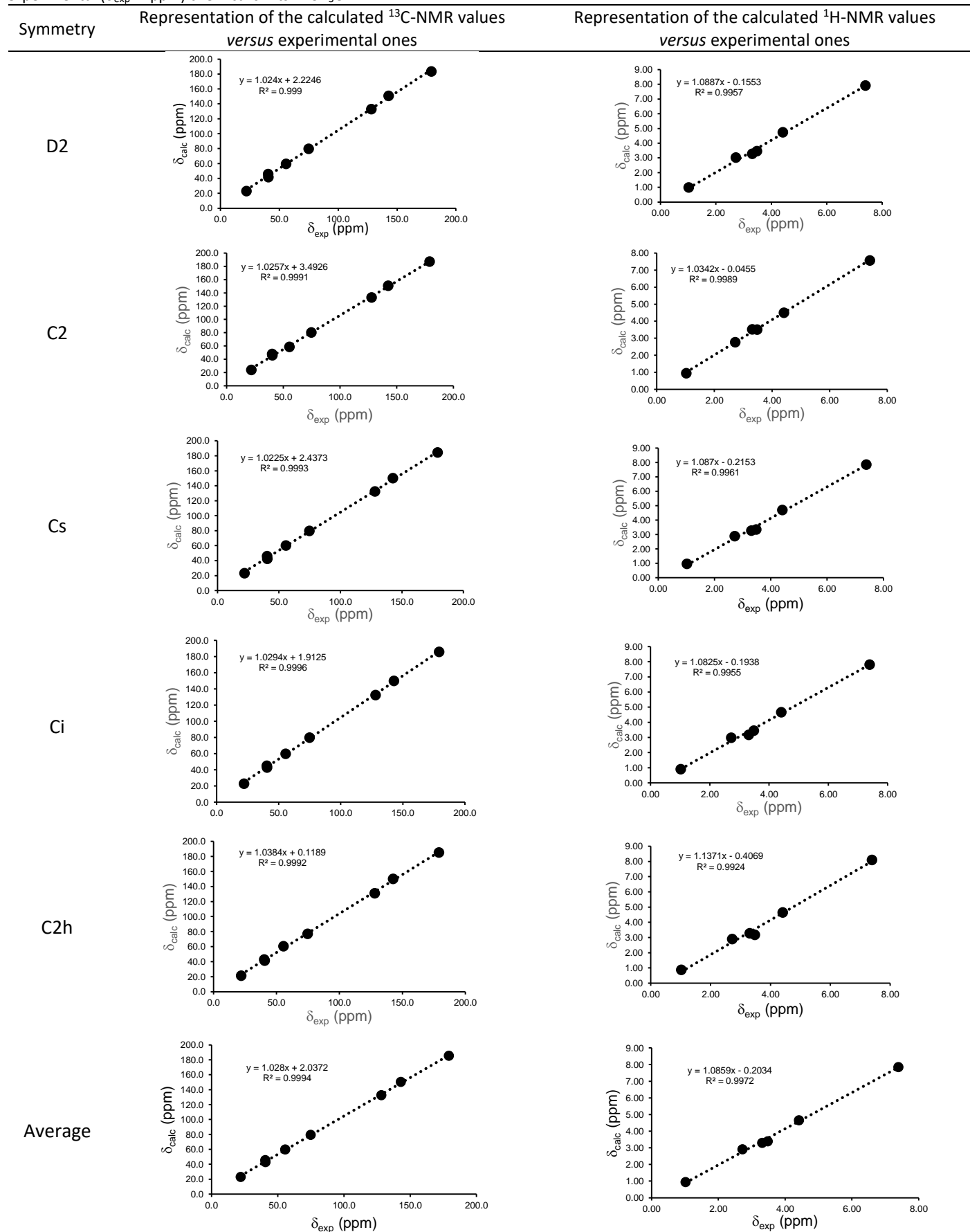
**Table S10:** Experimental and computed values of the  $^1\text{H}$ -NMR chemical shifts for compound **3a** in different geometries.

$^1\text{H}$ -NMR	Symm. D2		Symm. C2		Symm. Cs		Symm. Ci		Symm. C2h		Average <sup>a</sup>		
	$\delta_{\text{exp}}^b$	$\delta_{\text{calc}}^c$	$\Delta^d$	$\delta_{\text{calc}}^c$	$\Delta^d$	$\delta_{\text{calc}}^c$	$\Delta^d$	$\delta_{\text{calc}}^c$	$\Delta^d$	$\delta_{\text{calc}}^c$	$\Delta^d$	$\delta_{\text{calc}}^c$	$\Delta^d$
H_ arom	7.39	7.92	-0.53	7.57	-0.18	7.85	-0.46	7.82	-0.43	8.10	-0.71	7.85	-0.5
H_ aminal	4.41	4.73	-0.32	4.50	-0.09	4.70	-0.29	4.67	-0.26	4.64	-0.23	4.65	-0.2
CH <sub>2</sub> _ eda	3.48	3.46	0.02	3.51	-0.03	3.34	0.14	3.45	0.03	3.17	0.31	3.39	0.1
CH <sub>2</sub> _ ring	3.31	3.27	0.04	3.52	-0.21	3.26	0.05	3.18	0.13	3.27	0.04	3.30	0.0
CH <sub>2</sub> _ ring	2.72	3.02	-0.30	2.77	-0.05	2.87	-0.15	2.98	-0.26	2.90	-0.18	2.91	-0.2
CH <sub>3</sub>	1.02	0.98	0.04	0.95	0.07	0.96	0.06	0.91	0.11	0.87	0.15	0.93	0.1
<b>MAE<sup>e</sup></b>			0.21		0.11		0.19		0.20		0.27		0.18

<sup>a</sup>Values are reported as an average over a Boltzmann-weighted population of conformers. <sup>b</sup>Experimental chemical shift ( $\delta_{\text{exp}}$ ) in ppm obtained in CD<sub>3</sub>OD. <sup>c</sup>Calculated chemical shift ( $\delta_{\text{calc}}$ ) in ppm at PCM(MeOH)/6-311++G(2d,p)//PCM(MeOH)/6-311G(2d,p) level. <sup>d</sup>Difference ( $\Delta$ ) between  $\delta_{\text{exp}}$  and  $\delta_{\text{calc}}$ . <sup>e</sup>Mean absolute error. Amine protons were not used in the calculation of the MAE since they should be in exchange with the solvent.

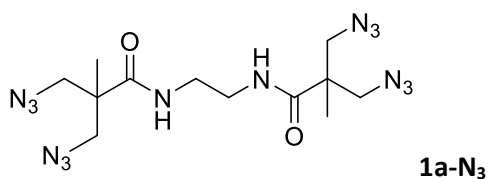
All the chemical shifts obtained are consistent with the experimental  $^{13}\text{C}$  and  $^1\text{H}$ -NMR spectra and within the mean absolute error (MAE) accepted for the method employed.<sup>[12]</sup> Due to the small energy difference between the others structures proposed for this compound (Table S2), we cannot totally discard any of the other structures, or even that there is a conformational equilibrium between them (Tables S9-S11).

**Table S11:** Calculated ( $\delta_{\text{calc}}$  in ppm)  $^{13}\text{C}$  and  $^1\text{H}$ -NMR chemical shifts at the GIAO/PCM(MeOH)/B3LYP/6-311++G(2d,p) level of theory *versus* experimental ( $\delta_{\text{exp}}$  in ppm) chemical shifts in  $\text{CD}_3\text{OD}$ .





## Characterization of compounds:



<sup>1</sup>H-NMR (400 MHz; CDCl<sub>3</sub>): δ 6.82 (2H, bs, NH), 3.56 (4H, d, <sup>2</sup>J = 12.2 Hz, CHHN<sub>3</sub>), 3.47 (4H, d, <sup>2</sup>J = 12.2 Hz, CHHN<sub>3</sub>), 3.44 (4H, m, CH<sub>2</sub>NH), 1.26 (6H, s, CH<sub>3</sub>).

<sup>13</sup>C-NMR (100 MHz; CDCl<sub>3</sub>): δ 174.0, 55.9, 47.2, 40.4, 18.8.

HRMS (ESI-TOF) m/z calcd. for C<sub>12</sub>H<sub>21</sub>N<sub>14</sub>O<sub>2</sub> [M+H]<sup>+</sup>: 393.19664. Found: 393.19645.

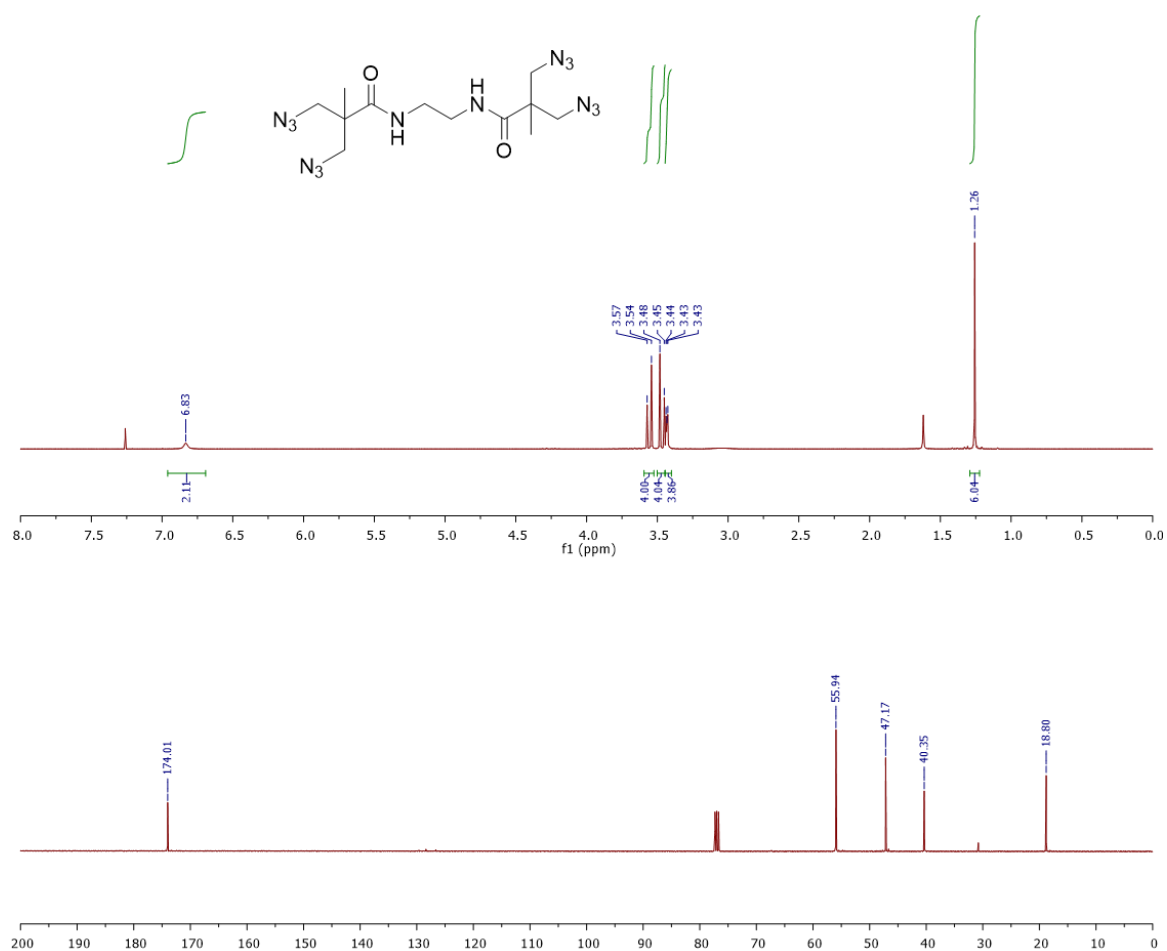
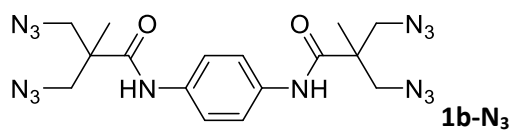


**Figure S1:** <sup>1</sup>H and <sup>13</sup>C NMR spectra of 1a-N<sub>3</sub>, CDCl<sub>3</sub>, 400 and 100 MHz respectively.



<sup>1</sup>H-NMR (400 MHz; CDCl<sub>3</sub>): δ 8.01 (2H, bs, NH), 7.48 (4H, m, CH<sub>ar</sub>), 3.64 (4H, d, <sup>2</sup>J = 12.4 Hz, CHHN<sub>3</sub>), 3.60 (4H, d, <sup>2</sup>J = 12.4 Hz, CHHN<sub>3</sub>), 1.36 (6H, s, CH<sub>3</sub>).

<sup>13</sup>C-NMR (100 MHz; CDCl<sub>3</sub>): δ 170.9, 134.0, 121.0, 56.1, 47.7, 19.4.

HRMS (ESI-TOF) m/z calcd. for C<sub>16</sub>H<sub>21</sub>N<sub>14</sub>O<sub>2</sub> [M+H]<sup>+</sup>: 441.19664. Found: 441.19745.

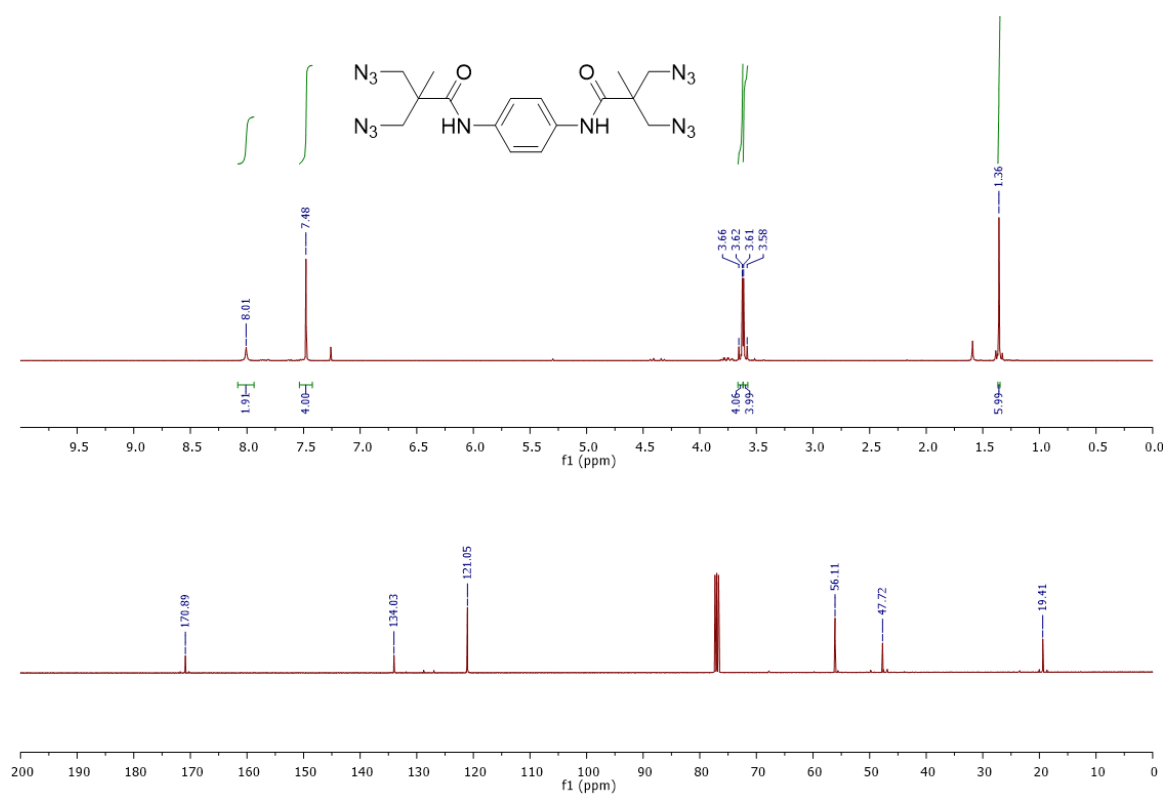
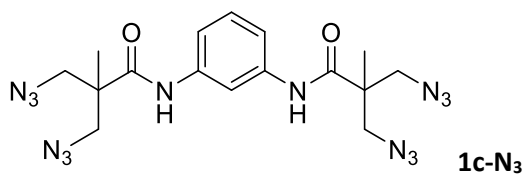


**Figure S2:** <sup>1</sup>H and <sup>13</sup>C NMR spectra of **1b-N<sub>3</sub>**, CDCl<sub>3</sub>, 400 and 100 MHz respectively.



<sup>1</sup>H-NMR (400 MHz; CDCl<sub>3</sub>): δ 8.02 (2H, bs, NH), 7.83 (1H, s, CH<sub>ar</sub>), 7.29 (3H, m, CH<sub>ar</sub>), 3.64 (4H, d, <sup>2</sup>J = 12.4 Hz, CHHN<sub>3</sub>), 3.60 (4H, d, <sup>2</sup>J = 12.4 Hz, CHHN<sub>3</sub>), 1.36 (6H, s, CH<sub>3</sub>).

<sup>13</sup>C-NMR (100 MHz; CDCl<sub>3</sub>): δ 171.2, 137.82, 129.4, 116.9, 112.7, 55.9, 47.8, 19.2.

HRMS (ESI-TOF) m/z calcd. for C<sub>16</sub>H<sub>21</sub>N<sub>14</sub>O<sub>2</sub> [M+H]<sup>+</sup>: 441.19664. Found: 441.19727.

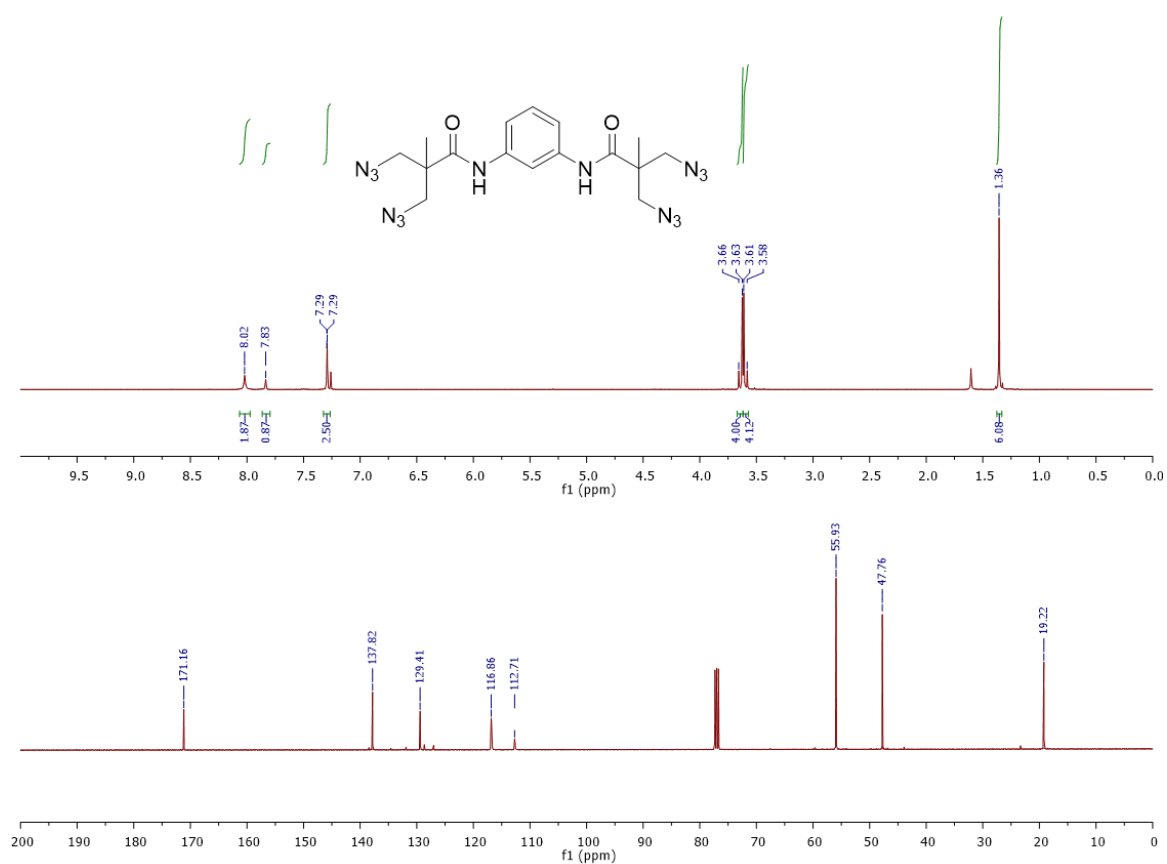
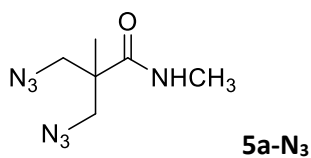


**Figure S3:** <sup>1</sup>H and <sup>13</sup>C NMR spectra of **1c-N<sub>3</sub>**, CDCl<sub>3</sub>, 400 and 100 MHz respectively.



<sup>1</sup>H-NMR (400 MHz; CDCl<sub>3</sub>): δ 6.11 (1H, bs, NH), 3.55 (2H, d, *J* = 12.3 Hz, CHHN<sub>3</sub>), 3.47 (2H, d, <sup>2</sup>*J* = 12.3 Hz, CHHN<sub>3</sub>), 2.83 (3H, d, <sup>2</sup>*J* = 4.8 Hz, NCH<sub>3</sub>), 1.25 (3H, s, CH<sub>3</sub>).

<sup>13</sup>C-NMR (100 MHz; CDCl<sub>3</sub>): δ 173.2, 55.9, 46.9, 26.4, 18.9.

HRMS (ESI-TOF) *m/z* calcd for C<sub>6</sub>H<sub>11</sub>N<sub>7</sub>NaO [M+Na]<sup>+</sup>: 220.09173. Found: 220.09149

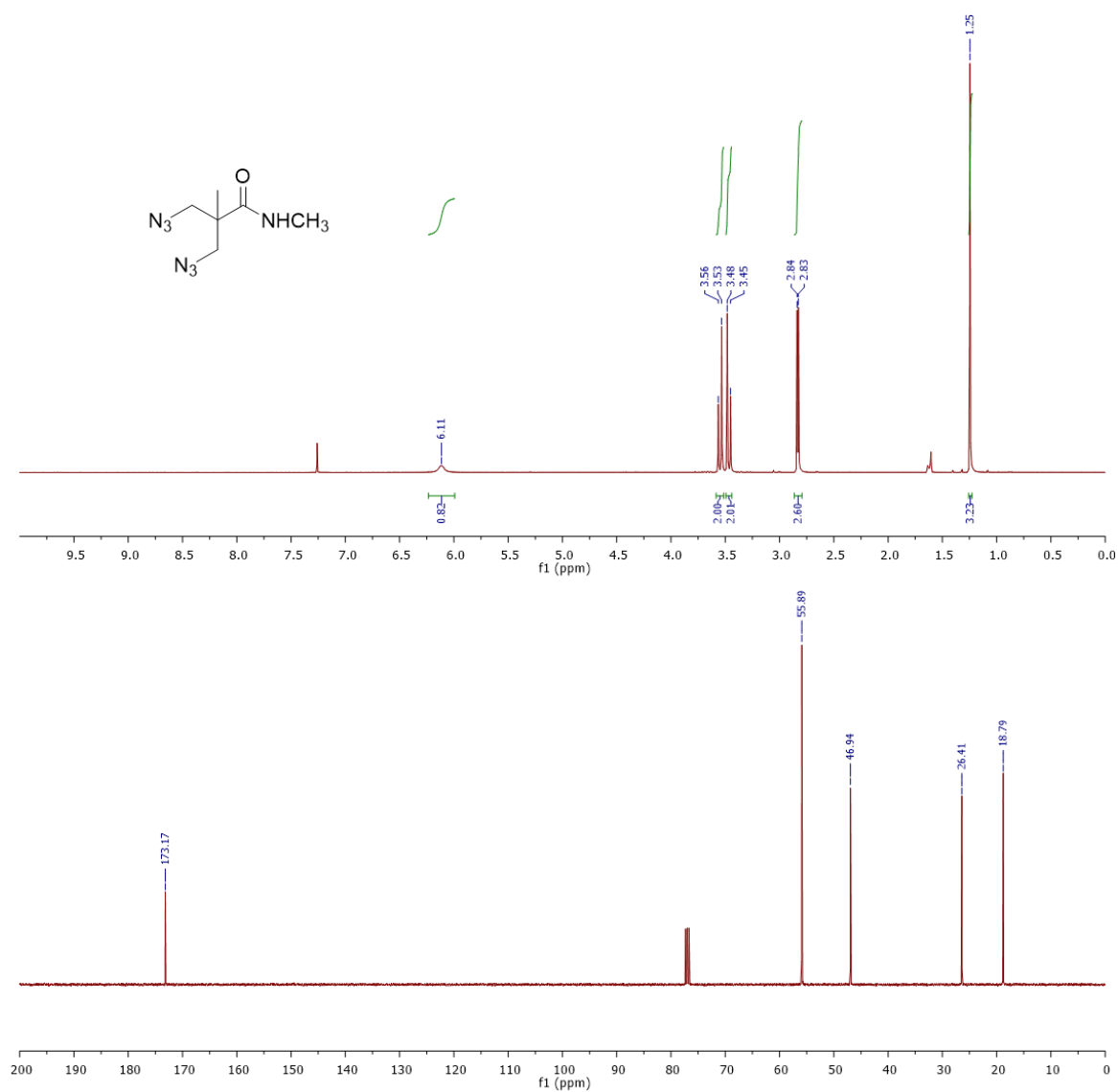
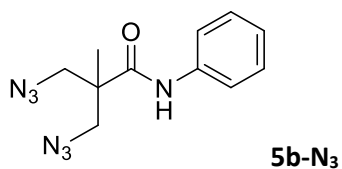


**Figure S4:** <sup>1</sup>H and <sup>13</sup>C NMR spectra of **5a-N<sub>3</sub>**, CDCl<sub>3</sub>, 400 and 100 MHz respectively.



<sup>1</sup>H-NMR (400 MHz; CDCl<sub>3</sub>): δ 8.00 (1H, bs, NH), 7.51 (2H, d, <sup>3</sup>J = 7.6 Hz CH<sub>ar</sub>), 7.34 (2H, t, <sup>3</sup>J = 7.6 Hz CH<sub>ar</sub>), 7.14 (1H, d, <sup>3</sup>J = 7.6 Hz CH<sub>ar</sub>), 3.64 (4H, d, <sup>2</sup>J = 12.4 Hz, CHHN<sub>3</sub>), 3.60 (4H, d, <sup>2</sup>J = 12.4 Hz, CHHN<sub>3</sub>), 1.36 (6H, s, CH<sub>3</sub>).

<sup>13</sup>C-NMR (100 MHz; CDCl<sub>3</sub>): δ 170.9, 137.3, 129.0, 124.8, 120.4, 56.2, 47.7, 19.4.

HRMS (ESI-TOF) m/z calcd. for C<sub>11</sub>H<sub>14</sub>N<sub>7</sub>O [M+H]<sup>+</sup>: 260.12543. Found: 260.12524.

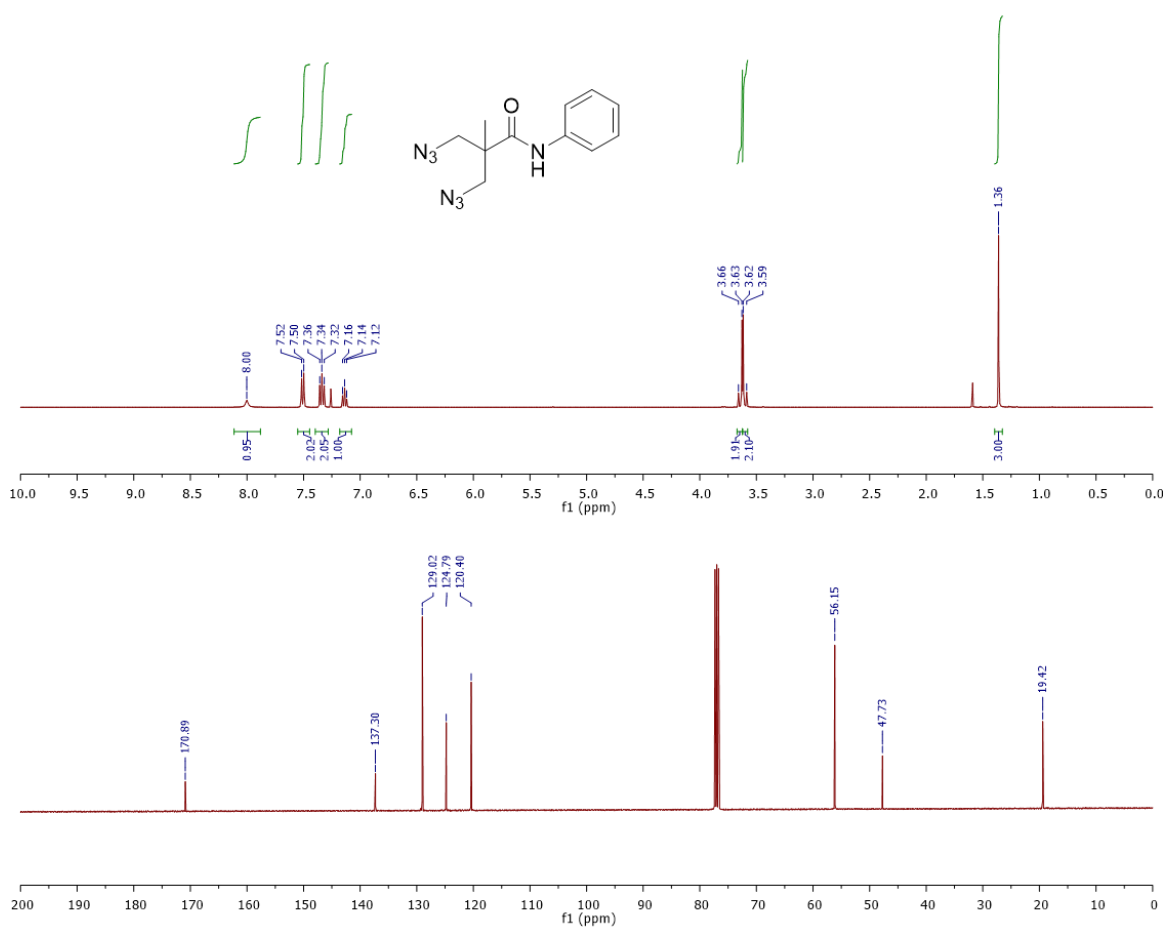
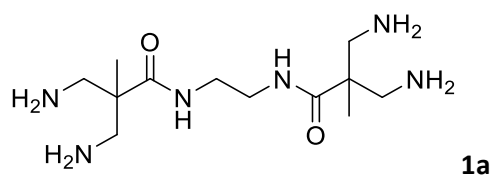


**Figure S5:** <sup>1</sup>H and <sup>13</sup>C NMR spectra of **5b-N<sub>3</sub>**, CDCl<sub>3</sub>, 400 and 100 MHz respectively.



$^1\text{H-NMR}$  (400 MHz;  $\text{DMSO-d}_6$ ):  $\delta$  8.51 (2H, bs, NH), 3.14 (4H, s,  $\text{CH}_2\text{N}$ ), 2.70 (8H, s,  $\text{NH}_2$ ), 2.64 (4H, d,  $^2J = 12.8$  Hz,  $\text{CHHNH}_2$ ), 2.58 (4H, d,  $^2J = 12.8$  Hz,  $\text{CHHNH}_2$ ), 0.95 (6H, s,  $\text{CH}_3$ ).

$^{13}\text{C-NMR}$  (100 MHz;  $\text{DMSO-d}_6$ ):  $\delta$  176.5, 47.3, 47.3, 38.6, 19.3.

HRMS (ESI-TOF)  $m/z$  calcd. for  $\text{C}_{12}\text{H}_{29}\text{N}_6\text{O}_2$   $[\text{M}+\text{H}]^+$ : 289.23465. Found: 289.23527.

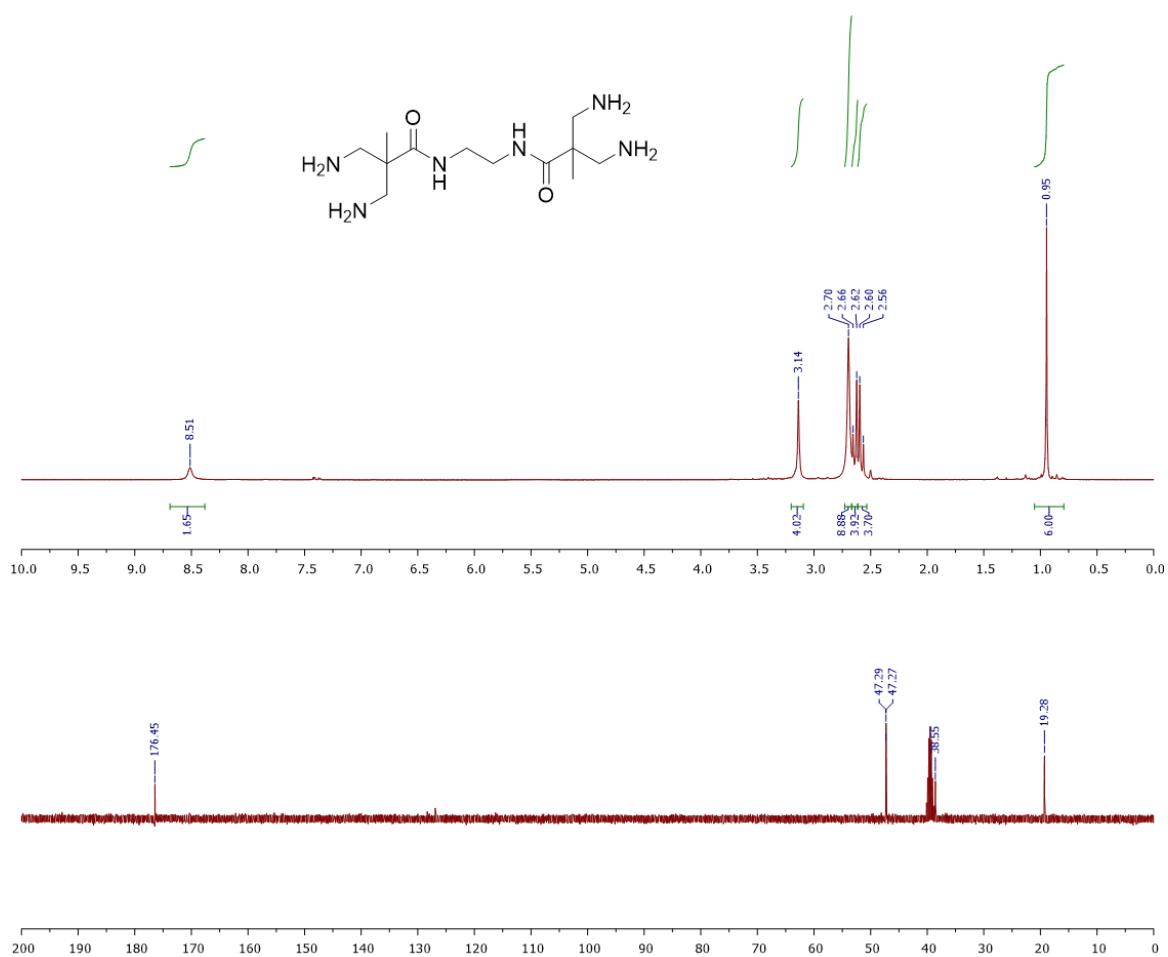
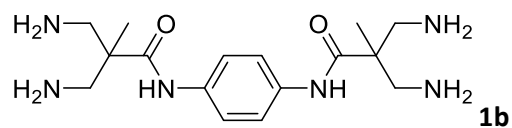


**Figure S6:**  $^1\text{H}$  and  $^{13}\text{C}$  NMR spectra of **1a**,  $\text{DMSO-d}_6$ , 400 and 100 MHz respectively.



$^1\text{H-NMR}$  (400 MHz;  $\text{DMSO-d}_6$ ):  $\delta$  7.44 (4H, s,  $\text{CH}_{ar}$ ), 2.72 (8H, s,  $\text{CH}_2\text{NH}_2$ ), 1.01 (6H, s,  $\text{CH}_3$ ).

$^{13}\text{C-NMR}$  (100 MHz;  $\text{DMSO-d}_6$ ):  $\delta$  175.0, 134.5, 119.7, 47.1, 46.9, 19.6.

HRMS (ESI-TOF)  $m/z$  calcd. for  $\text{C}_{16}\text{H}_{30}\text{N}_6\text{O}_2$   $[\text{M}+2\text{H}]^{2+}$ : 169.12096. Found: 169.12129.

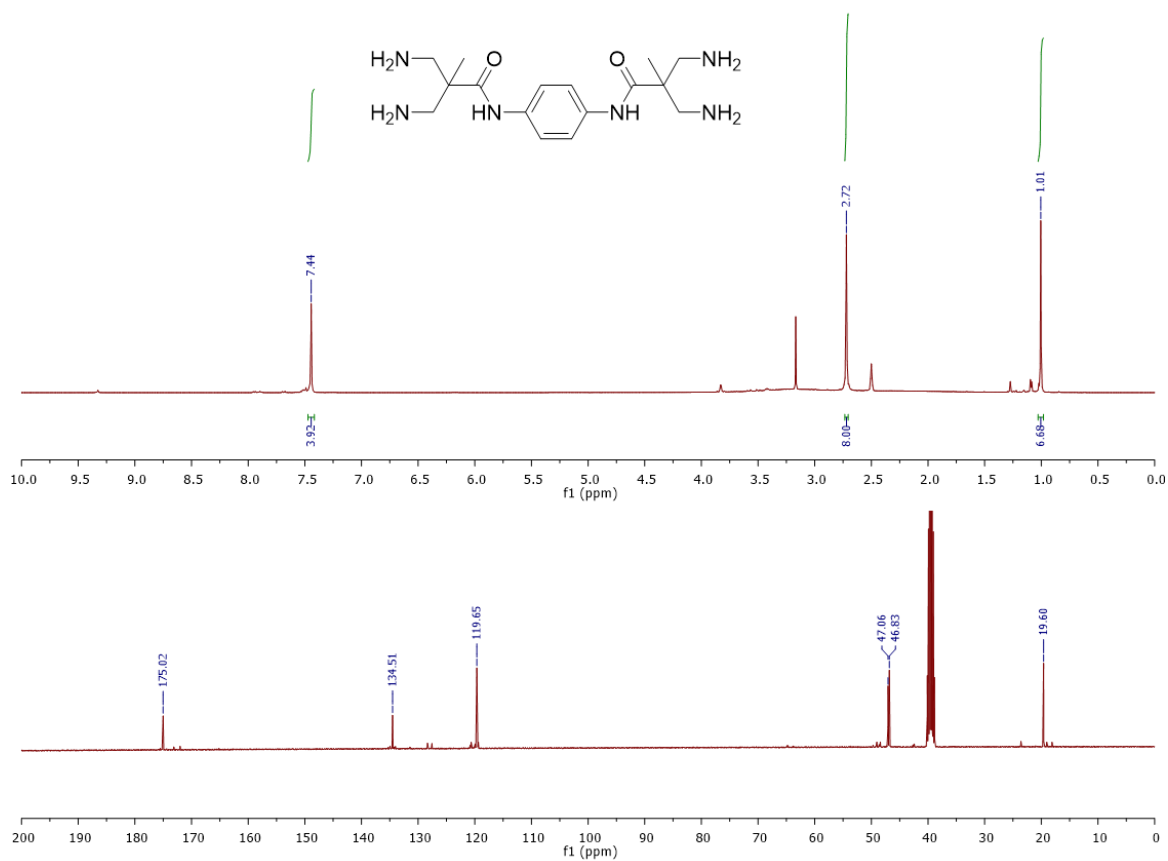
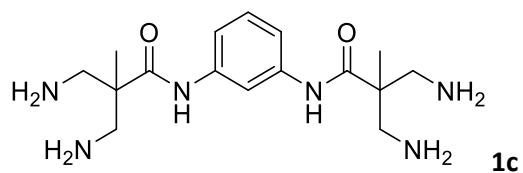


**Figure S7:**  $^1\text{H}$  and  $^{13}\text{C}$  NMR spectra of **1b**,  $\text{DMSO-d}_6$ , 400 and 100 MHz respectively.



$^1\text{H-NMR}$  (400 MHz;  $\text{DMSO-d}_6$ ):  $\delta$  7.76 (1H, m,  $\text{CH}_{ar}$ ), 7.22 (2H, dd,  $3J = 7.1, 1.7$  MHz,  $\text{CH}_{ar}$ ), 7.16 (1H, m,  $\text{CH}_{ar}$ ), 2.72 (8H, s,  $\text{CH}_2\text{NH}_2$ ), 1.00 (6H, s,  $\text{CH}_3$ ).

$^{13}\text{C-NMR}$  (100 MHz;  $\text{DMSO-d}_6$ ):  $\delta$  175.4, 139.7, 128.8, 114.0, 110.2, 47.1, 46.8, 19.6.

HRMS (ESI-TOF)  $m/z$  calcd. for  $\text{C}_{16}\text{H}_{30}\text{N}_6\text{O}_2$   $[\text{M}+2\text{H}]^{+2}$ : 169.12096. Found: 169.12119.

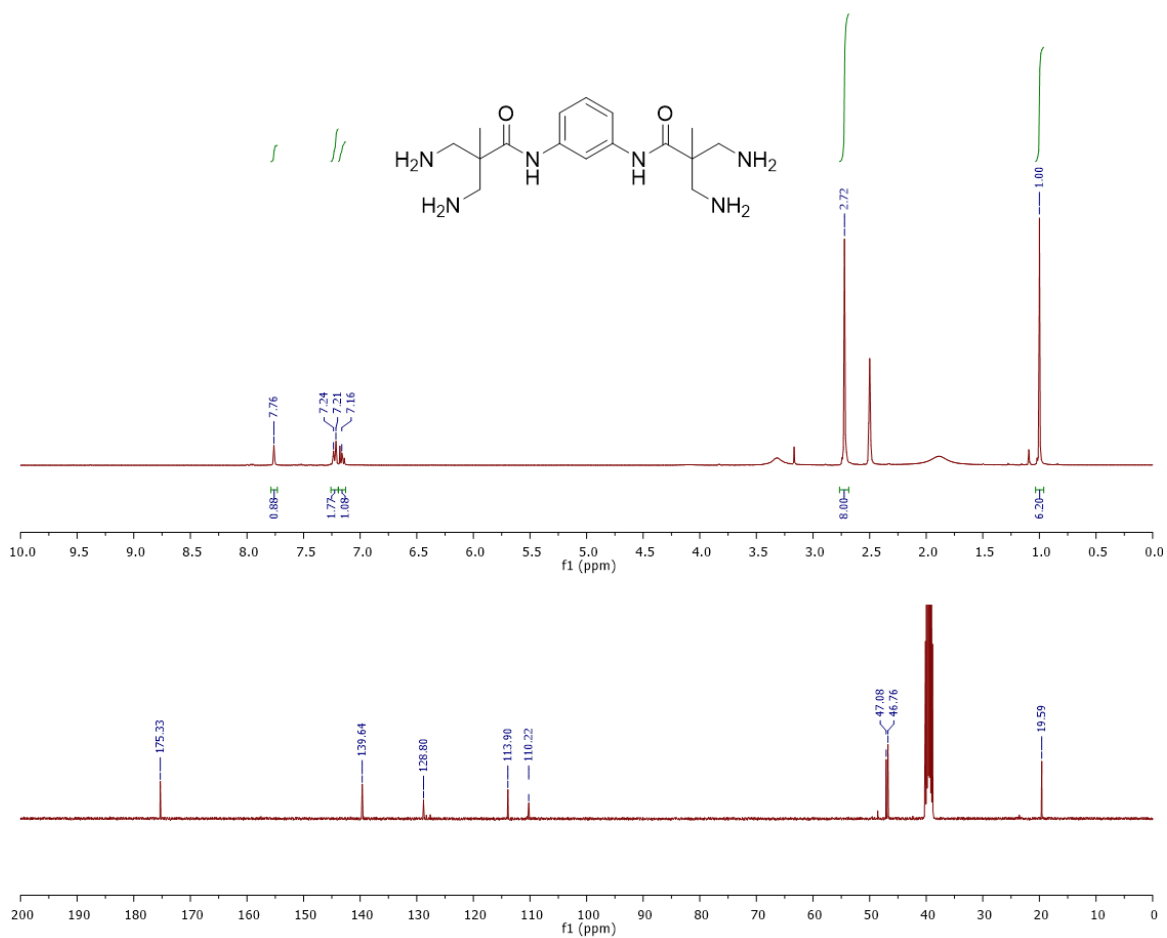
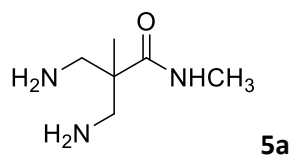


**Figure S8:**  $^1\text{H}$  and  $^{13}\text{C}$  NMR spectra of **1c**,  $\text{DMSO-d}_6$ , 400 and 100 MHz respectively.





$^1\text{H-NMR}$  (400 MHz;  $\text{DMSO-d}_6$ ):  $\delta$  8.31 (1H, bs, NH), 2.57 (7H, m,  $\text{CH}_2\text{NH}_2$ ,  $\text{NCH}_3$ ), 0.93 (3H, s,  $\text{CH}_3$ ).

$^{13}\text{C-NMR}$  (100 MHz;  $\text{DMSO-d}_6$ ):  $\delta$  176.7, 47.5, 47.4, 25.5, 19.3.

HRMS (ESI-TOF)  $m/z$  calcd. for  $\text{C}_6\text{H}_{16}\text{N}_3\text{O}$   $[\text{M}+\text{H}]^+$ : 146.18279. Found: 146.12862.

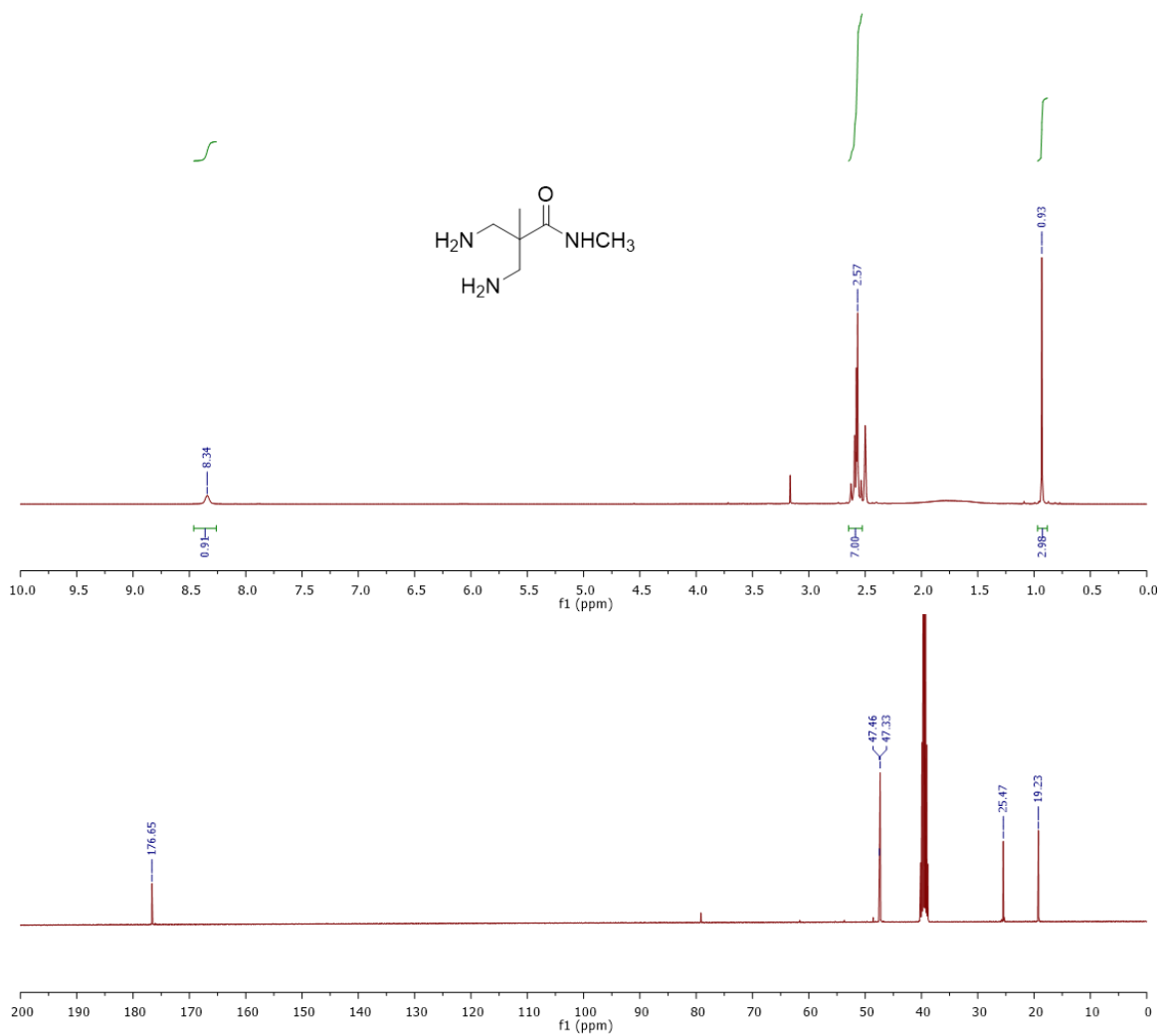
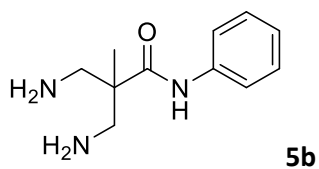


**Figure S9:**  $^1\text{H}$  and  $^{13}\text{C}$  NMR spectra of **5a**,  $\text{DMSO-d}_6$ , 400 and 100 MHz respectively.



$^1\text{H-NMR}$  (400 MHz;  $\text{DMSO-d}_6$ ):  $\delta$  7.53 (2H, d,  $J = 7.4$  MHz,  $\text{CH}_{ar}$ ), 7.28 (2H, t,  $3J = 7.4$  MHz,  $\text{CH}_{ar}$ ), 7.00 (1H, t,  $^3J = 7.4$  MHz,  $\text{CH}_{ar}$ ), 2.73 (4H, s,  $\text{CH}_2\text{NH}_2$ ), 1.01 (3H, s,  $\text{CH}_3$ ).

$^{13}\text{C-NMR}$  (100 MHz;  $\text{DMSO-d}_6$ ):  $\delta$  175.4, 139.4, 128.7, 122.8, 119.3, 47.2, 46.8, 19.6.

HRMS (ESI-TOF)  $m/z$  calcd. for  $\text{C}_{11}\text{H}_{18}\text{N}_3\text{O}$   $[\text{M}+\text{H}]^+$ : 208.14444. Found: 208.14424.

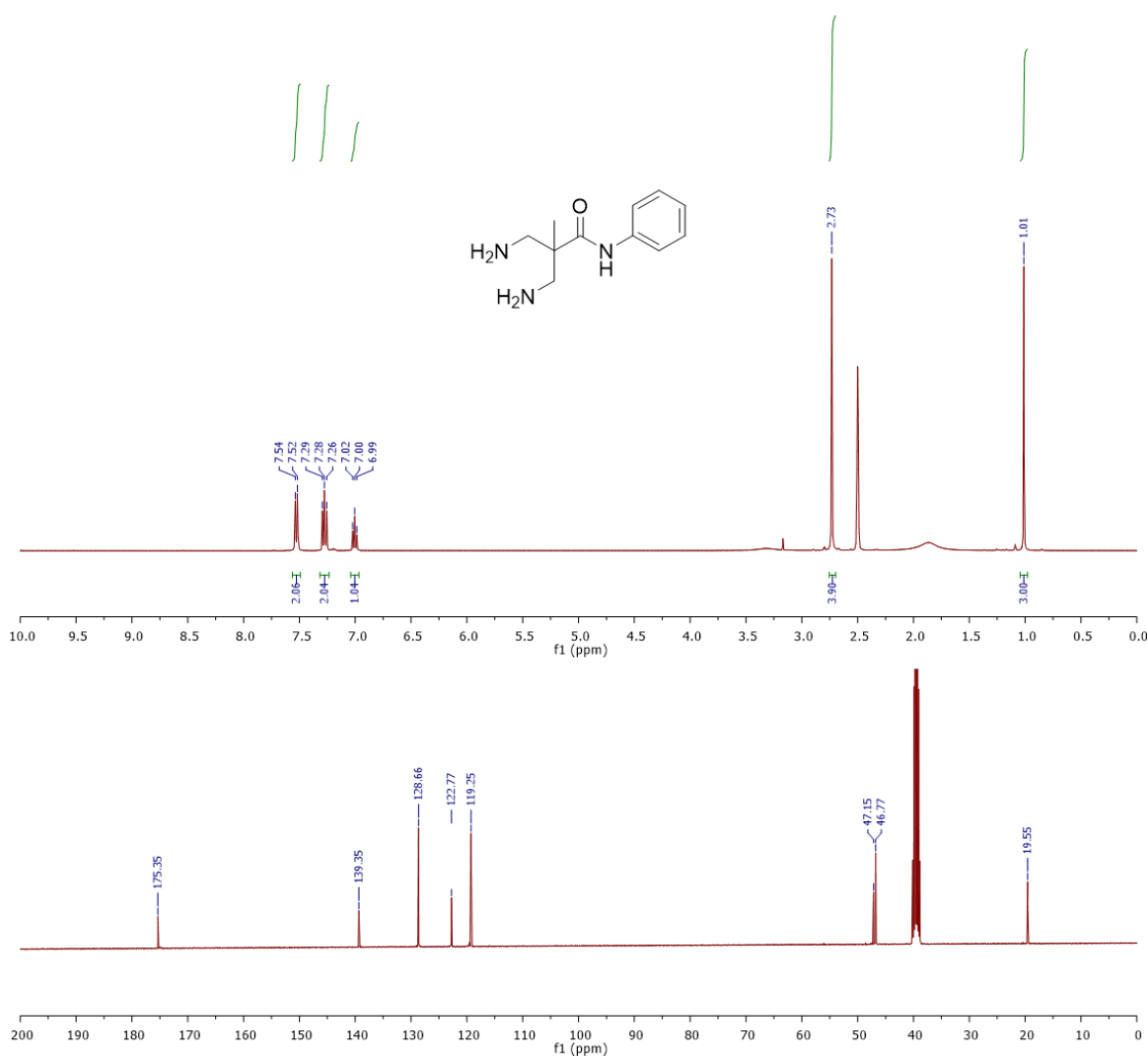
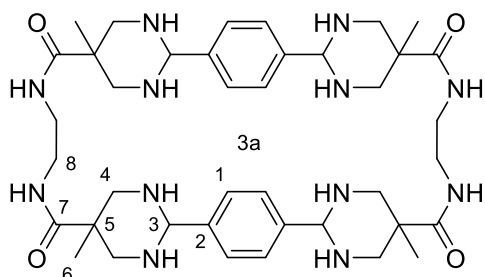


**Figure S10:**  $^1\text{H}$  and  $^{13}\text{C}$  NMR spectra of **5b**,  $\text{DMSO-d}_6$ , 400 and 100 MHz respectively.

## General procedure to macrocyclization

0.5mg (1.73 $\mu$ mol) of **1x** was introduced in an NMR tube from a stock solution at 150mM in CD<sub>3</sub>OD. To that, 1 equivalent of **2x** was added coming from a stock solution of 100mM in CD<sub>3</sub>OD. CD<sub>3</sub>OD was then added to the tube to a volume of 700 $\mu$ L, so [reactives]=2.5mM. The tube is then left reacting at room temperature, with gentle manual shaking at regular times. Advance of the reaction is controlled by NMR. Reaction is performed in CD<sub>3</sub>OD, so incorporation of deuterium in amines is expected.



<sup>1</sup>H-NMR (400 MHz; CD<sub>3</sub>OD):  $\delta$  7.39 (8H, s, H1), 4.41 (4H, s, H3), 3.48 (8H, s, H8), 3.31 (8H, H4a, H4b) 2.72 (8H, d, H4a', H4b', <sup>2</sup>J = 12Hz), 1.02 (12H, s, H6).

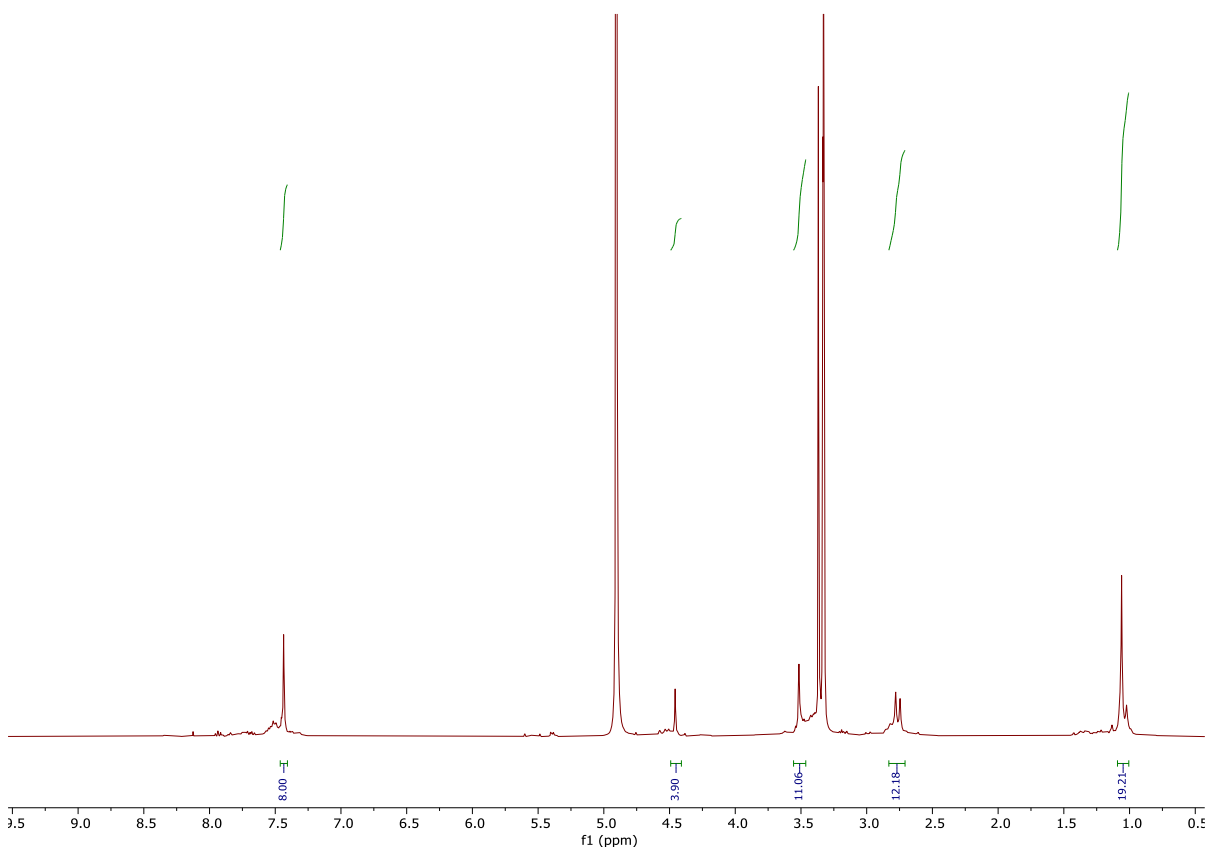


**Figure S11:** <sup>1</sup>H NMR spectrum of **3a**. CD<sub>3</sub>OD, 400MHz.

<sup>13</sup>C-NMR (100 MHz; CD<sub>3</sub>OD):  $\delta$  177.6 (C7), 141.2 (C2), 126.5 (C1), 73.4 (C5), 54.1 (C4), 39.1 (C8a), 39.0 (C8b), 20.6 (C6).

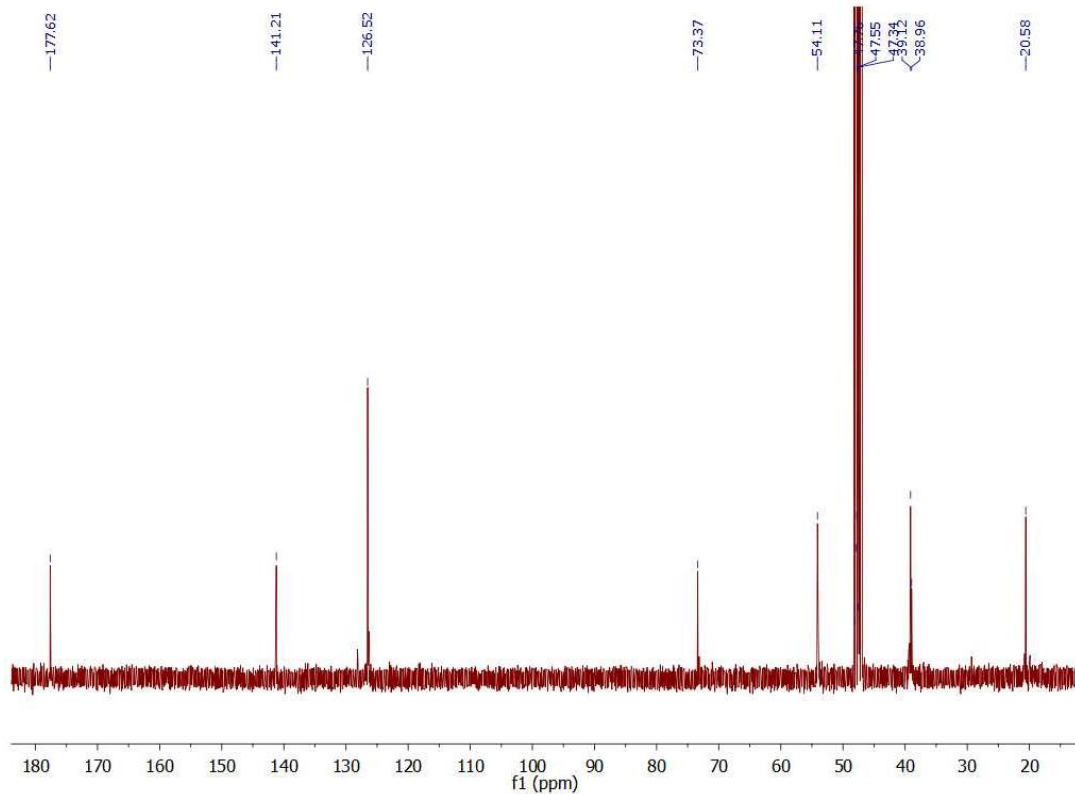


**Figure S12:**  $^{13}\text{C}$  NMR spectrum of **3a**.  $\text{CD}_3\text{OD}$ , 100MHz.

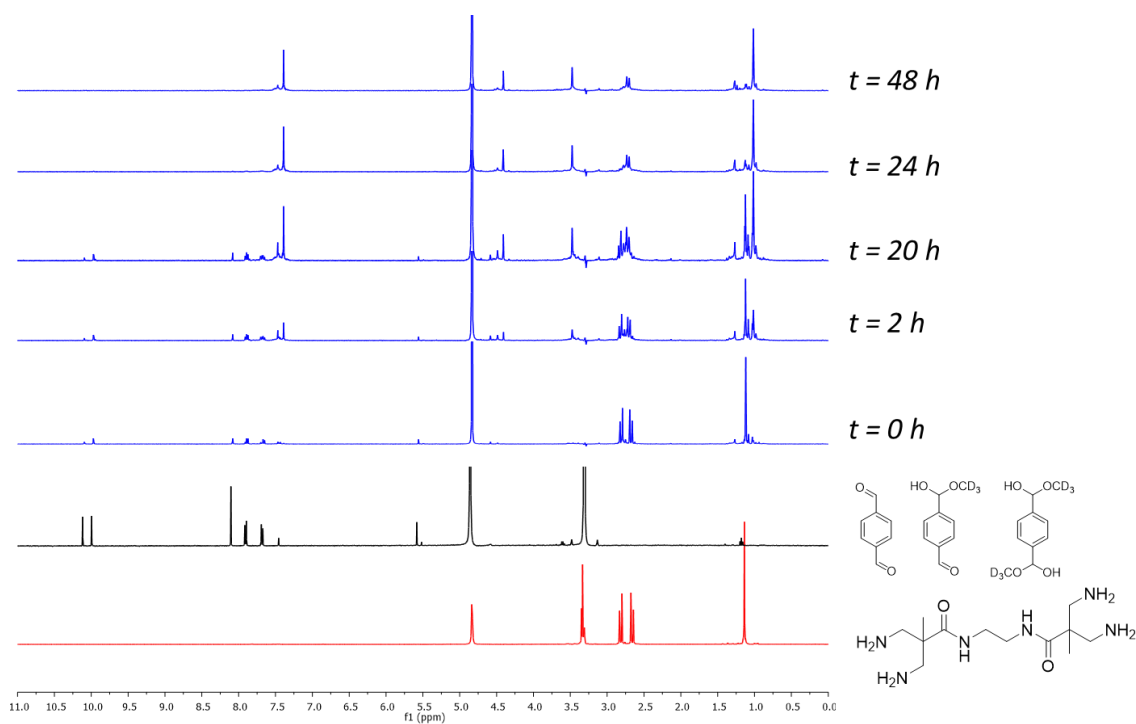


**Figure S13:**  $^1\text{H}$  NMR spectra (WET solvent suppression) of **3a** within time course of the reaction until reaction finishes.  $\text{CD}_3\text{OD}$ , 400MHz.

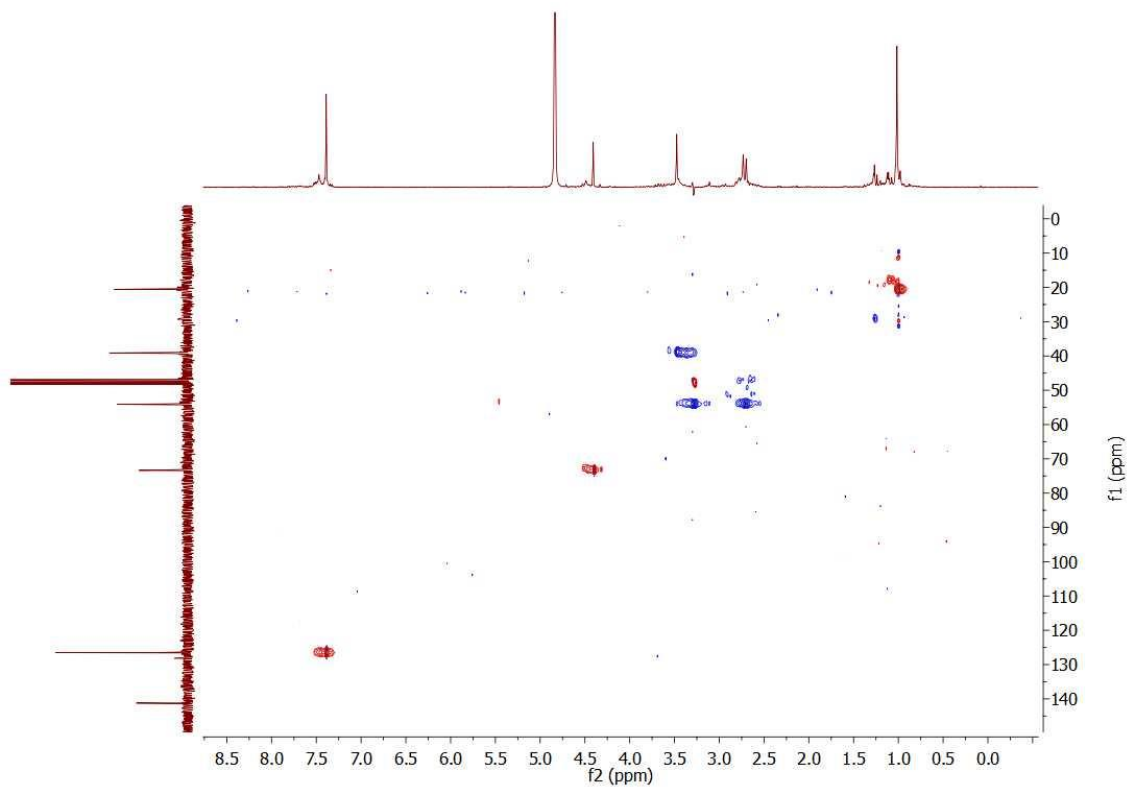
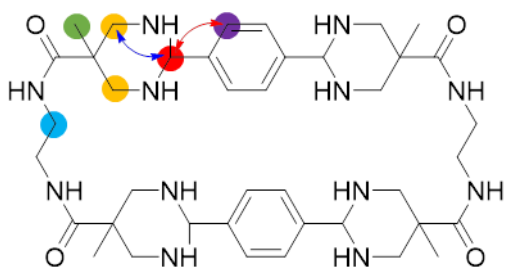


**Figure S14:** HSQC NMR spectrum of **3a** (WET solvent suppression).



The HMBC experiment (Figure S15) gives support to the proposed structure, as proton in red gives response to both carbons in yellow and the ones in purple. This identifies the presence of a covalent aminal linkage, providing a closed macrocyclic conformation, which is in agreement with the high symmetry of the molecule and further confirmed by MALDI-TOF measurements.

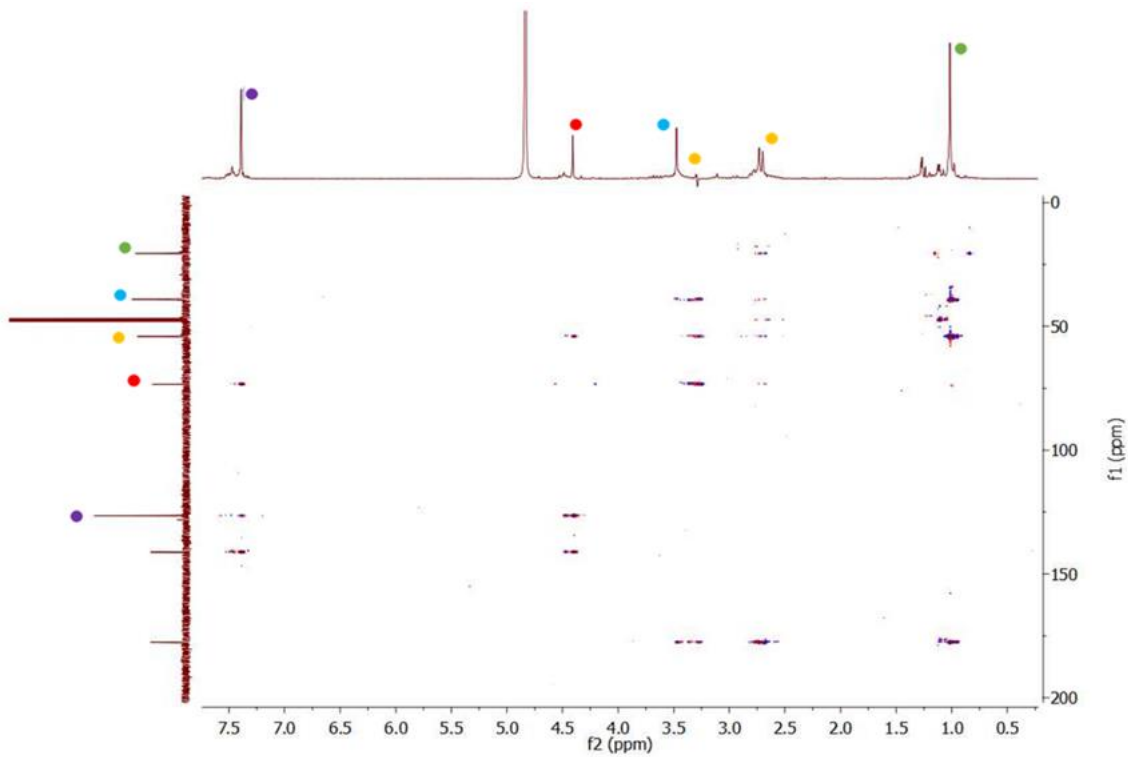


Figure S15: HMBC NMR spectrum of 3a (WET solvent suppression).

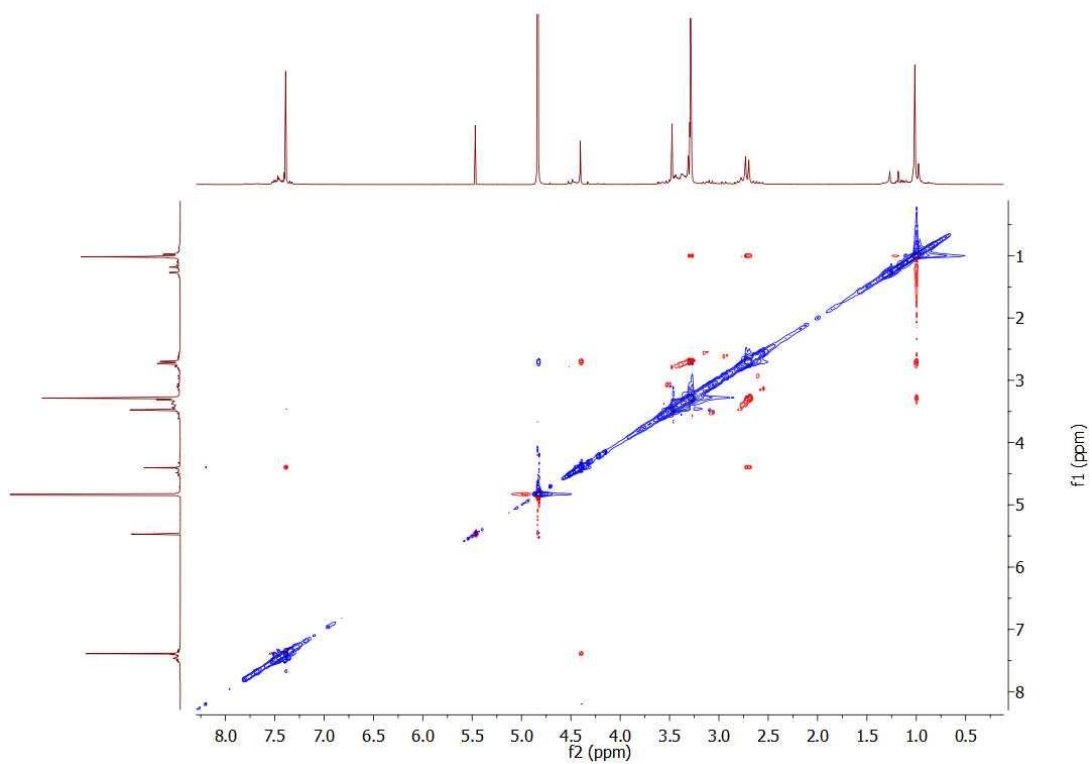
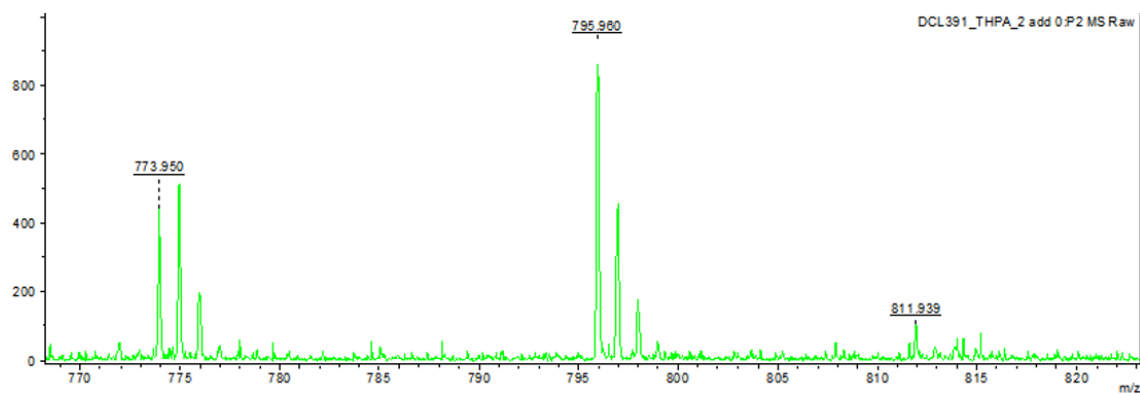
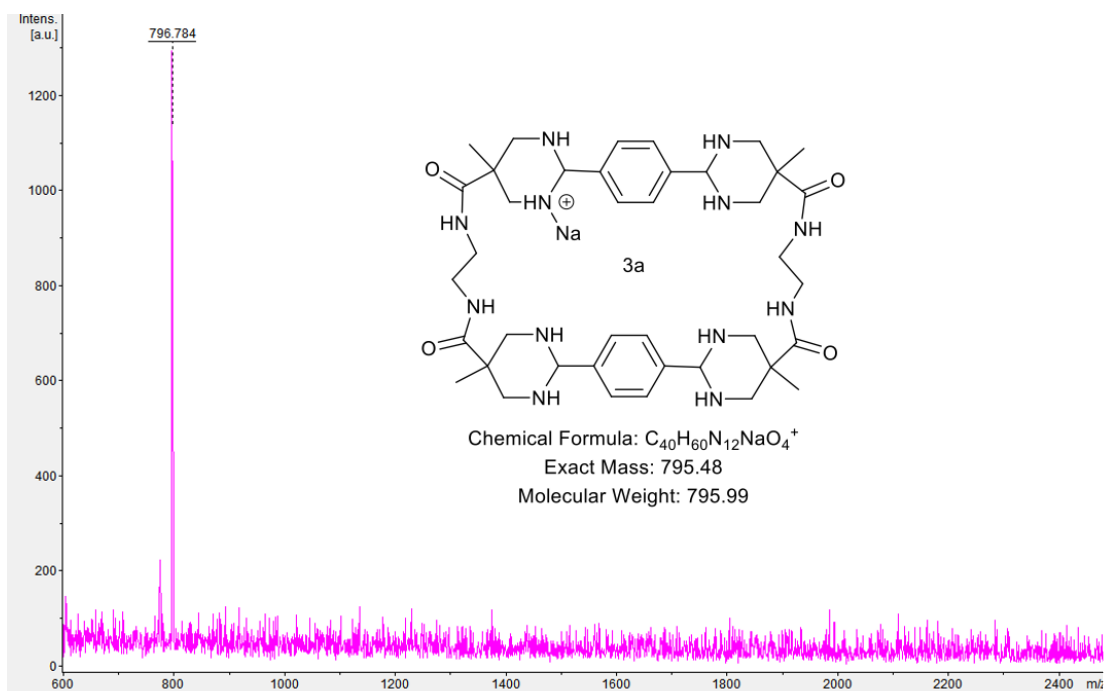
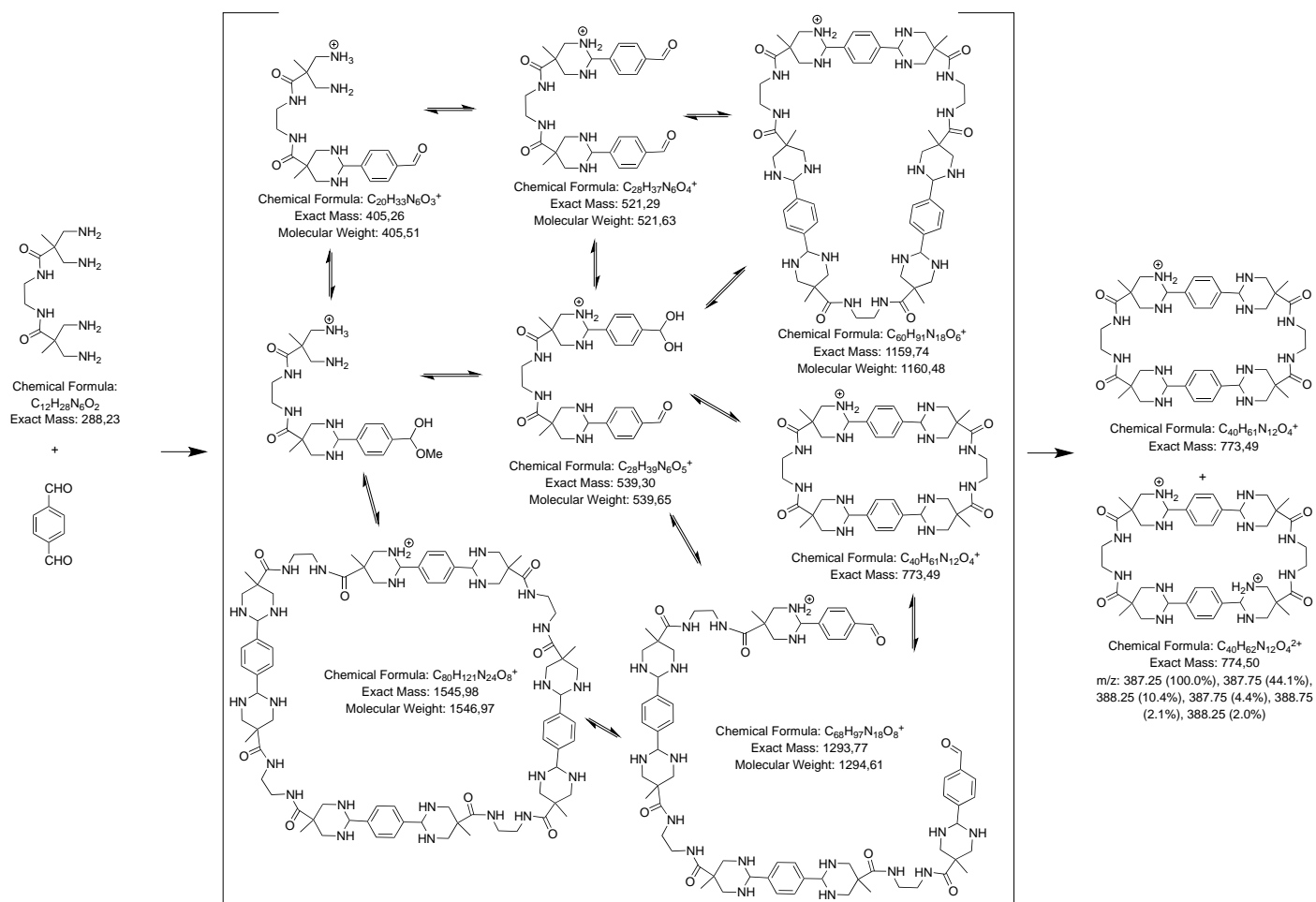


Figure S16: NOESY NMR spectrum of 3a

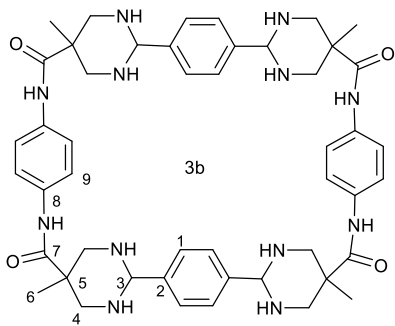


**Figure S17:** MALDI-TOF MS trace of **3a**. The upper trace shows the 600-2500 m/z range, while the bottom trace is focused on the mass corresponding to the [2+2] macrocycle. Calculated theoretical MS for **3a**: 772.4860. Found MS: 773.950 (Mw and partially deuterated **3a**)<sup>+</sup>. 795.960 (M and partially deuterated compound + Na)<sup>+</sup>. 811.939 (M + K)<sup>+</sup>



**Scheme S2:** Reaction progress for the formation of **3a**, monitored by ESI-MS. The intermediate species here depicted were identified while reaction proceeds before equilibration to the formation of **3a**.





$^1\text{H-NMR}$  (400 MHz;  $\text{CD}_3\text{OD}$ ):  $\delta$  7.58 (8H, s, H9), 7.5 (8H, s, H1), 4.56 (4H, s, H3), 3.46 (8H, d, H4a, H4b,  $^2J=12\text{Hz}$ ), 2.87 (8H, d, H4a', H4b',  $^2J=12\text{Hz}$ ), 1.13 (12H, s, H6).

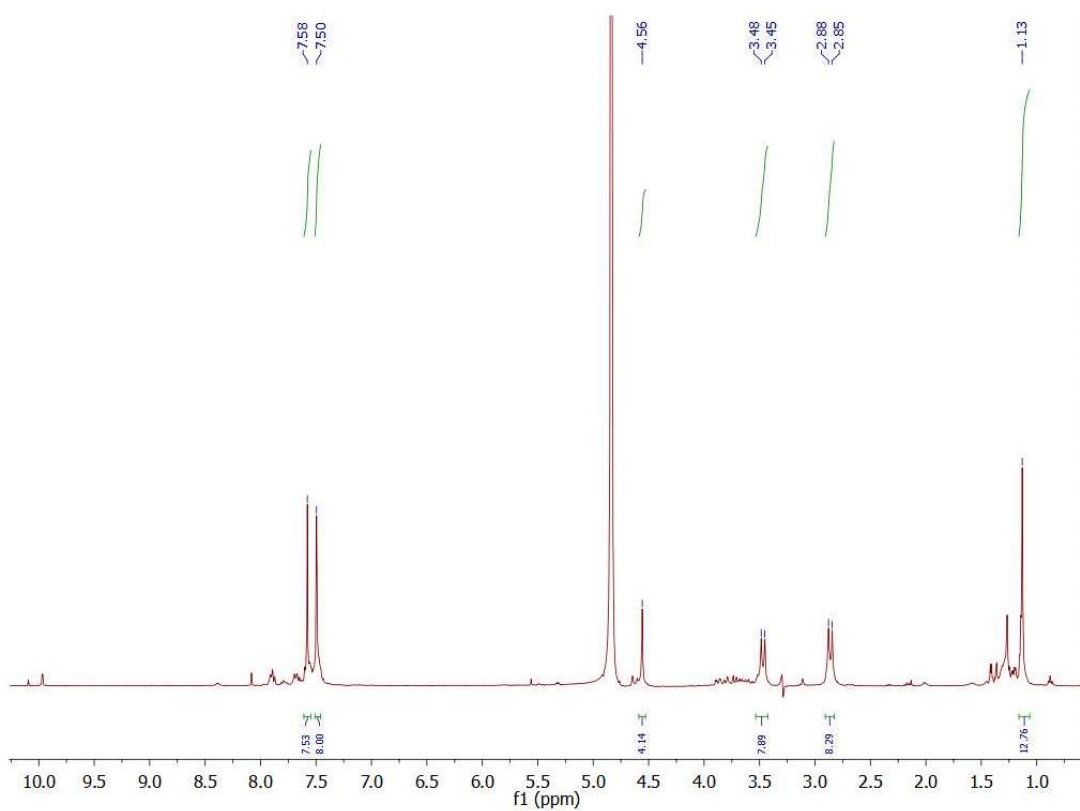


**Figure S18:**  $^1\text{H NMR}$  spectrum of **3b** (WET solvent suppression),  $\text{CD}_3\text{OD}$ , 400MHz.

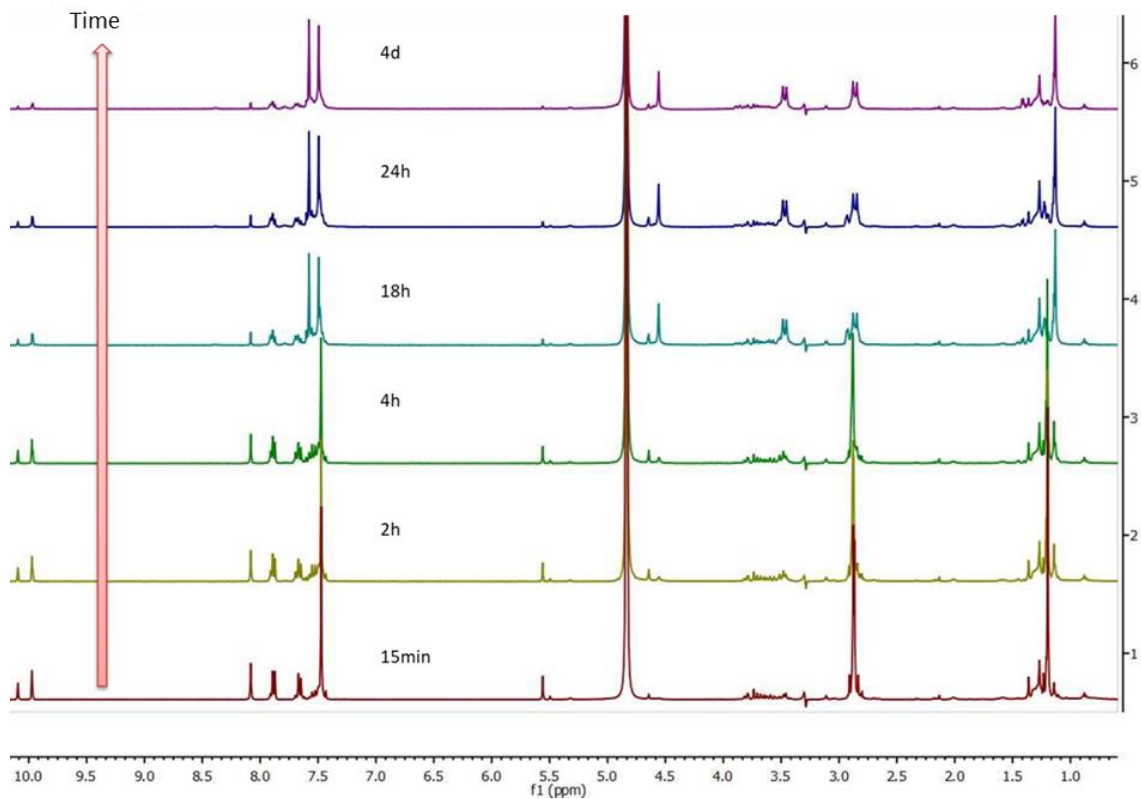


**Figure S19:**  $^1\text{H}$  NMR spectra of **3b** (WET solvent suppression) within time course of the reaction until reaction finishes. MeOD, 400MHz.

$^{13}\text{C}$ -NMR (100 MHz;  $\text{CD}_3\text{OD}$ ):  $\delta$  175.4 (C7), 141.4 (C9), 134.5 (C1), 126.6 (C8), 120.7 (C2), 73.5 (C3), 54.0(C4), 40.0 (C5), 20.3 (C6).

1D  $^{13}\text{C}$  NMR was not acquired as the cycle greatly precipitates at higher concentration. C atoms have been assigned by HSQC and HMBC NMR spectra.

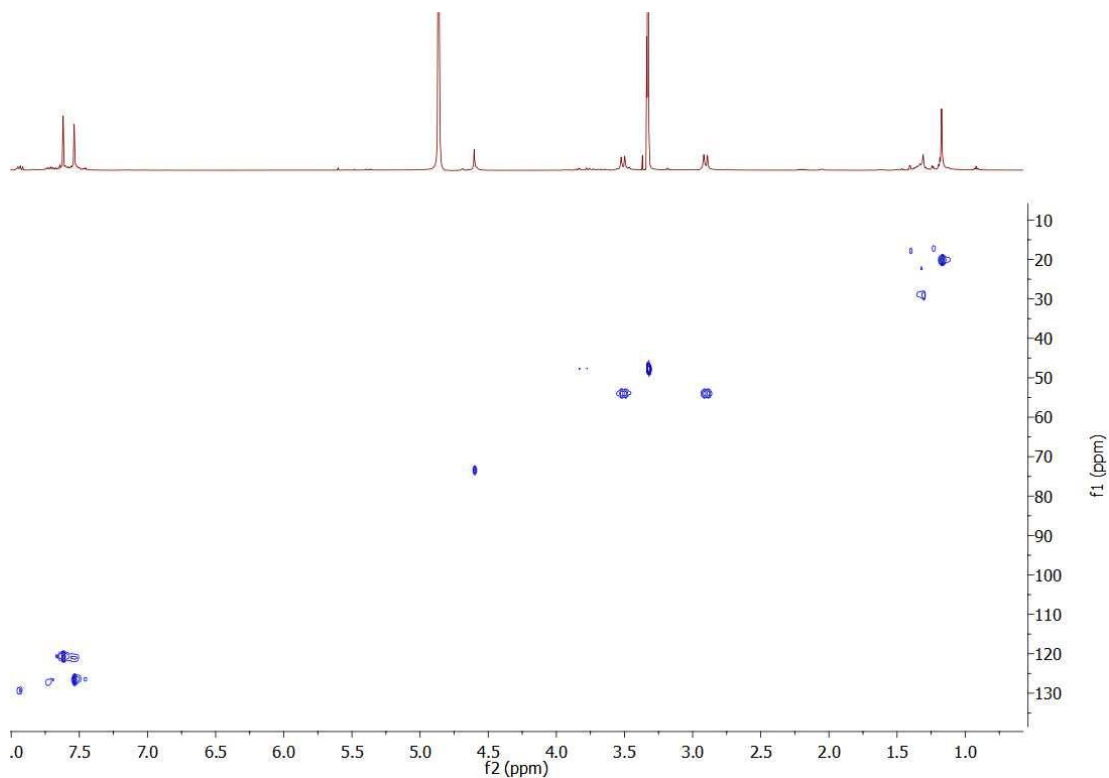


**Figure S20:** HSQC NMR spectrum of **3b**

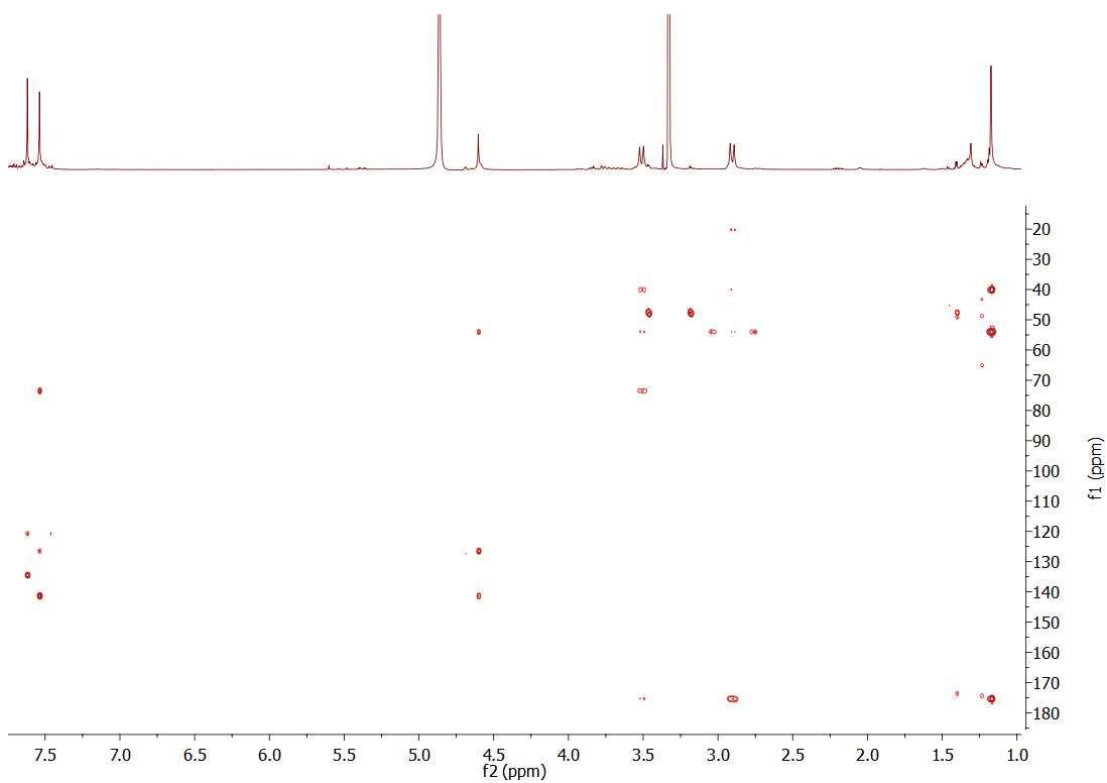


Figure S21: HMBC NMR spectrum of 3b

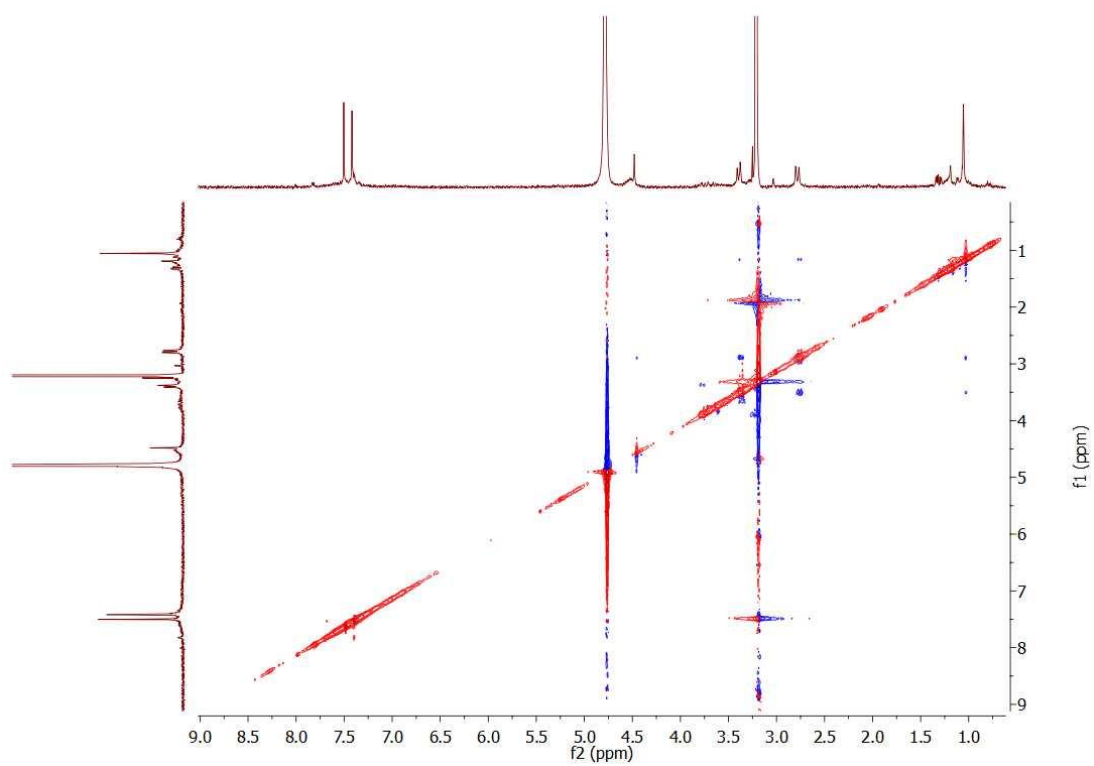
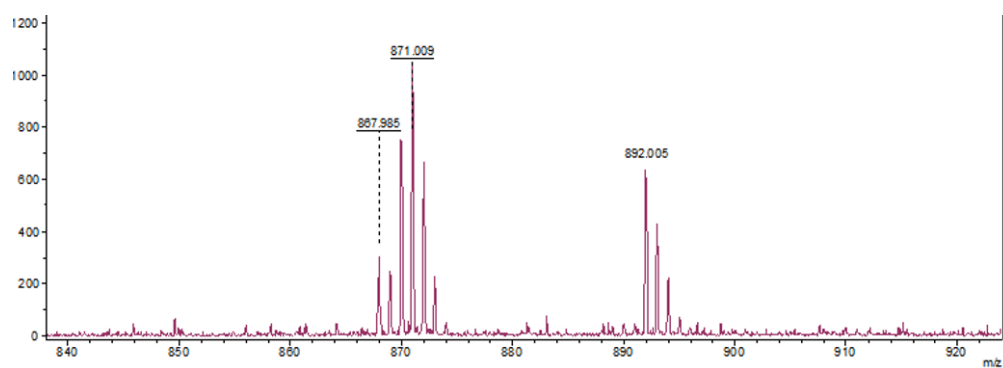
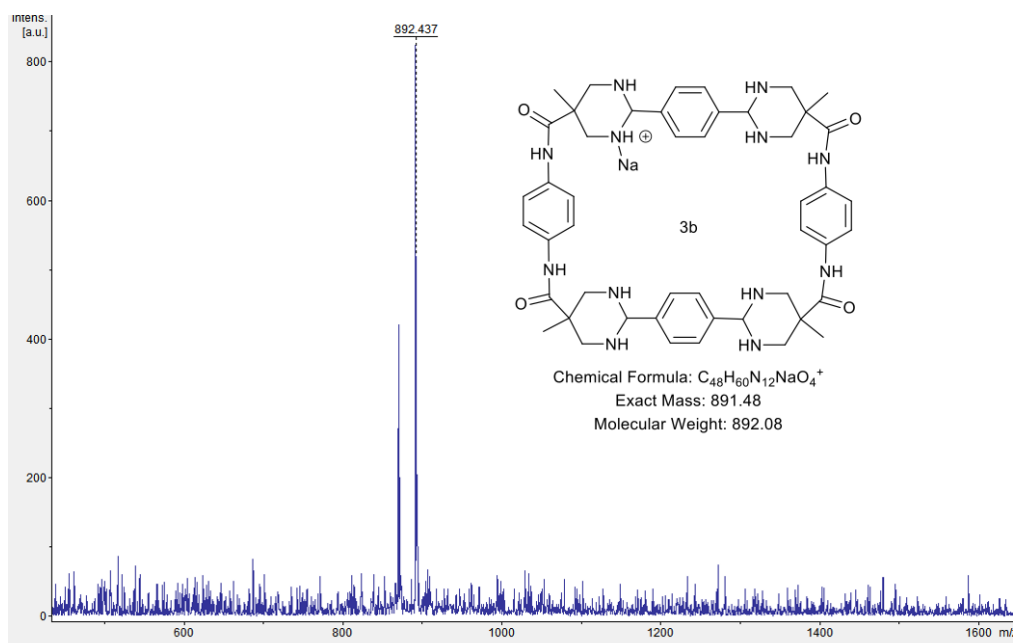
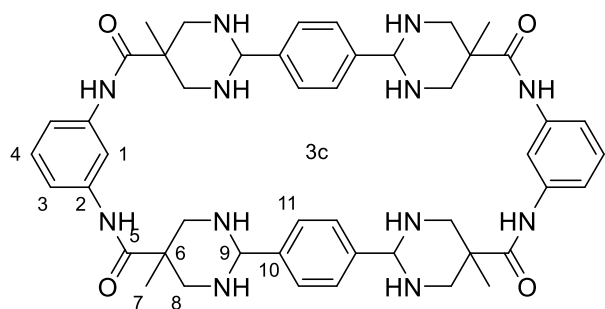


Figure S22: NOESY NMR spectrum of 3b



**Figure S23:** MALDI-TOF MS trace of **3b**. The upper trace shows the 400-1600 m/z range, while the bottom trace is focused on the mass corresponding to the [2+2] macrocycle. Calculated theoretical MS for **3b**: 868.4860. Found MS: 867.985 (Mw and partially deuterated **3b**)<sup>+</sup>. 892.005 (M and partially deuterated compound + Na)<sup>+</sup>.



$^1\text{H-NMR}$  (400 MHz;  $\text{CD}_3\text{OD}$ ):  $\delta$  7.96 (2H, s, H1), 7.43 (6H, m, H3, H4), 7.33 (8H, s, H11), 4.65 (4H –integration distorted due to water suppression-, s, H9), 3.52 (8H, d,  $^2J=12\text{Hz}$ , H8a, H8b), 2.95 (8H, d,  $^2J=12\text{Hz}$ , H8a', H8b'), 1.21 (12H, s, H7)

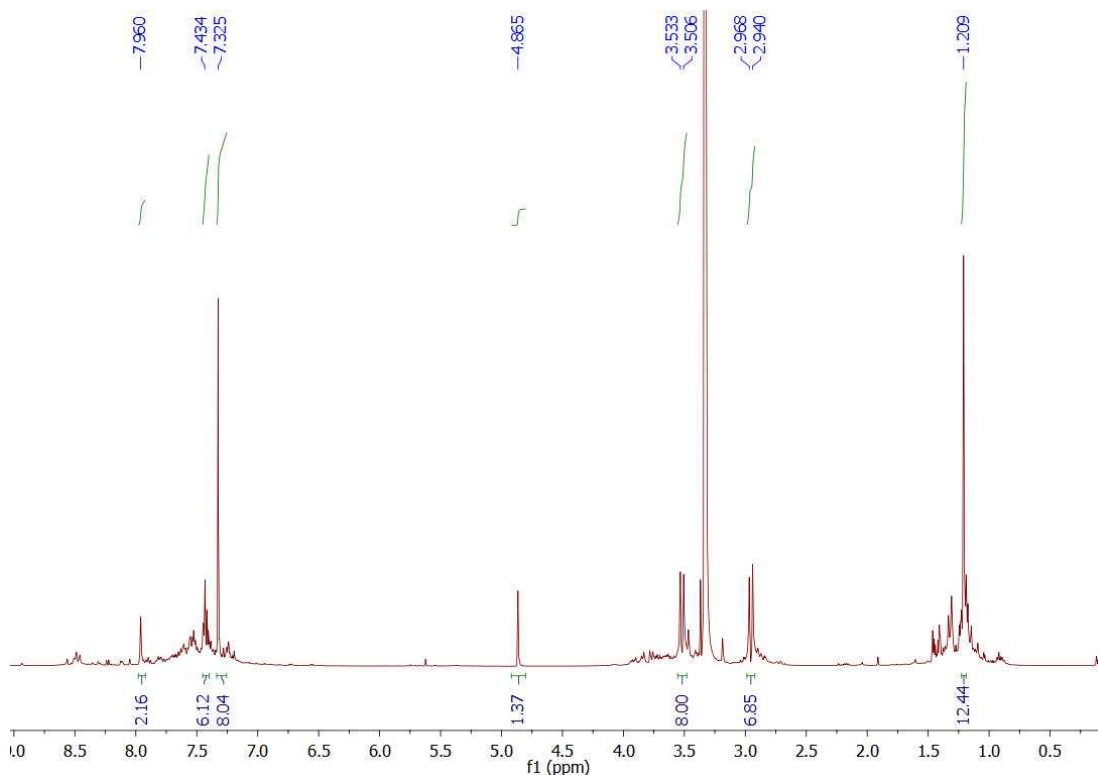


**Figure S24:**  $^1\text{H}$  NMR spectrum of **3c**.  $\text{CD}_3\text{OD}$ , 400MHz.

$^{13}\text{C-NMR}$  (100 MHz;  $\text{CD}_3\text{OD}$ ):  $\delta$  175.2 (C5), 141.9 (C2), 133.8 (C10), 128.5 (C4), 121.1 (C1), 120.8 (C3), 120.5 (C11), 73.5 (C9), 54.2 (C8), 39.7 (C6) 17.3 (C7)

1D  $^{13}\text{C}$  NMR was not acquired as the cycle greatly precipitates at higher concentration. C atoms have been assigned by HSQC and HMBC NMR spectra.

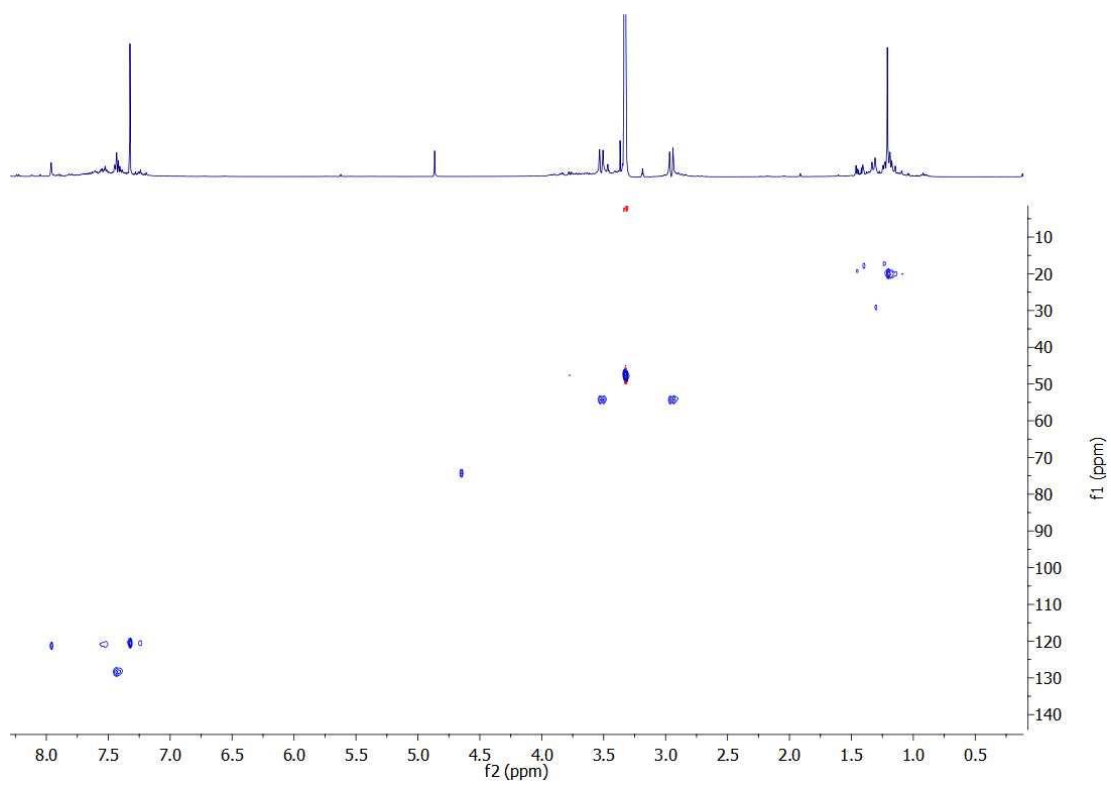


Figure S25: HSQC NMR spectrum of 3c

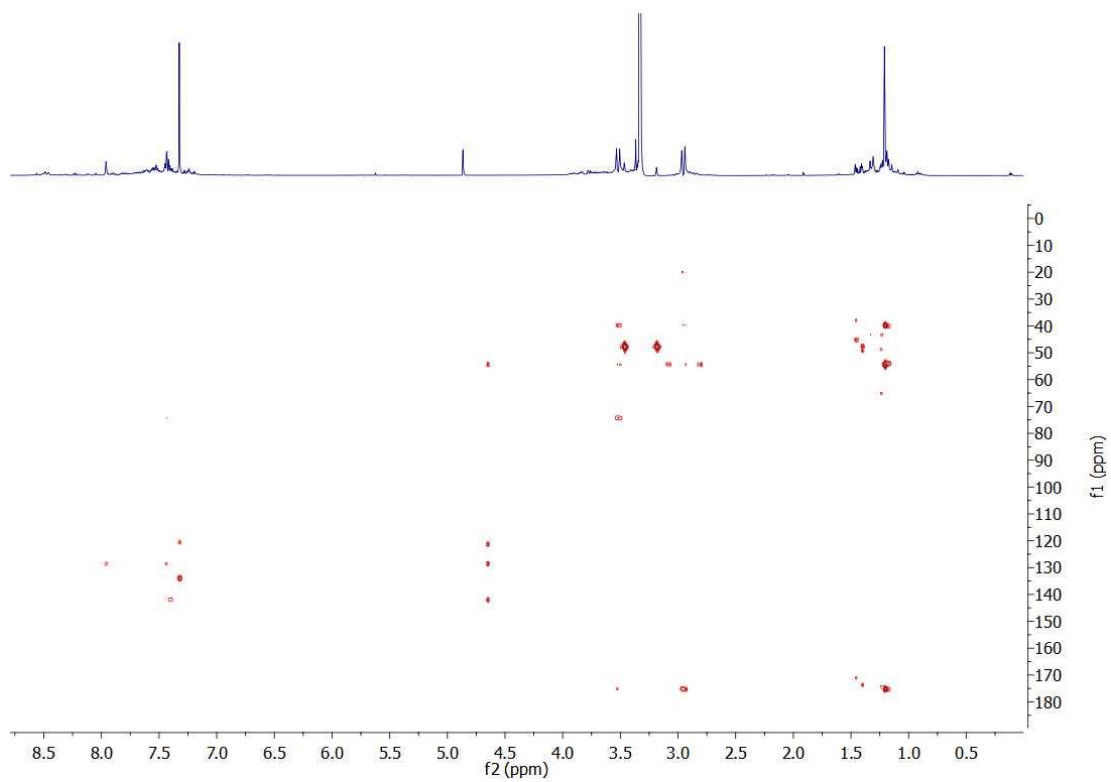
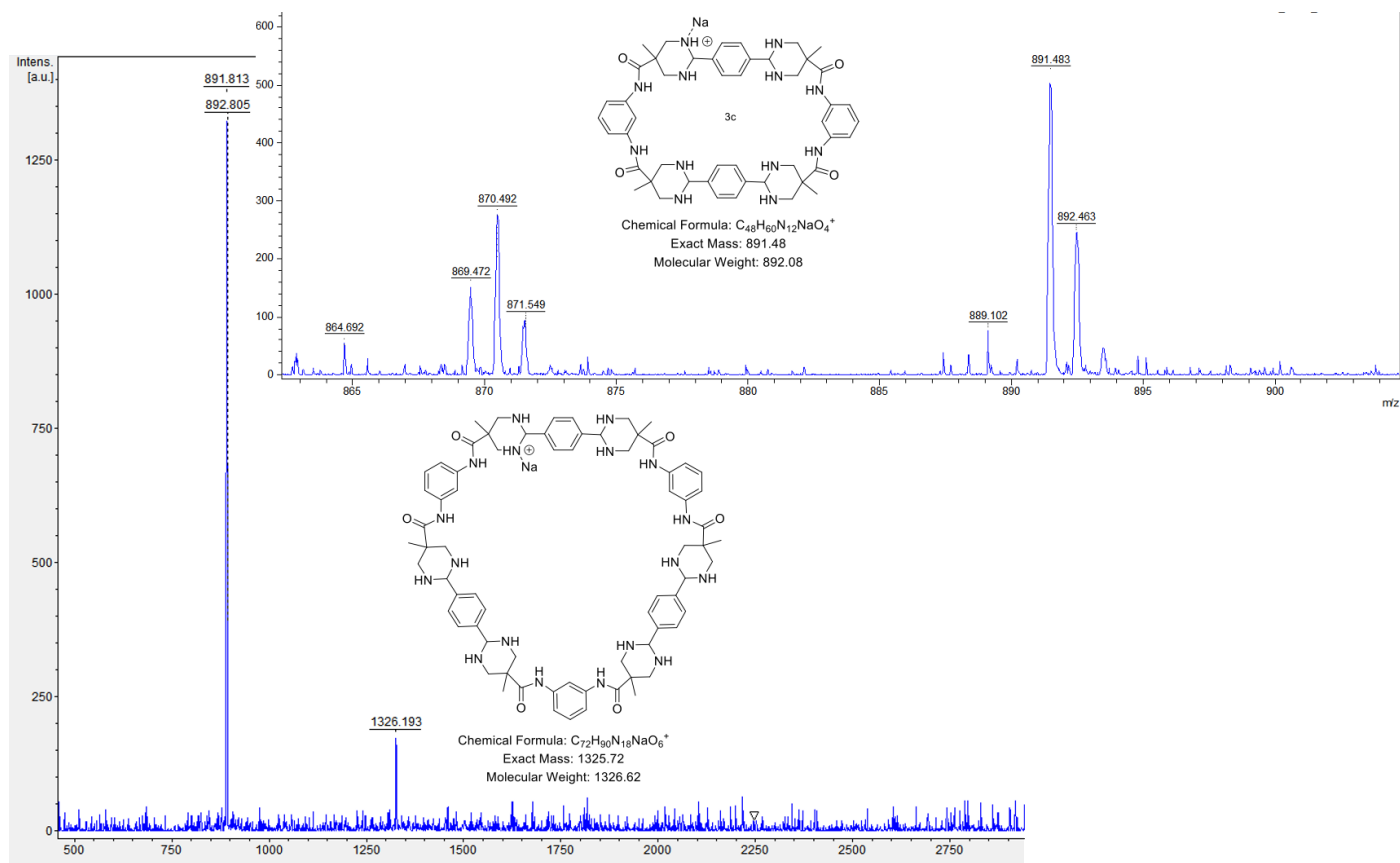
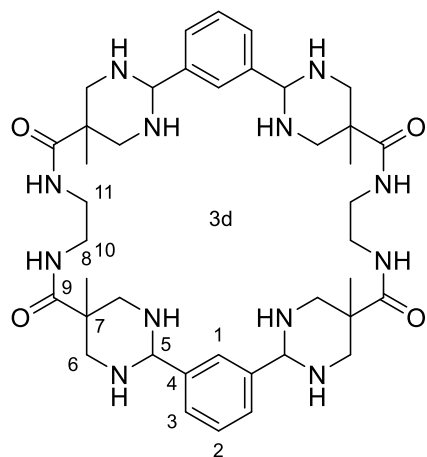


Figure S26: HMBC NMR spectrum of 3c



**Figure S27:** MALDI-TOF MS trace of **3c**. The lower trace shows the 500-3000 m/z range, while the upper inset is focused on the mass corresponding to the [2+2] macrocycle. Calculated theoretical MS for **3c**: 868.4860. Found MS: 869.472 (Mw and partially deuterated **3c**)<sup>+</sup>. 891.483 (M and partially deuterated compound + Na)<sup>+</sup>. The MS spectra shows the presence of a minor amount of the [3+3] macrocycle as a byproduct.



$^1\text{H-NMR}$  (400 MHz;  $\text{CD}_3\text{OD}$ ):  $\delta$  8.04 (2H, s, H1). 7.3 (6H, m, H2, H3), 4.51 (4H, s, H5), 3.55 (8H, m, H10, H11), 3.27 (8H, m, H6a, H6b), 2.77 (8H, d, H6a', H6b',  $^2J=12\text{Hz}$ ), 1.03 (12H, s, H8).

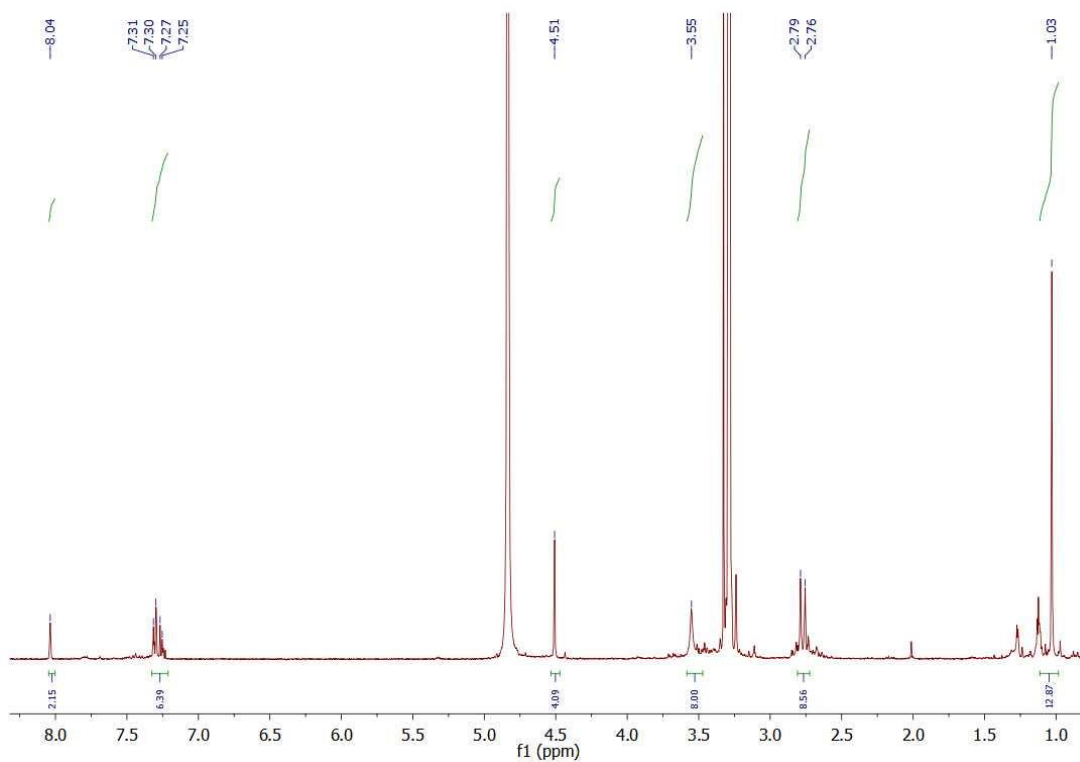


**Figure S28:**  $^1\text{H}$  NMR spectrum of **3d**.  $\text{CD}_3\text{OD}$ , 400MHz.

$^{13}\text{C-NMR}$  (100 MHz;  $\text{CD}_3\text{OD}$ ):  $\delta$  178.1 (C9), 142.6 (C4), 127.7 (C3), 127.5 (C2), 125.7 (C1), 72.6 (C5), 53.5 (C6), 40.7 (C10), 39.9 (C11), 20.6 (C8)



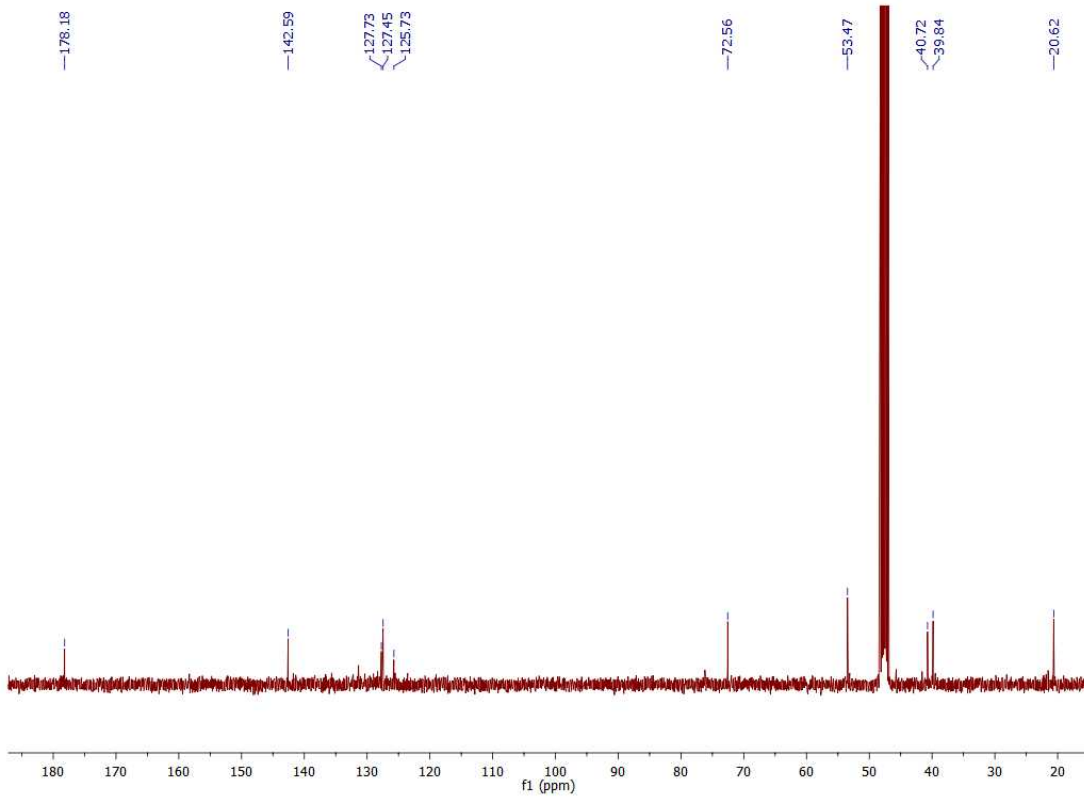


Figure S29:  $^{13}\text{C}$  NMR spectrum of **3d**.  $\text{CD}_3\text{OD}$ , 400MHz.

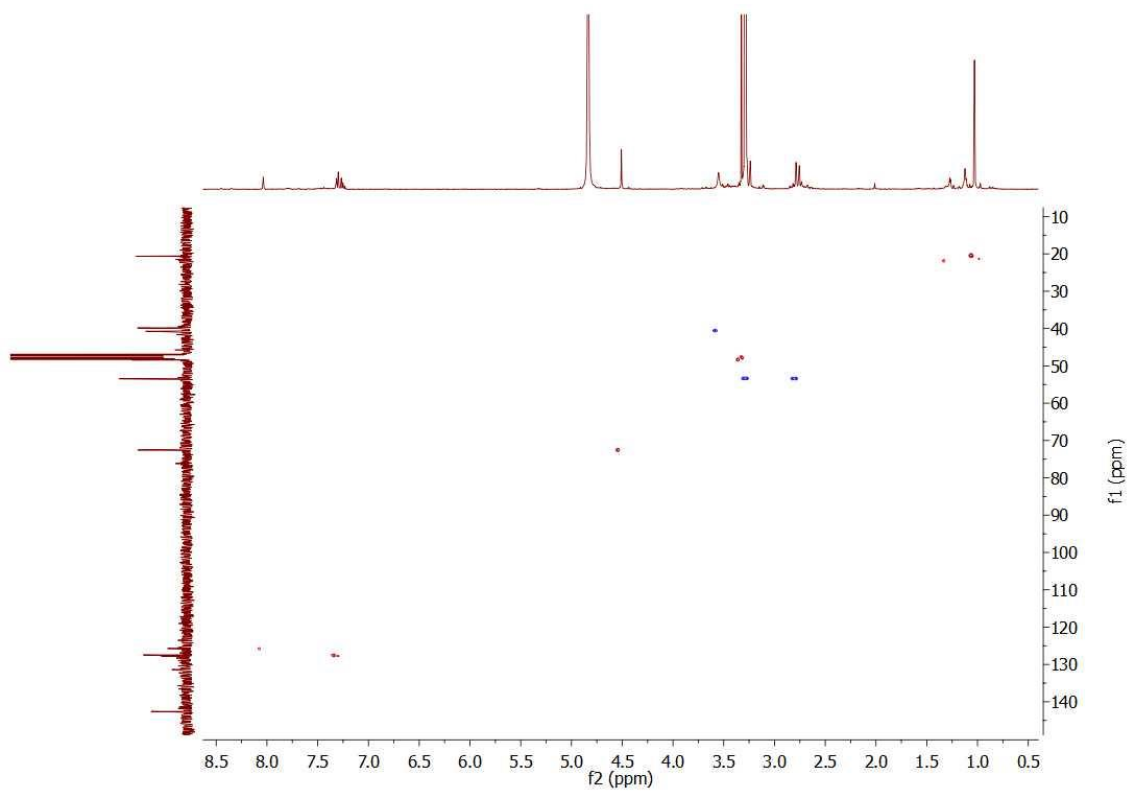


Figure S30: HSQC NMR spectrum of **3d**

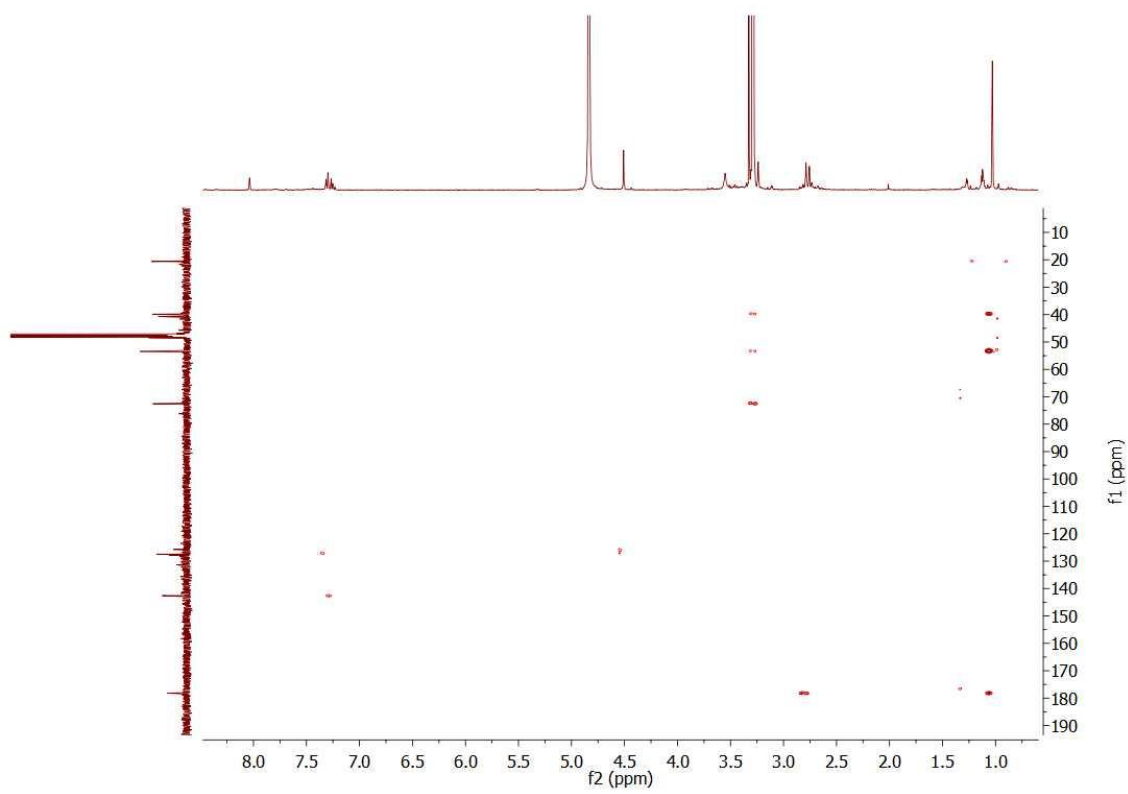
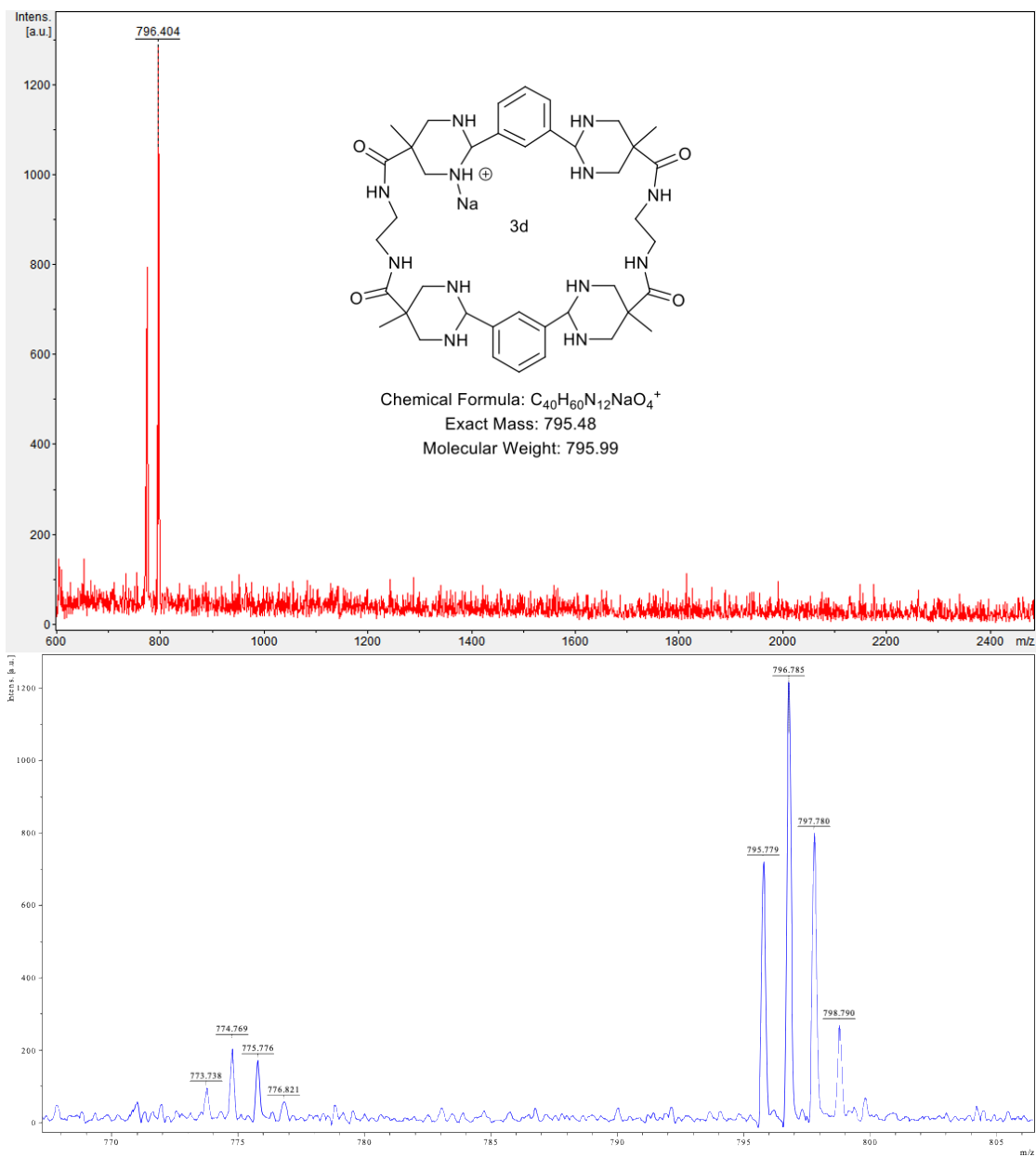
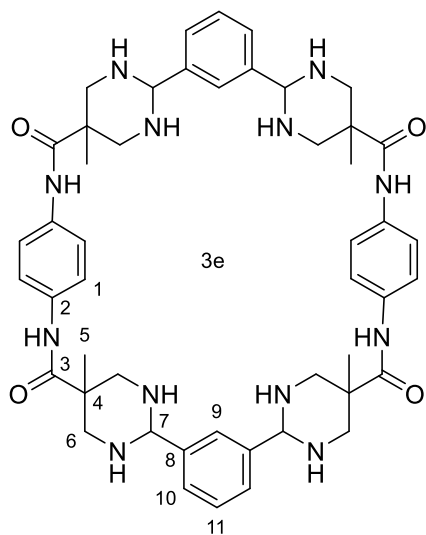


Figure S31: HMBC NMR spectrum of **3d**



**Figure S32:** MALDI TOF MS trace of **3d**. The upper trace shows the 400-1600 m/z range, while the bottom trace is focused on the mass corresponding to the [2+2] macrocycle. Calculated theoretical MS for **3a**: 772.4860. Found MS: 773.738 (Mw and partially deuterated **3a**)<sup>+</sup>. 795.779 (M and partially deuterated compound + Na)<sup>+</sup>.



$^1\text{H-NMR}$  (400 MHz;  $\text{CD}_3\text{OD}$ ):  $\delta$  7.96 (2H, s, H9), 7.52 (4H, m, H1), 7.43 (6H, m, H10, H11), 7.33 (4H, s, H1), 4.65 (4H, s, H7), 3.52 (4H, d,  $^2J=8\text{Hz}$ , H6a, H6b), 2.96 (4H, d,  $^2J=8\text{Hz}$ , H6a', H6b'), 1.21 (12H, s, H5).

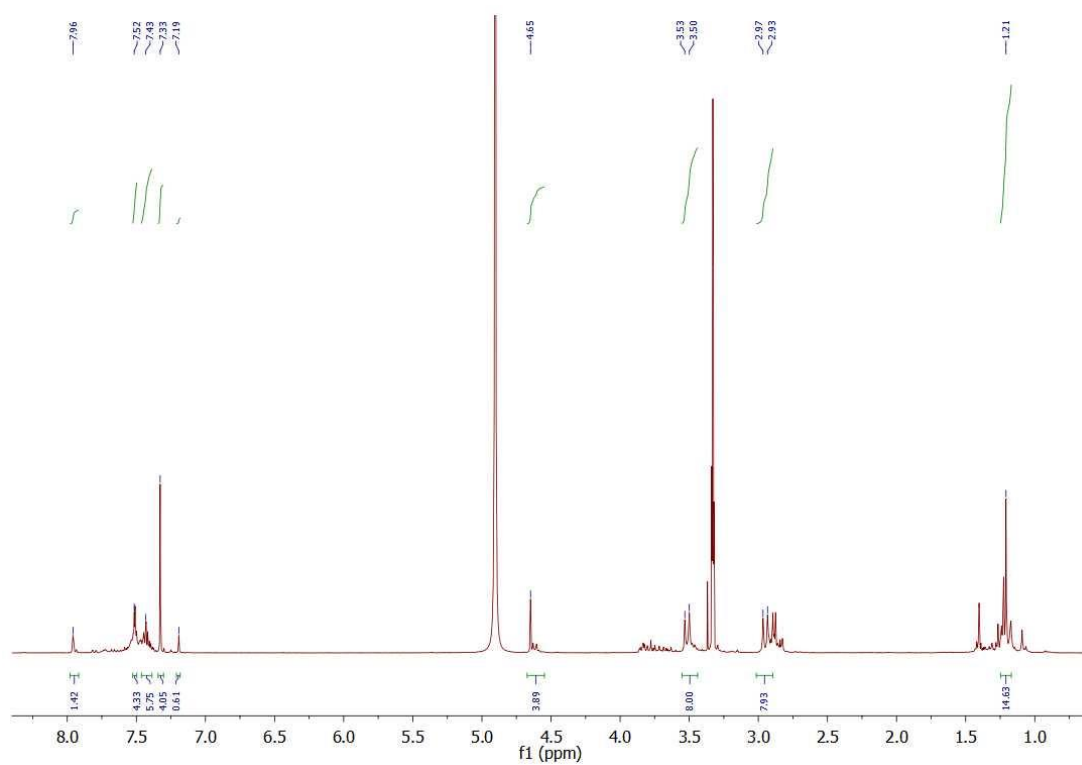


**Figure S33:**  $^1\text{H NMR}$  spectrum of **3e**.  $\text{CD}_3\text{OD}$ , 400MHz.

$^{13}\text{C}$ -NMR (100 MHz;  $\text{CD}_3\text{OD}$ ):  $\delta$  175.2 (C3), 142.1 (C8), 134.6 (C2), 134.0 (C9), 128.6 (C10), 121.3 (C11), 120.6 (C1), 74.4 (C7), 54.5 (C6), 40.0 (C4), 20.0 (C5).

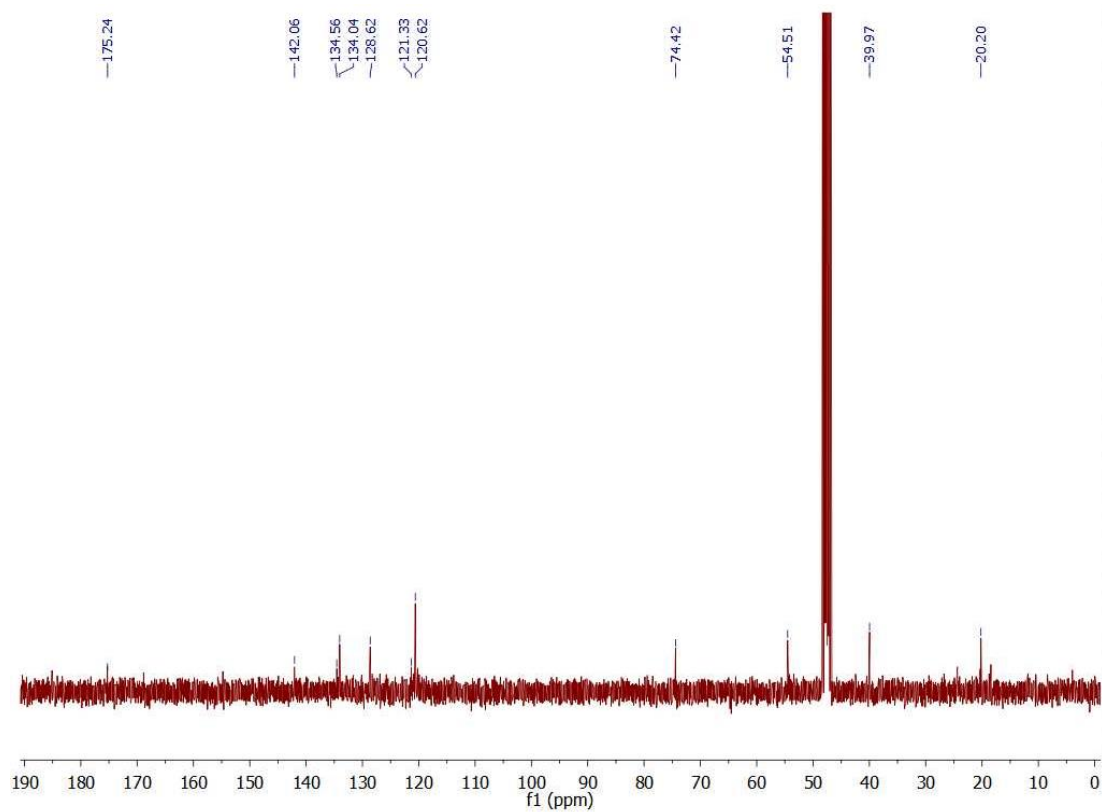


**Figure S34:**  $^{13}\text{C}$  NMR spectrum of **3e**.  $\text{CD}_3\text{OD}$ , 400MHz.

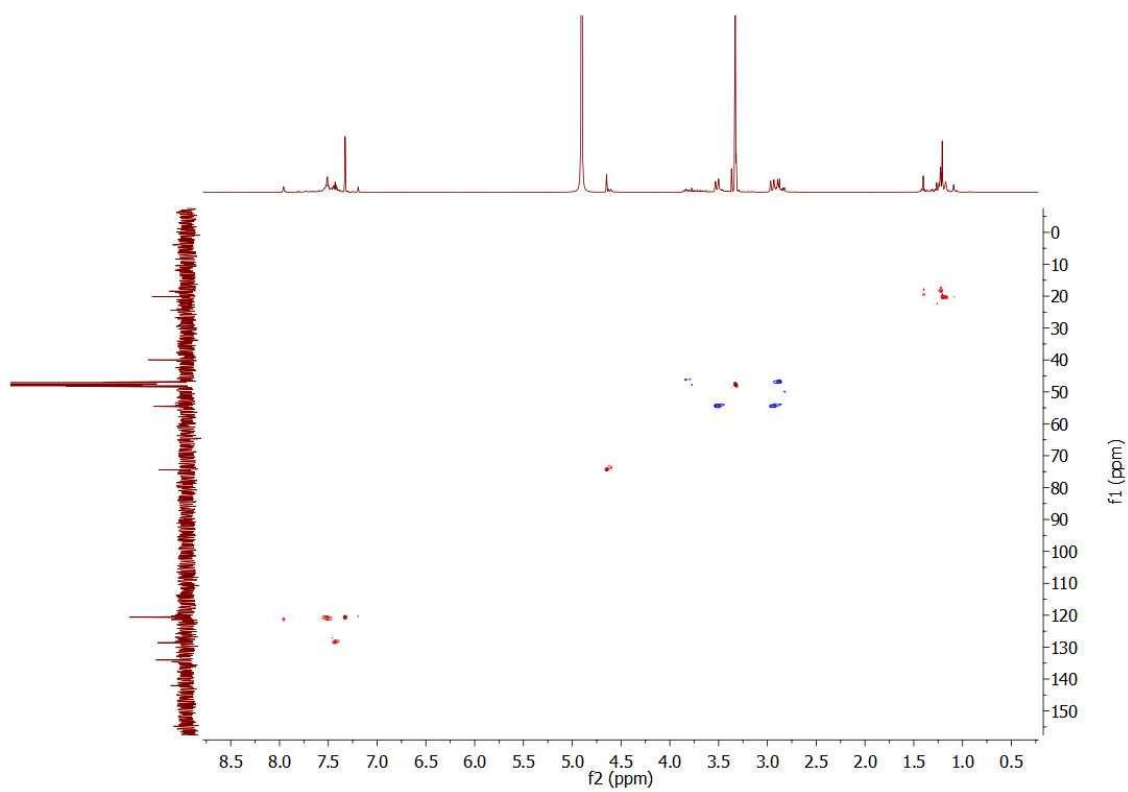


**Figure S35:** HMBC NMR spectrum of **3e**

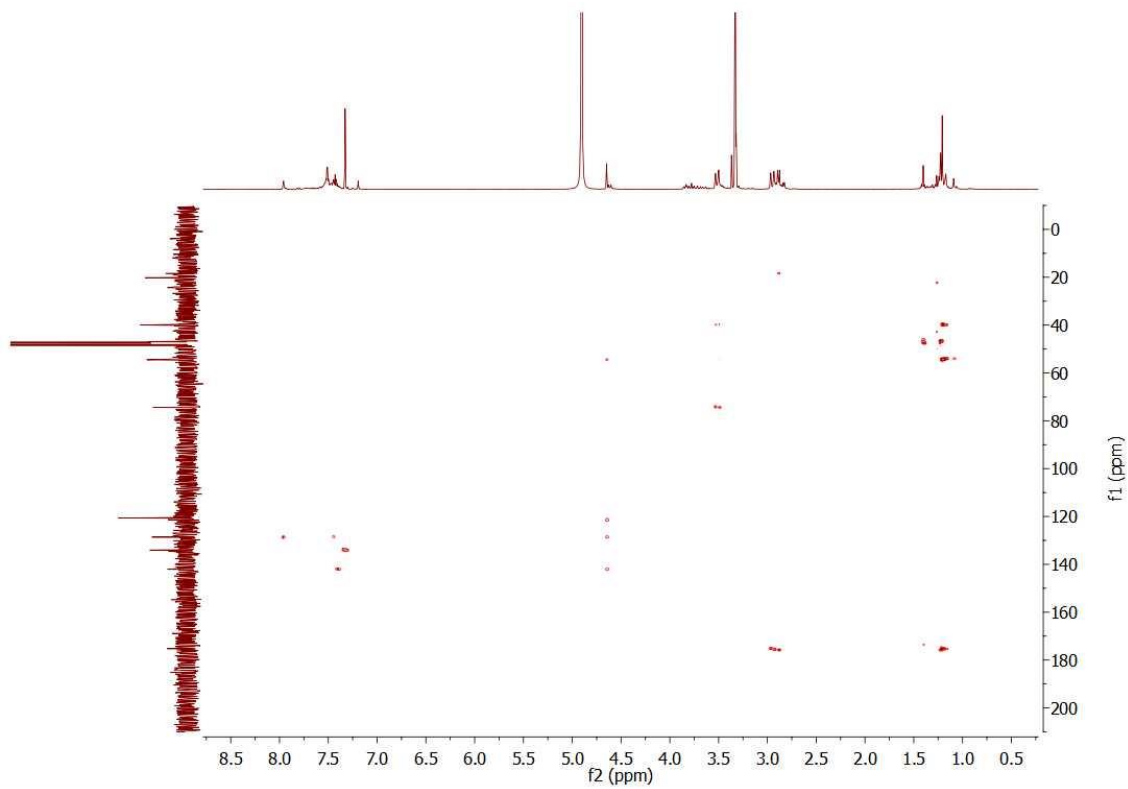


**Figure S36:** HSQC NMR spectrum of **3e**

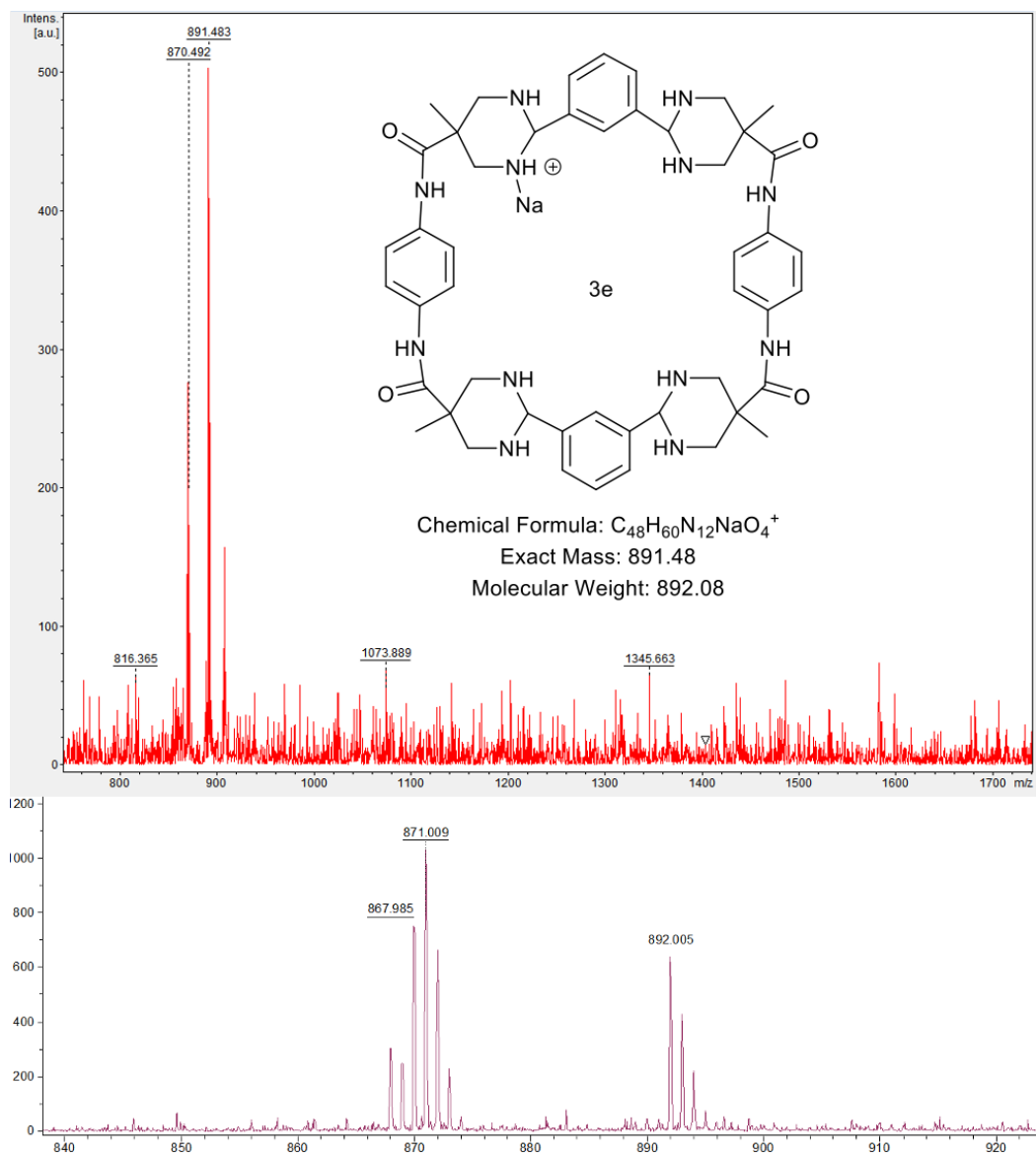
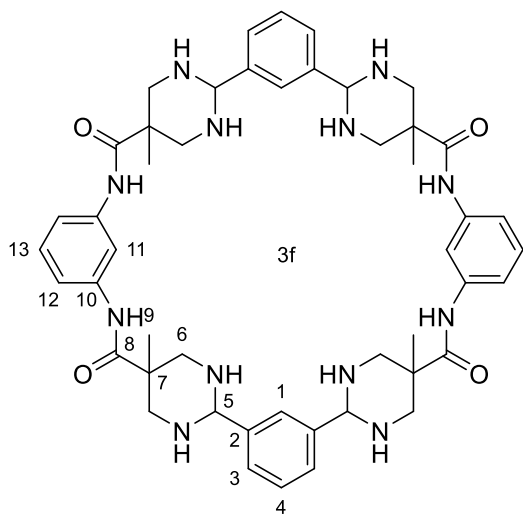


**Figure S37:** MALDI TOF MS trace of **3e**. The upper trace shows the 750-1750 m/z range, while the bottom trace is focused on the mass corresponding to the [2+2] macrocycle. Calculated theoretical MS for **3e**: 868.4860. Found MS: 867.985 (Mw and partially deuterated **3e**)<sup>+</sup>. 892.005 (M and partially deuterated compound + Na)<sup>+</sup>.



$^1\text{H-NMR}$  (400 MHz;  $\text{CD}_3\text{OD}$ ):  $\delta$  8.11 (1H, s, H11), 7.73 (1H, s, H1), 7.37 (12H, m, H3, H4, H12, H13), 4.62 (4H, s, H5), 3.46 (8H, d, H6a, H6b,  $^2J=12\text{Hz}$ ), 2.87(8H, d, H6a', H6b',  $^2J=12\text{Hz}$ ), 1.18 (H9, s, 12H)

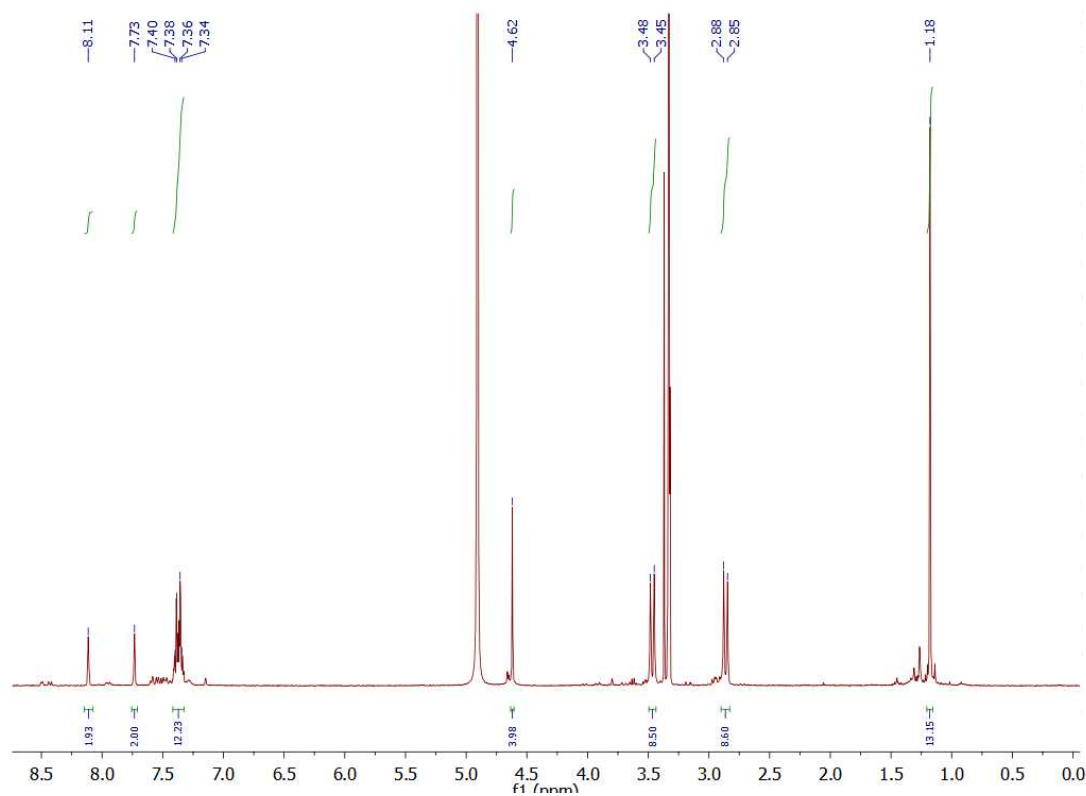


**Figure S38:**  $^1\text{H-NMR}$  spectrum of **3f**.  $\text{CD}_3\text{OD}$ , 400MHz.

$^{13}\text{C-NMR}$  (100 MHz;  $\text{CD}_3\text{OD}$ ):  $\delta$  177.6 (C8), 142.5 (C2), 138.9 (C10), 129.2 (C13), 129.1 (C4), 128.2 (C1), 122.5 (C11), 118.9 (C3), 118.3 (C12), 74.7(C5), 54.6 (C6), 40.7 (C7), 19.3 (C9)



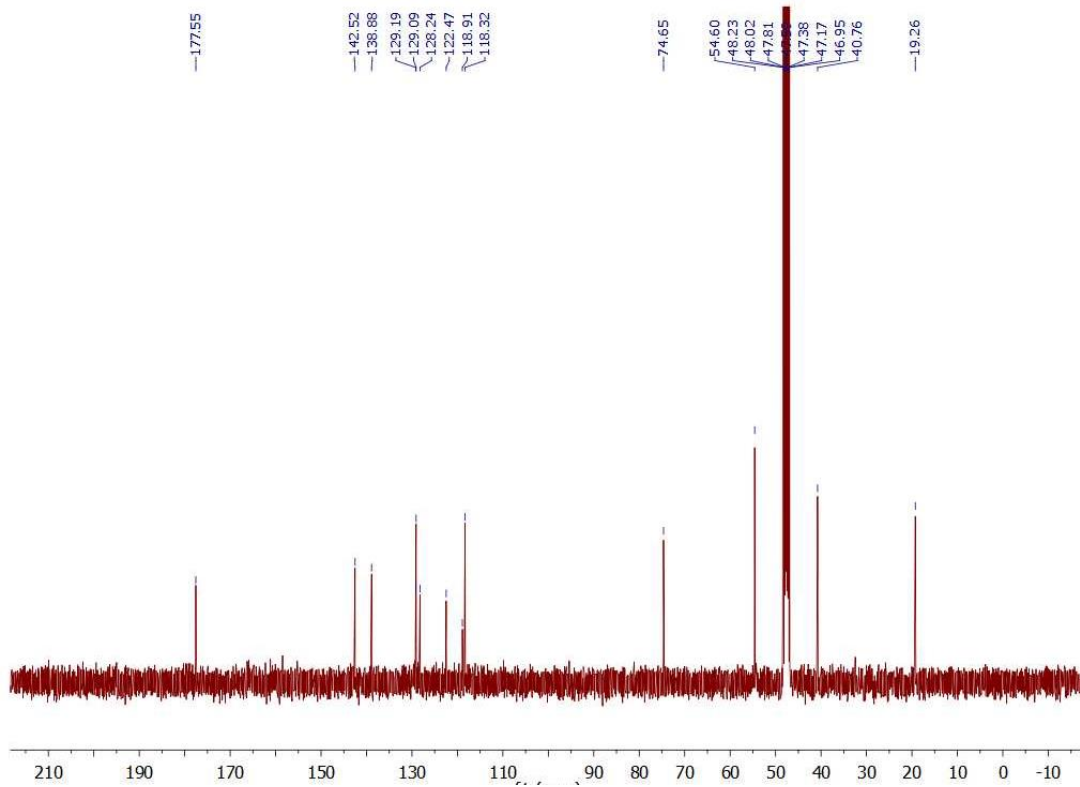


Figure S39:  $^{13}\text{C}$  NMR spectrum of **3f**.  $\text{CD}_3\text{OD}$ , 400MHz.

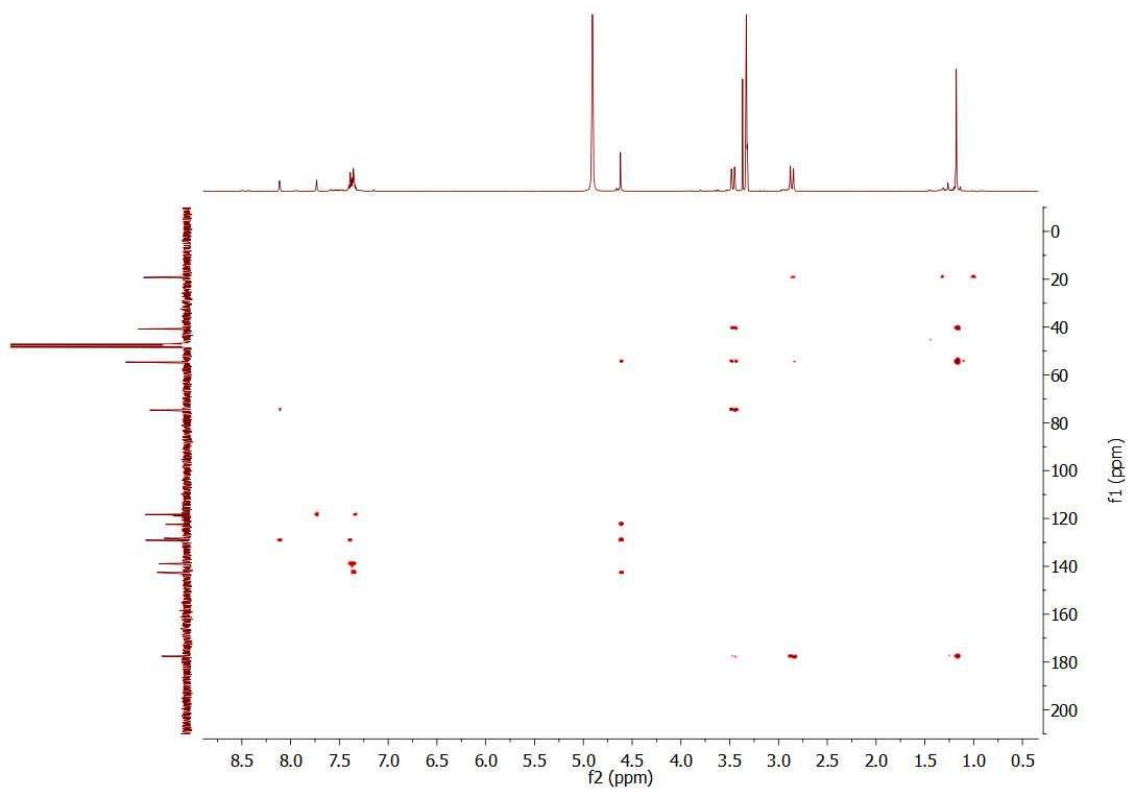


Figure S40: HMBC NMR spectrum of **3f**

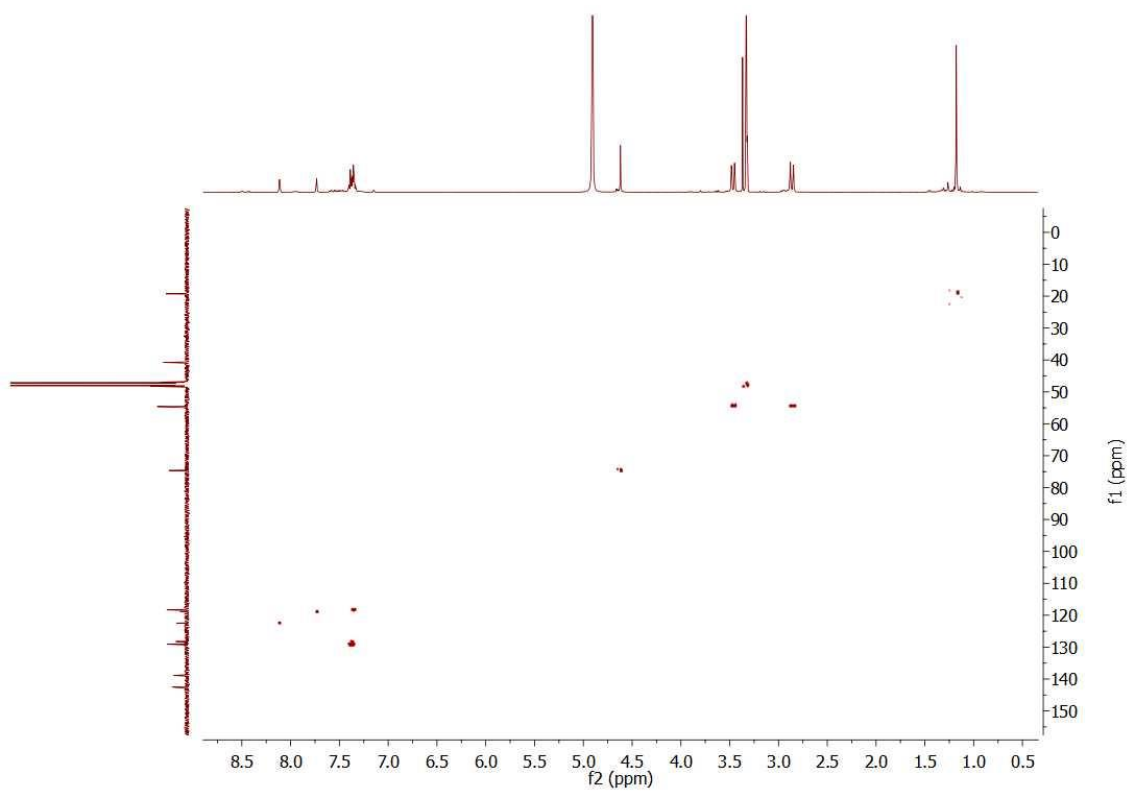
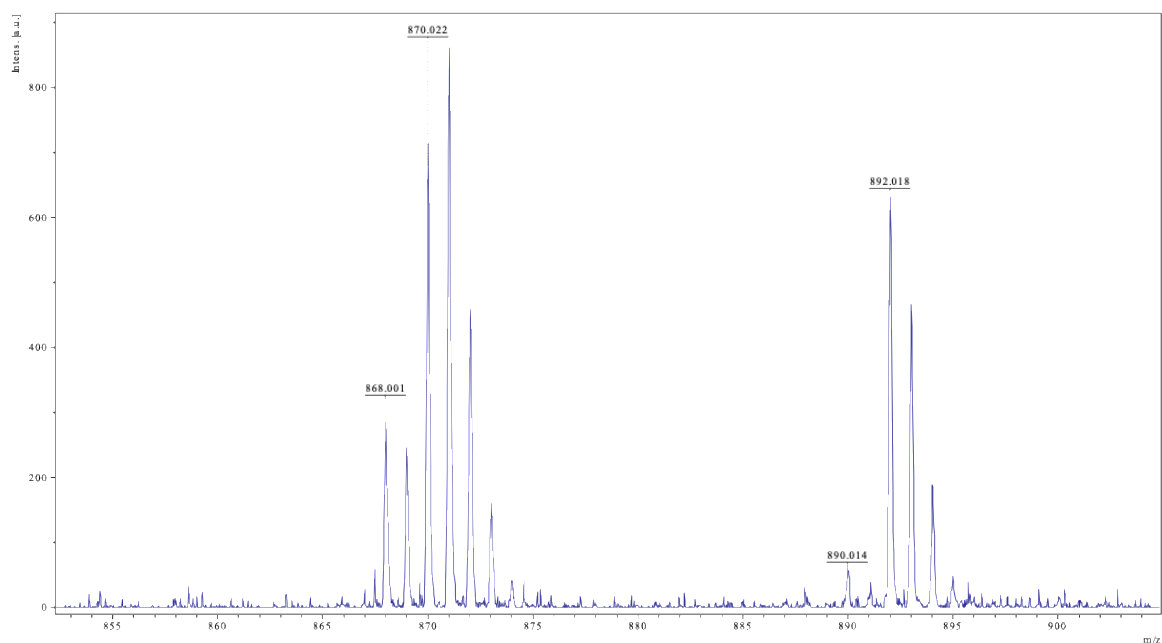
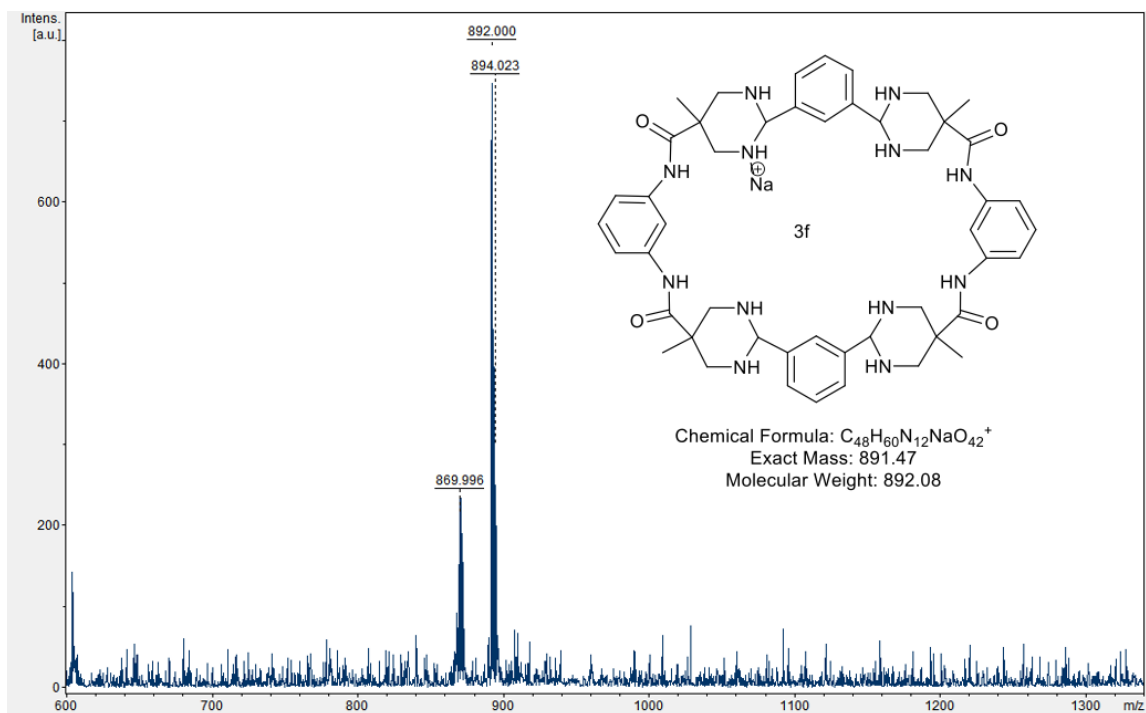
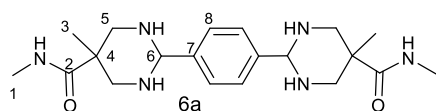


Figure S41: HSQC NMR spectrum of **3f**



**Figure S42:** MALDI TOF MS trace of **3f**. The upper trace shows the 600-1350 m/z range, while the bottom trace is focused on the mass corresponding to the [2+2] macrocycle. Calculated theoretical MS for **3f**: 868.4860. Found MS: 868.001 (Mw and partially deuterated **3f**)<sup>+</sup>. 890.014 (M and partially deuterated compound + Na)<sup>+</sup>.



$^1\text{H-NMR}$  (400 MHz;  $\text{CD}_3\text{OD}$ ):  $\delta$  7.45 (4H, s, H8), 4.5 (2H, s, H6), 3.39 (4H, d,  $^2J=12\text{Hz}$ , H5a, a'), 2.78 (4H, d,  $^2J=12\text{Hz}$ , 5b, b'), 1.25 (6H, m, H1), 1.04 (6H, s, H3)

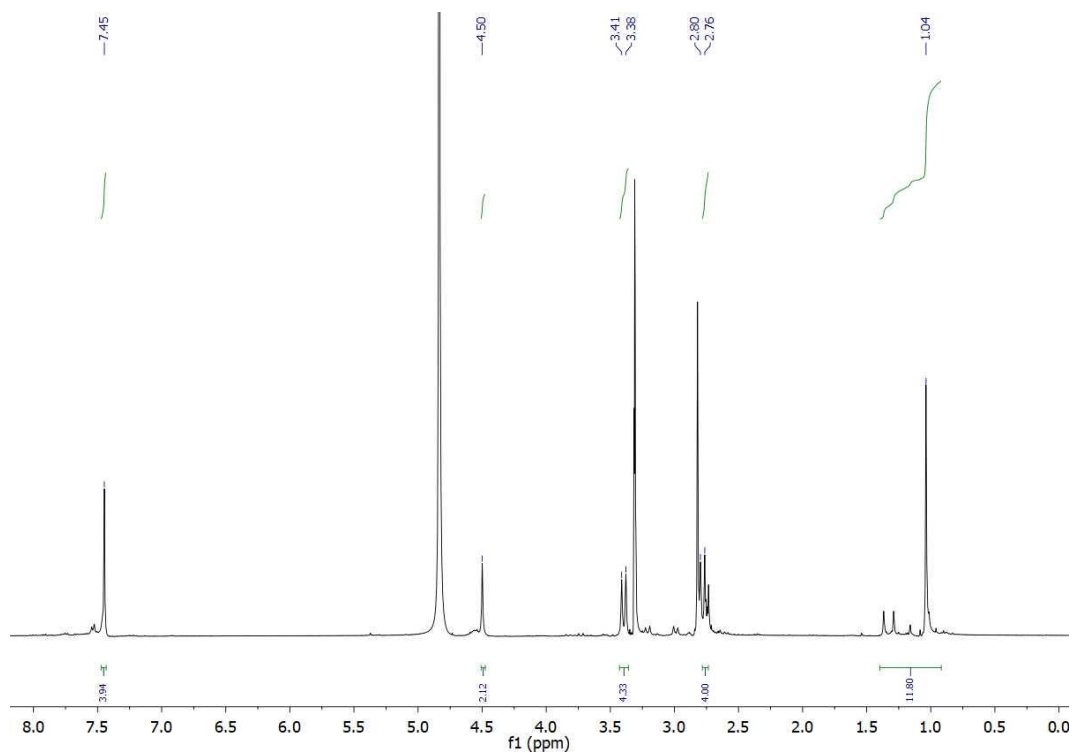


**Figure S43:**  $^1\text{H-NMR}$  spectrum of 6a.  $\text{CD}_3\text{OD}$ , 400MHz.

$^{13}\text{C-NMR}$  (100 MHz;  $\text{CD}_3\text{OD}$ ):  $\delta$  179.2 (C2), 142.7 (C7), 127.9 (C8), 74.7 (C6), 55.4 (C5), 41.0 (C4), 26.5 (C1), 22.1 (C3).

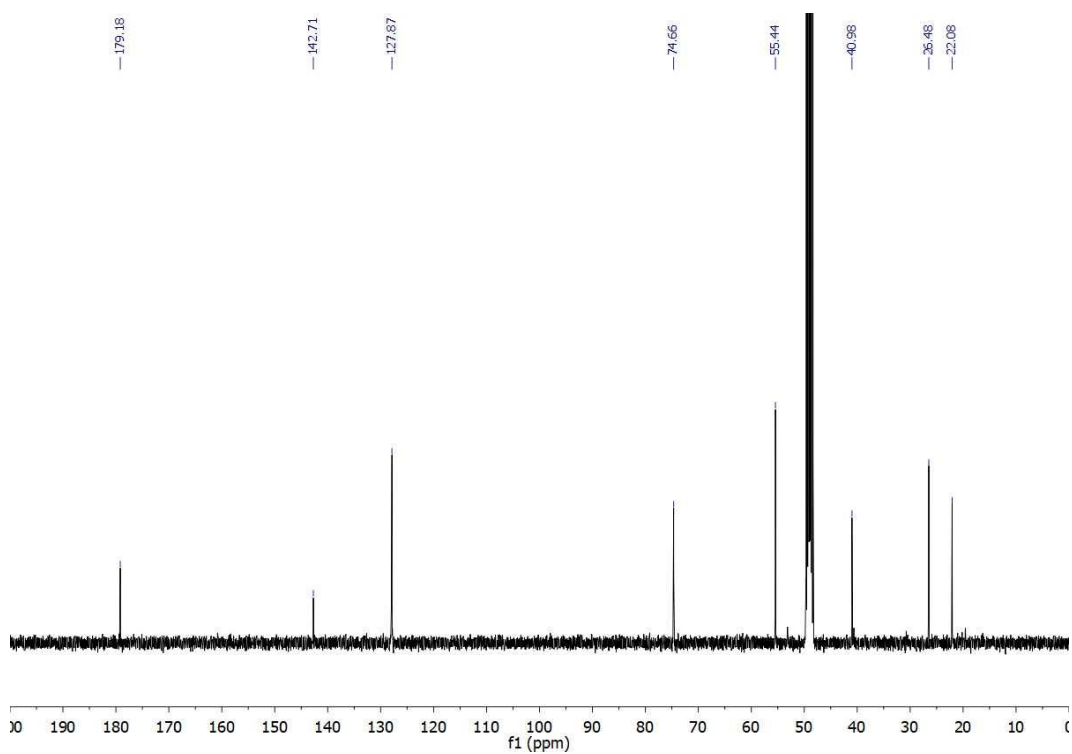


**Figure S44:**  $^{13}\text{C-NMR}$  spectrum of 6a.  $\text{CD}_3\text{OD}$ , 400MHz.

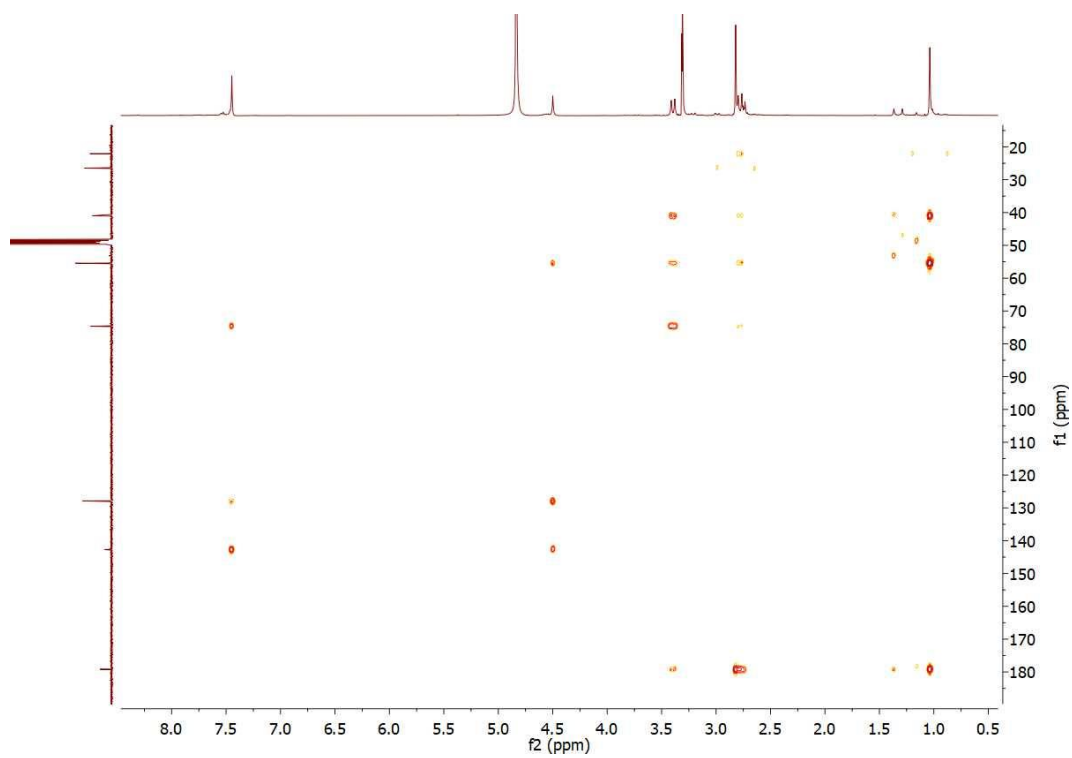


Figure S45: HMBC NMR spectrum of 6a

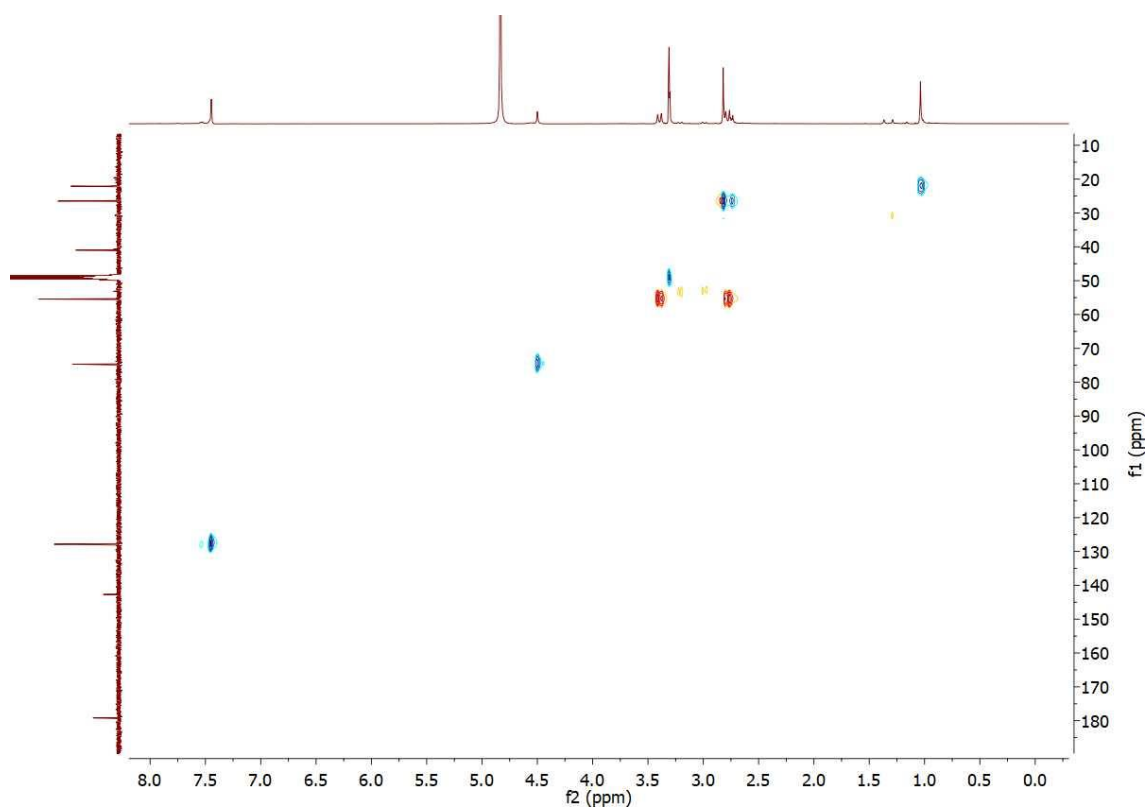


Figure S46: HSQC NMR spectrum of 6a

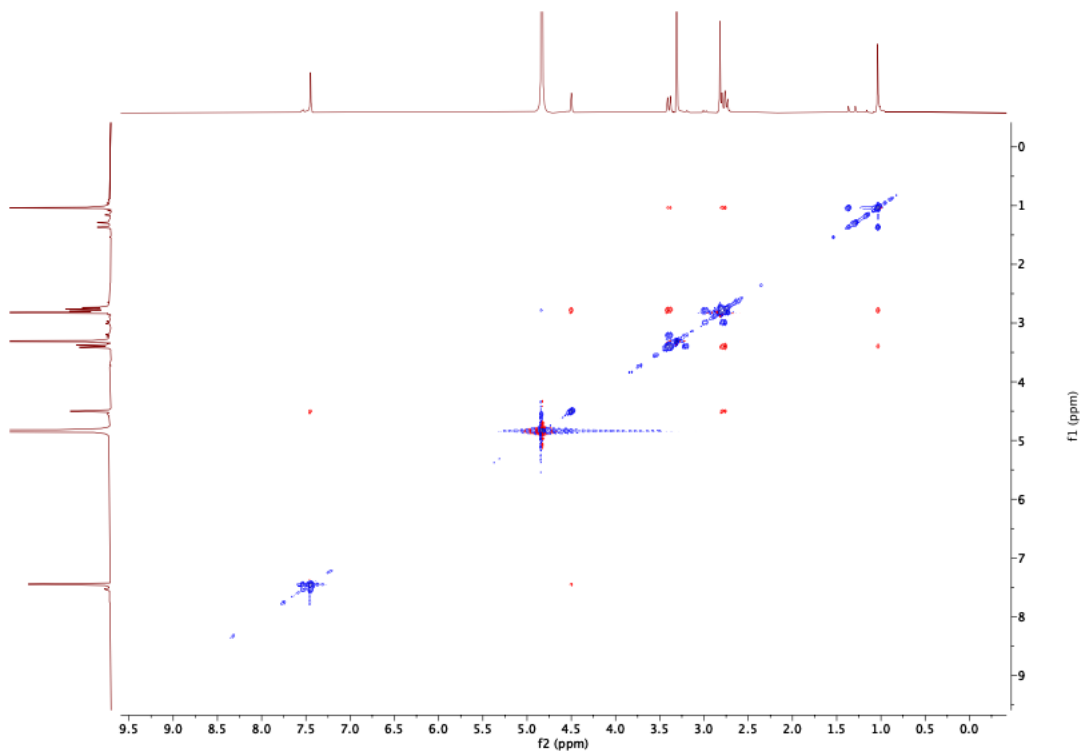


Figure S47: NOESY NMR spectrum of 6a

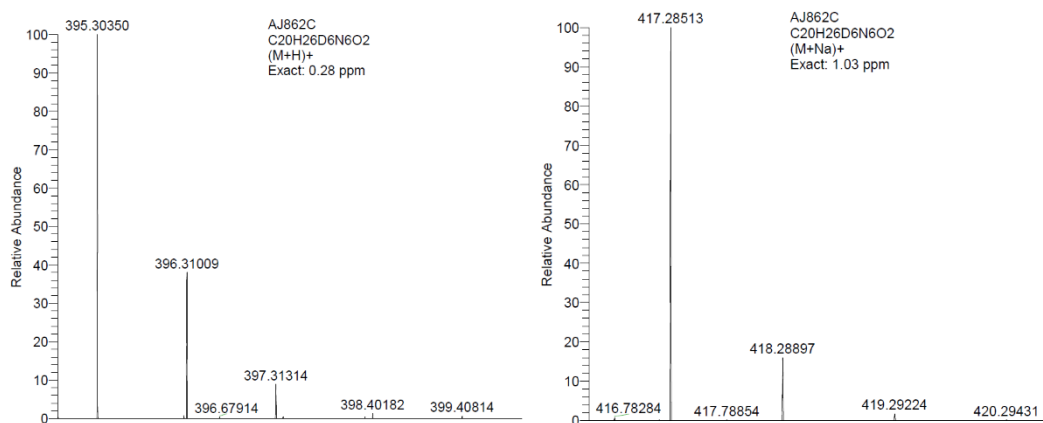
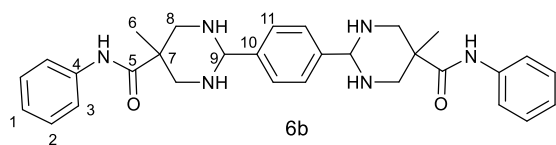
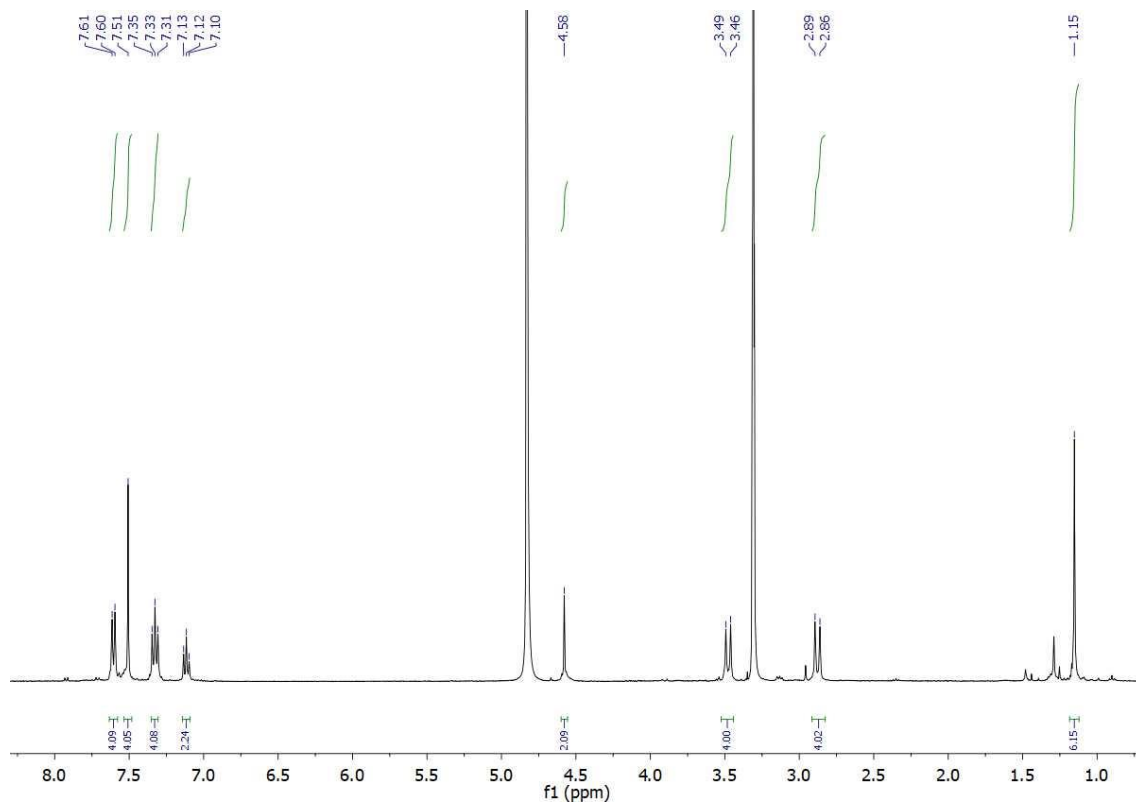


Figure S48: MALDI trace of 6a. Expected MS after deuterium exchange: 394.29633. Found MS 395.30350 ( $M + H$ )<sup>+</sup>, 417.28513 ( $M + Na$ )<sup>+</sup>. MS of partially deuterated compounds are also present.



$^1\text{H-NMR}$  (400 MHz;  $\text{CD}_3\text{OD}$ ):  $\delta$  7.6 (4H, d, H3,  $J_1=4\text{Hz}$ ), 7.51 (4H, s, H11), 7.33 (4H, dd, H2,  $^3J_1=4\text{Hz}$ ,  $^3J_2=4\text{Hz}$ ), 7.12 (2H, t,  $^3J_2=4\text{Hz}$ ), 4.58 (4H, s, H9), 3.47 (4H, d, H8a, H8a',  $^2J=12\text{Hz}$ ), 2.87 (4H, d, H8b, H8b',  $^2J=12\text{Hz}$ ), 1.15 (6H, s, H6).



**Figure S49:**  $^1\text{H NMR}$  spectrum of **6b**.  $\text{CD}_3\text{OD}$ , 400MHz.

$^{13}\text{C}$ -NMR (100 MHz;  $\text{CD}_3\text{OD}$ ):  $\delta$  177.0 (C5), 143.0 (C10), 139.8 (C4), 129.7 (C2), 128.1 (C11), 125.3 (C1), 121.7 (C3), 75.0 (C9), 55.5 (C8), 41.7 (C7), 21.8 (C6).

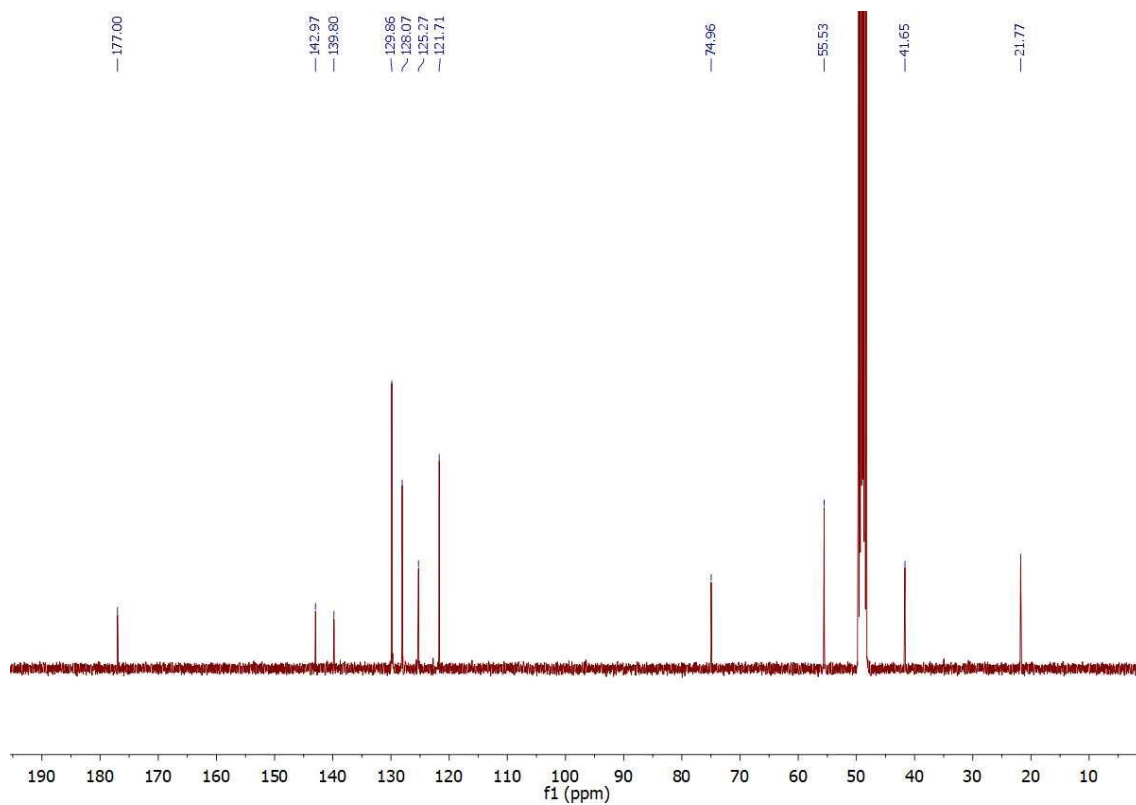


Figure S50:  $^{13}\text{C}$  NMR spectrum of **6b**.  $\text{CD}_3\text{OD}$ , 400MHz.

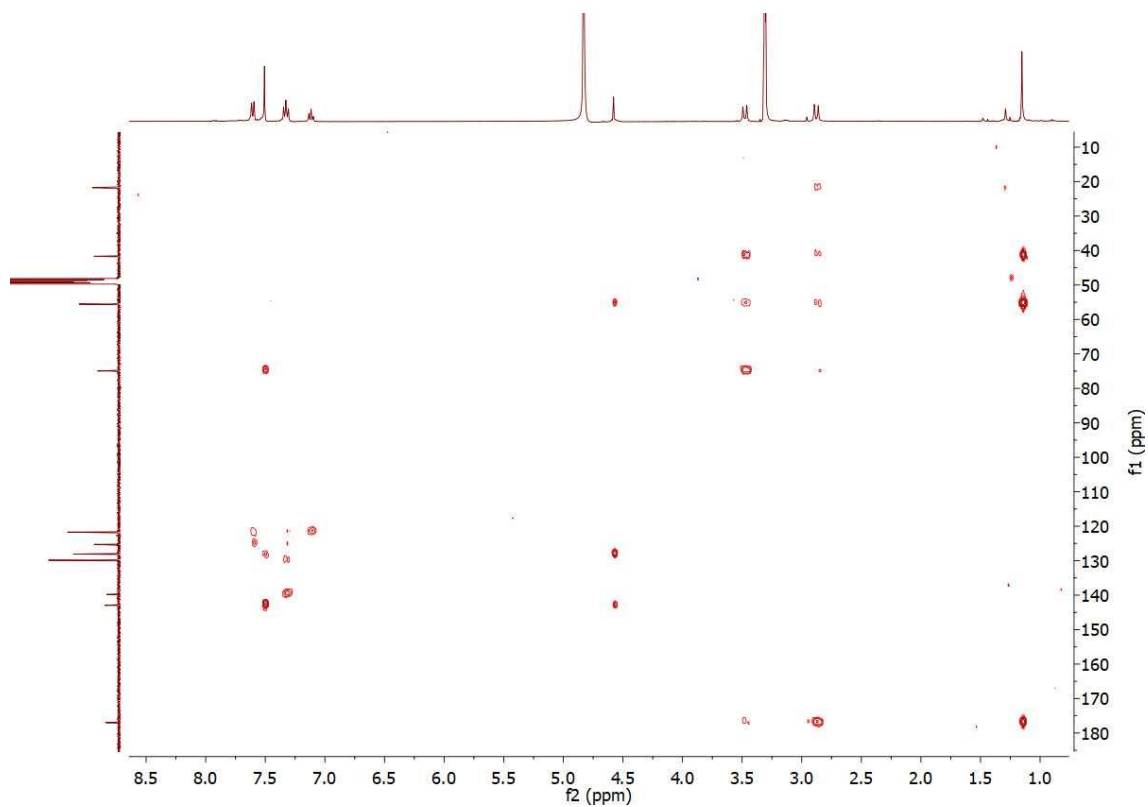


Figure S51: HMBC NMR spectrum of **6b**



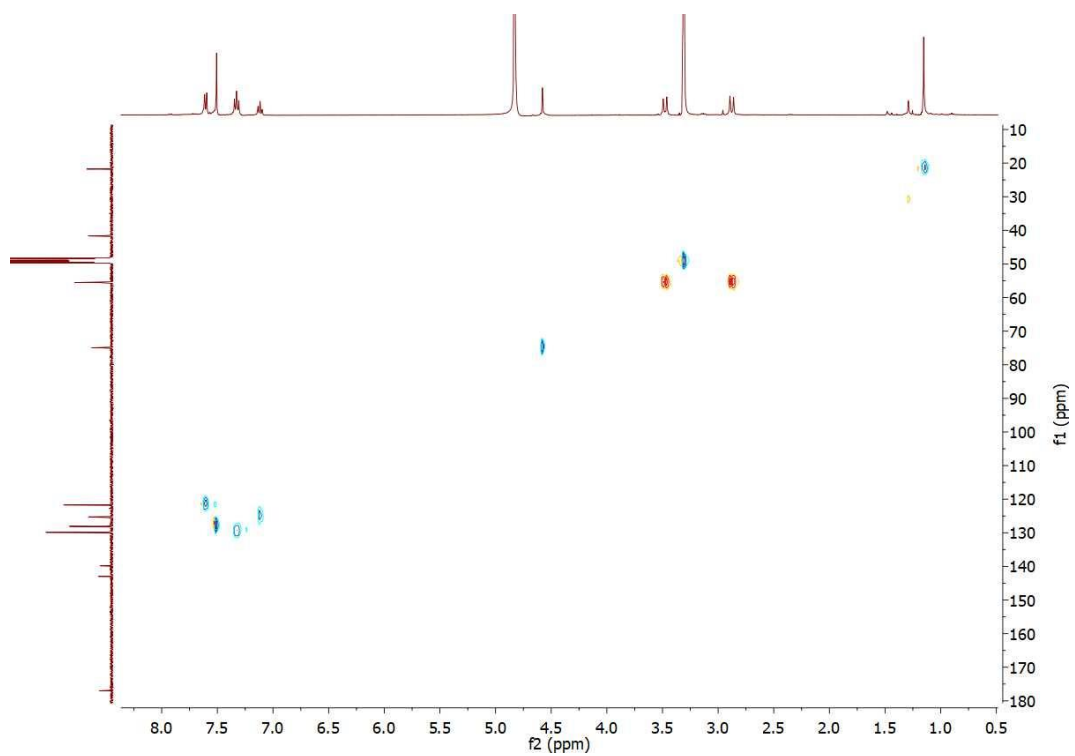


Figure S52: HSQC NMR spectra of 6b

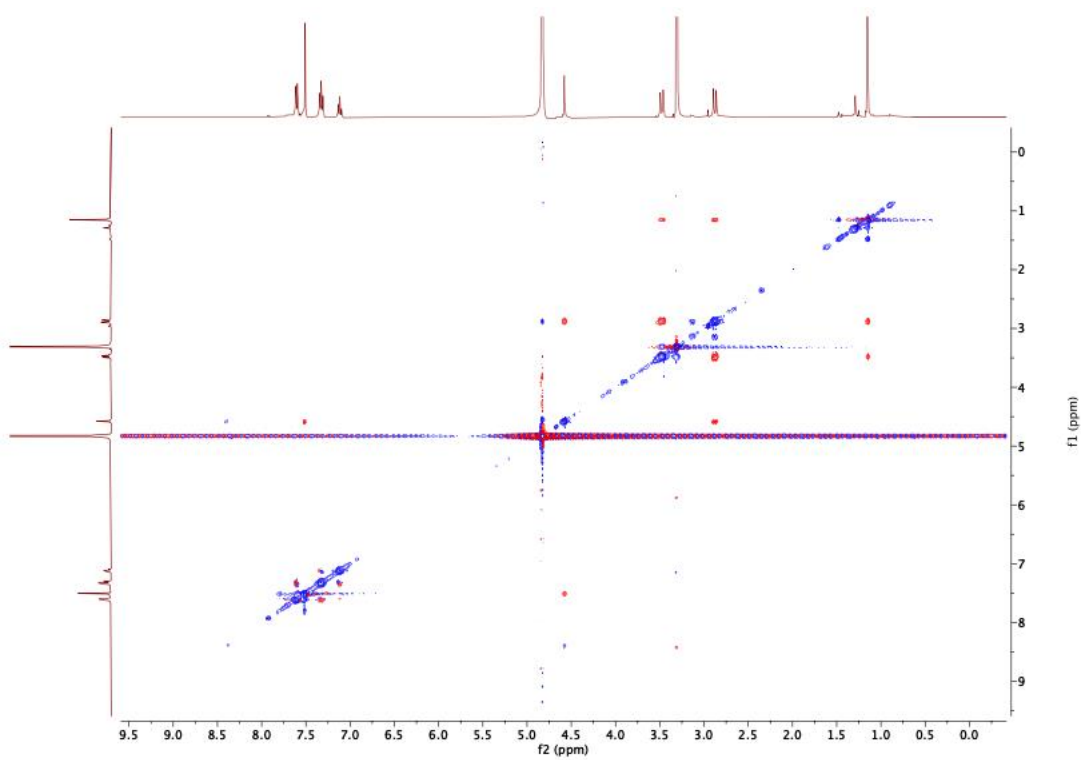
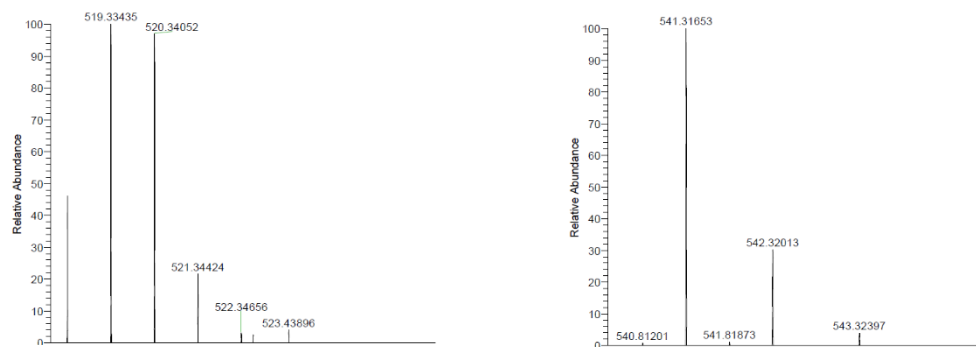
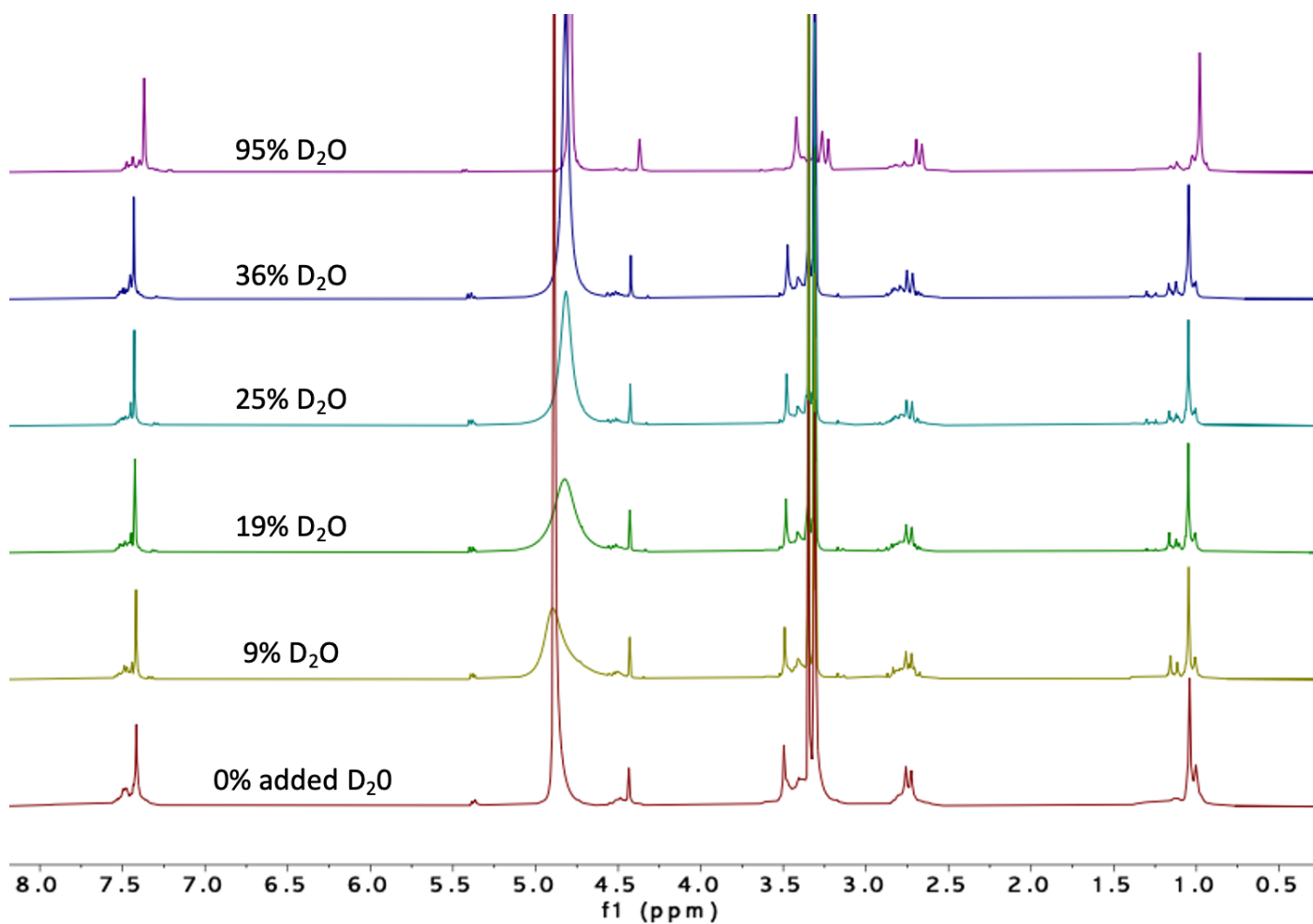


Figure S53: NOESY NMR spectrum of 6b



**Figure S54:** MALDI trace of **6b**. Expected MS after deuterium exchange: 518.3276. Found MS 519.3344 ( $M + H$ )<sup>+</sup>, 541.3163 ( $M + Na$ )<sup>+</sup>. MS of partially deuterated compounds are also present.



**Figure S55:** NMR spectra of **3a** with increasing amounts of added  $D_2O$ . Spectra were acquired at least 1h after  $D_2O$  addition. Purple upper trace corresponds to a cyclization performed from **1a** + **2a** in  $D_2O$  containing the minimal amount of MeOD (5%) required to solubilize starting material.

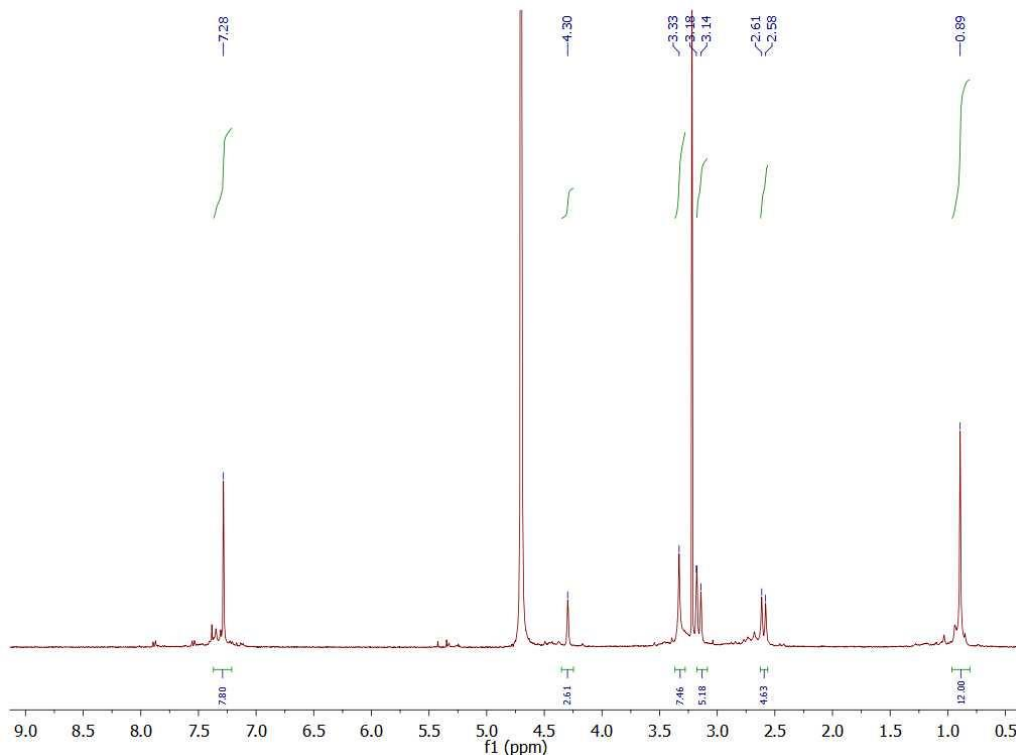


**Figure S56:** NMR spectra of **3a** after cyclization in 95% D<sub>2</sub>O.

#### Catalytic effect of aromatic carboxylic diacids

Kinetic study of the catalytic effect of aromatic carboxylic acids was performed on the formation of **3a**. Reaction was launched in the same conditions as previously but with the addition of 1 eq of the respective aromatic diacid. NMR was acquired at different timepoints to assess the progress of the reaction. Conversion was calculated by comparison of the integrals of the NMR signals corresponding to the final aminal peaks and those of the aldehyde. The presence of the aromatic diacids greatly reduced the time to reach equilibrium in cases **4a-4c**. On the other hand, no changes were observed for **4d**.

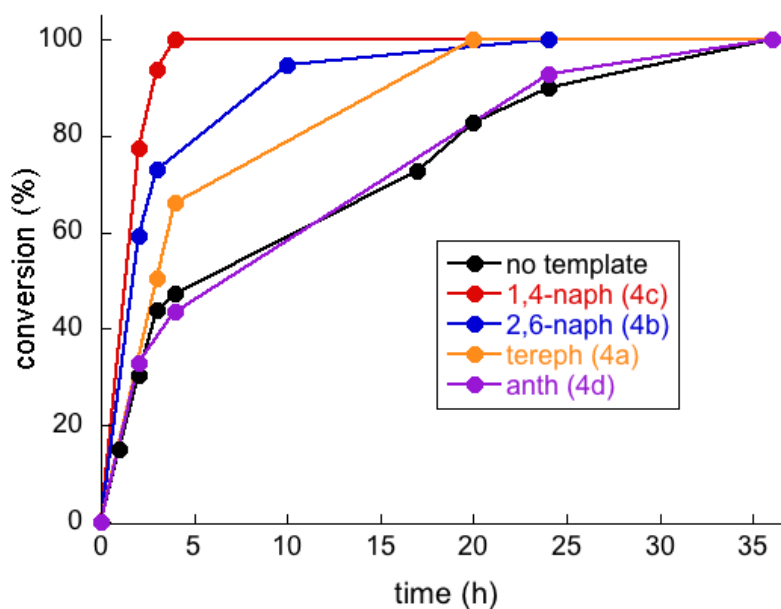


**Figure S57:** Plot of the conversion towards the formation of macrocycle **3a** in the absence and in the presence of aromatic carboxylic diacids **4a-4d**.

We performed MALDI mass spectra at the end of the reactions to further confirm the interaction between aromatic carboxylic diacids and **3a** cycle. MS of the [macrocycle + diacid] supramolecular complex was detected in two cases.

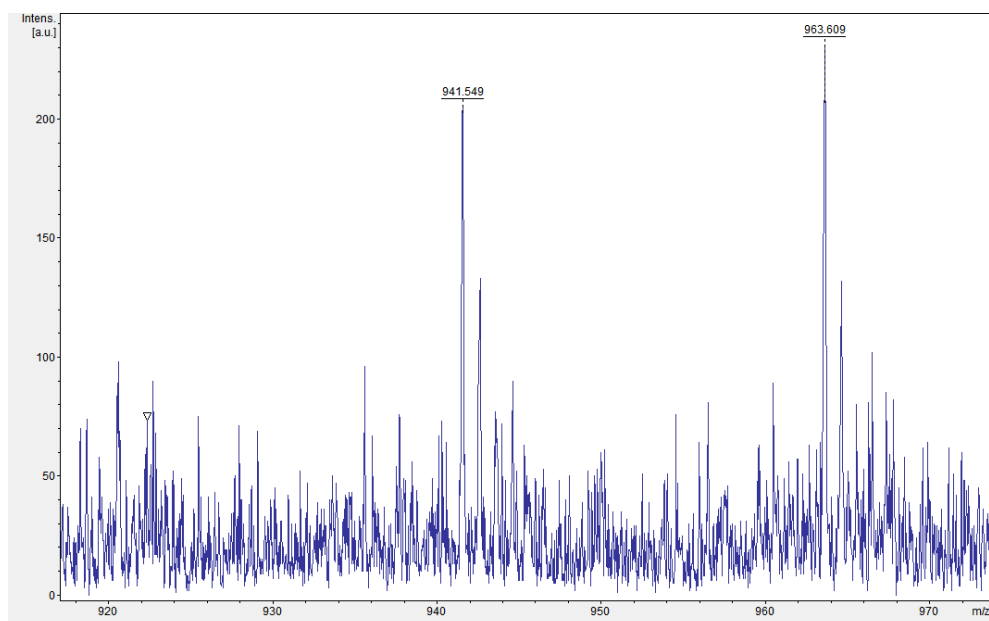


**Figure S58:** MALDI trace of **3a** in the presence of **4a**. Expected MS: 939.1320. Found MS: 941.549 (Mw and partially deuterated **3a-4a**) and 963.609 (Mw and partially deuterated compound + Na<sup>+</sup>)

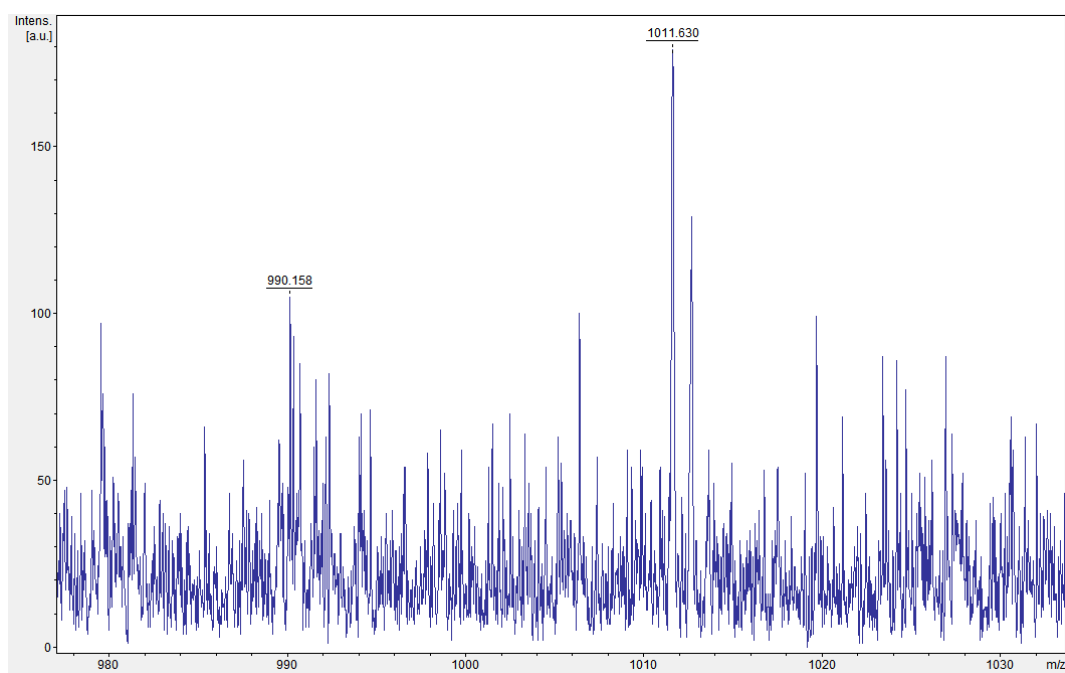


**Figure S59:** MALDI trace of **3a** in the presence of **4c**. Expected MS: 989.1920. Found MS: 990.158 (Mw and partially deuterated **3a-4c**) and 1011.630 (Mw and partially deuterated compound + Na<sup>+</sup>)

### Formation of hybrid mixed macrocycles.

The experiments depicted in Figure S60 were performed by mixing 700  $\mu\text{L}$  of preformed **3a** dissolved in  $\text{CD}_3\text{OD}$  and 700  $\mu\text{L}$  of preformed **3b** dissolved in  $\text{CD}_3\text{OD}$ , both at 2.5mM. NMR spectra was performed 30 minutes after and show no changes, just the addition of the corresponding NMR signals of each compound. Three days after, another NMR was performed, showing that there were no changes.

Upon addition of 0.3 eq of **1a** and **1b**, we observed the fast apparition of a new set of signals (Figure S61-S62), which correspond to the formation of a hybrid cycle **1a-2a-1b-2a**, as confirmed by MALDI-TOF measurements (Figure S65).

This shows that the cycles are stable in solution, but once there is excess of amine, the exchange is possible and hybrid cycles are generated, which proves the reversibility of the system.

Figure S63 depicts a similar experiment that further proves the stability of the cycles once equilibrium has been established, this time mixing **3a** and **3d**.

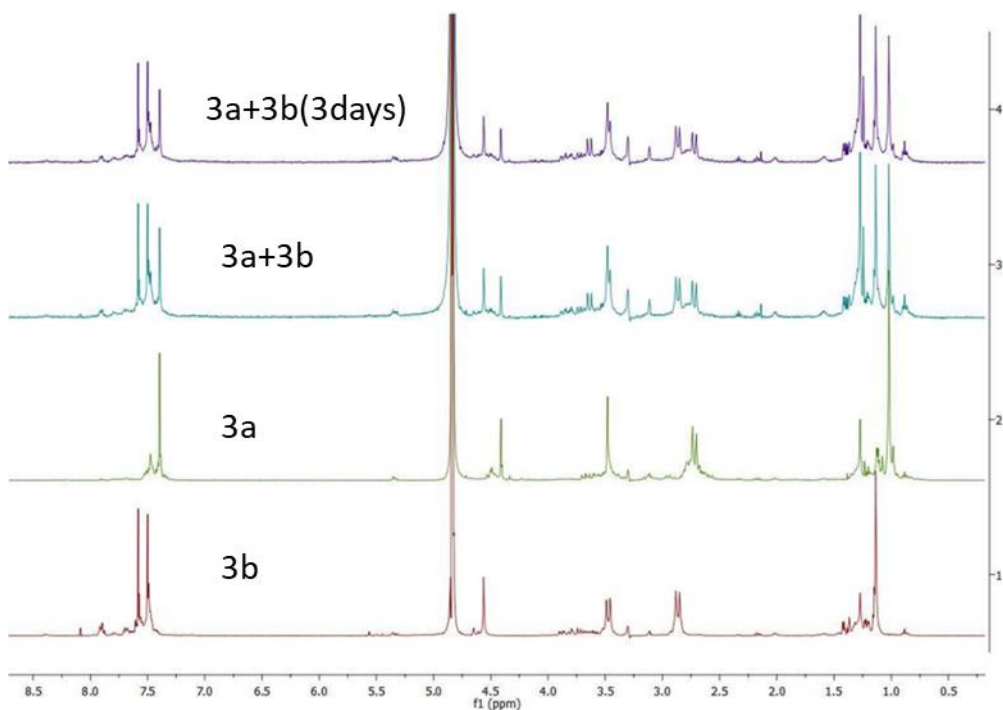


**Figure S60:** NMR showing the mixture of cycles **3a** and **3b**. No changes are detected even after 3 days. MeOD, 400MHz.

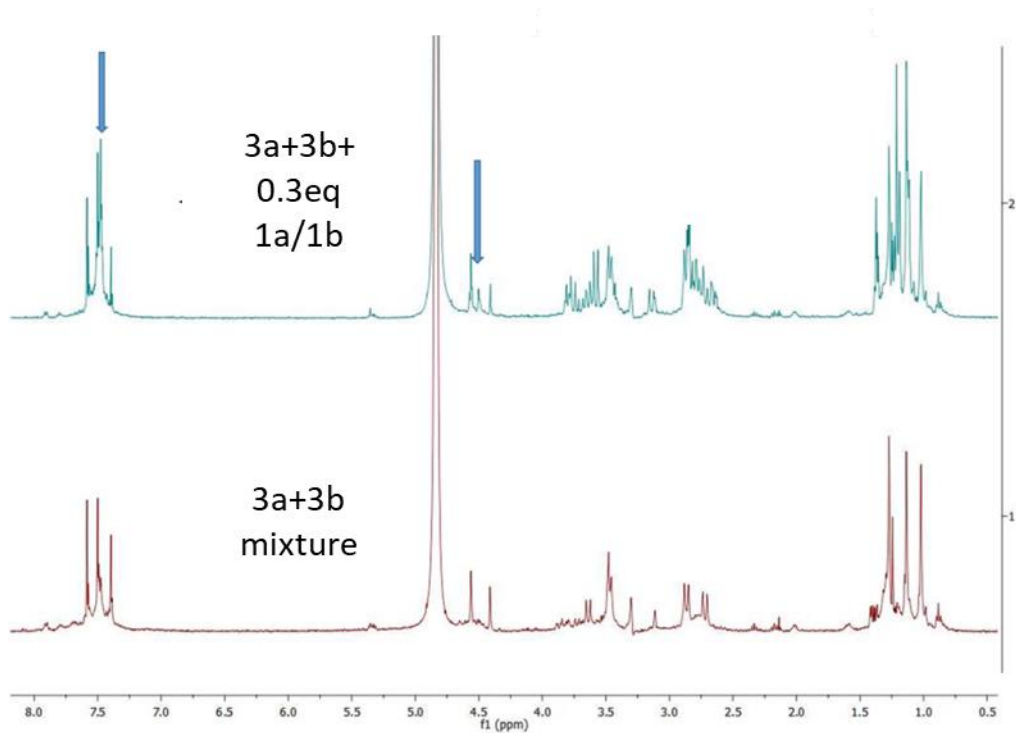


**Figure S61:** Changes in NMR spectra after addition of additional tetraamines. Proton signals that correspond to the hybrid cycle are detected, which show that the exchange is now possible, as there are some amines available to entwine with the existing cycles.

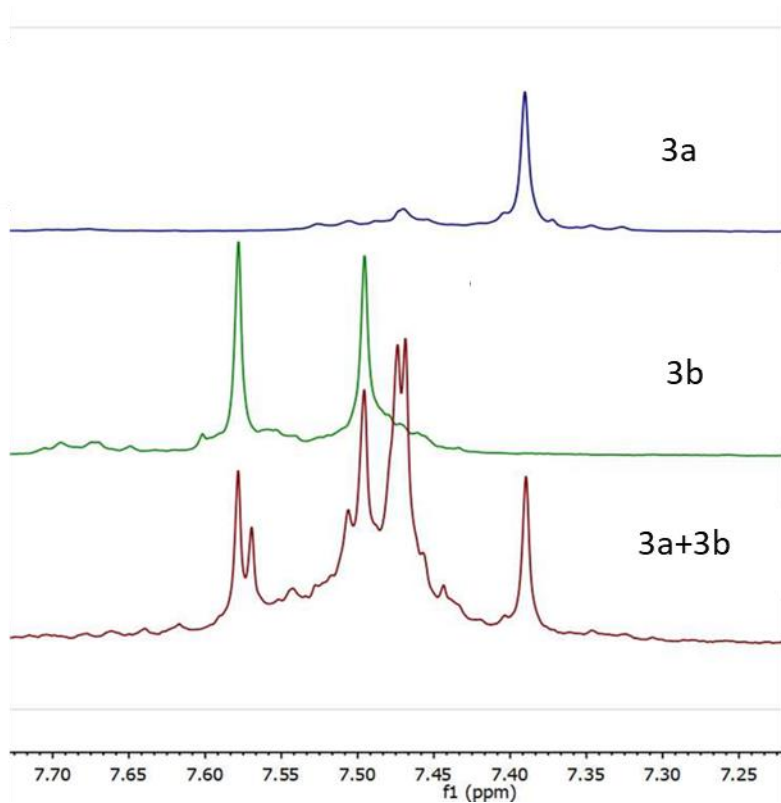


**Figure S62:** Detail of  $^1\text{H}$  NMR spectra of **3a**, **3b**, and **1b+1a+2a (3a+3b+hybrid cycle)**. The combination of products detected at the end of the reaction follows approx. a 1:2:1 proportion, as statistically expected if no other factors interfere. MeOD, 400MHz.

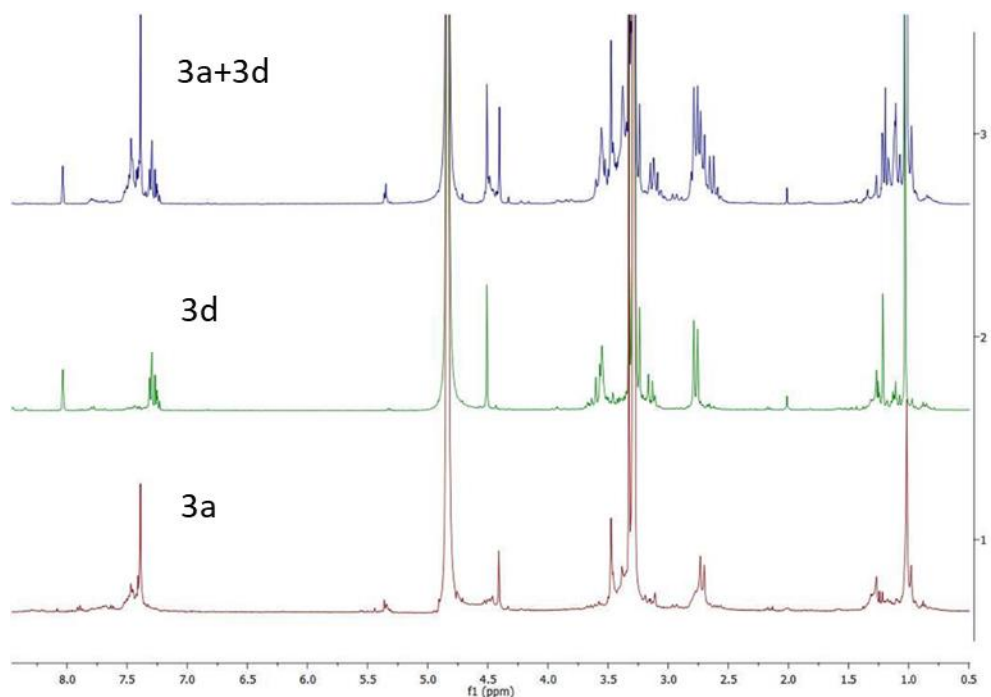


**Figure S63:** NMR showing the mixture of cycles **3a** and **3d**. Again, no changes are detected even after 3 days. MeOD, 400MHz.

Figure S64 shows a different experiment. Here we mixed in the same NMR tube **1a**, **1b**, **2a** and **2b** to a final concentration of 1.25mM each. We followed the course of the reaction by NMR. Spectra initially showed a complex array of signal, corresponding to an unsolved mixture. Within time, signals got simplified, as the equilibria shifted towards the formation of the [2+2] macrocycles. The three different combinations were found in an almost statistical distribution. This supports the reversibility of the system, as the system arrives to the same conclusion either when all compounds are present from the beginning or we open preformed cycles.

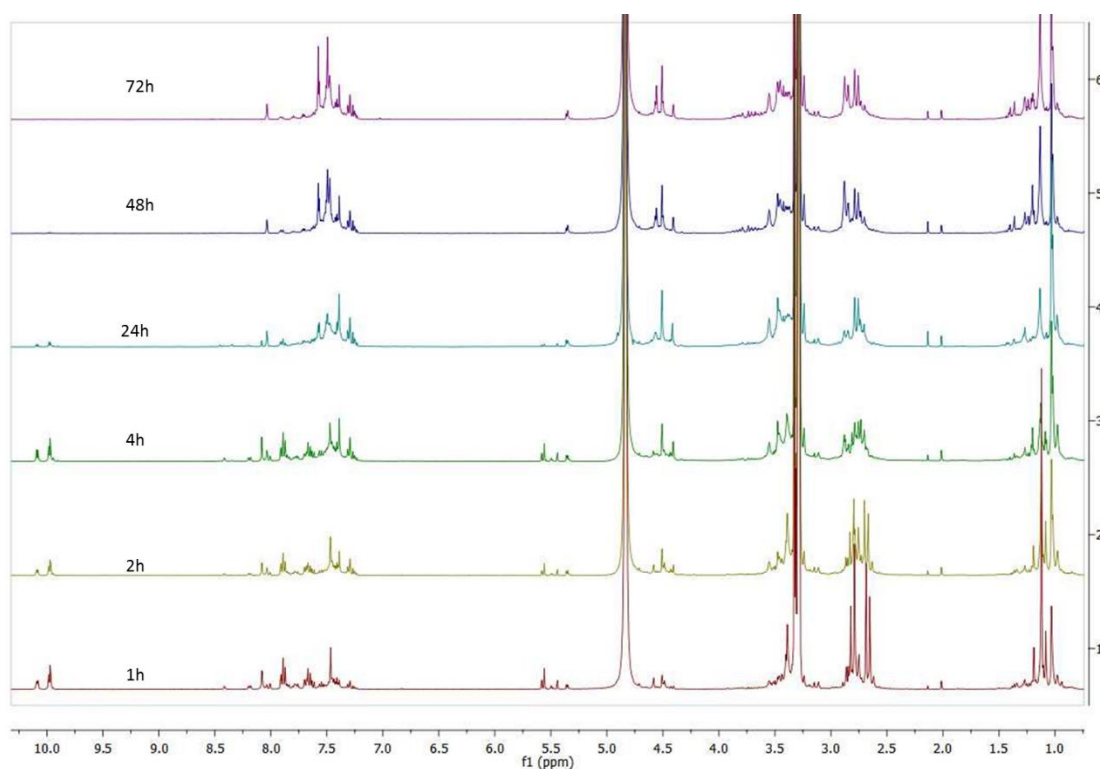


**Figure S64:** Example of NMR following the evolution of reaction **1a+1b+2a+2b**. The signals are complicated at the earlier stages of the reaction, but when the cycles get stabilized, spectra get simplified to a mixture of all possible macrocycles.

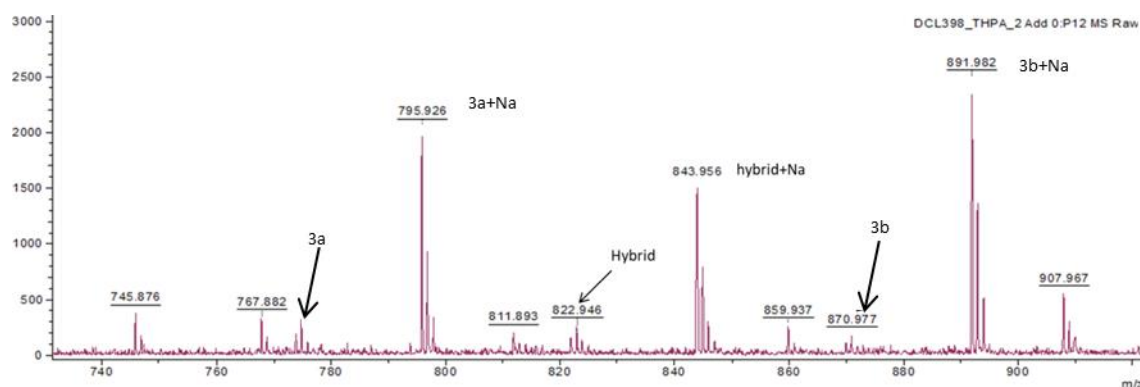


**Figure S65:** MALDI trace depicting the presence of cycles **3a**, **3b** and its corresponding hybrid cycle.

## References

- [1] A. J. Ruiz-Sanchez, P. Mesa-Antunez, N. Barbero, D. Collado, Y. Vida, F. Najera, E. Perez-Inestrosa, *Polym. Chem.* **2015**, *6*, 3031.
- [2] Tinker Molecular Modeling Package, v. 4.2; <http://dasher.wustl.edu/tinker/> (accessed 2020/12/7).
- [3] J. Wang, R. M. Wolf, J. W. Caldwell, P. A. Kollman, D. A. Case, *J. Comput. Chem.* **2005**, *26*, 114.
- [4] Gaussian 16, Revision A.03, M. J. Frisch, G. W. Trucks, H. B. Schlegel, G. E. Scuseria, M. A. Robb, J. R. Cheeseman, G. Scalmani, V. Barone, G. A. Petersson, H. Nakatsuji, X. Li, M. Caricato, A. V. Marenich, J. Bloino, B. G. Janesko, R. Gomperts, B. Mennucci, H. P. Hratchian, J. V. Ortiz, A. F. Izmaylov, J. L. Sonnenberg, D. Williams-Young, F. Ding, F. Lipparini, F. Egidi, J. Goings, B. Peng, A. Petrone, T. Henderson, D. Ranasinghe, V. G. Zakrzewski, J. Gao, N. Rega, G. Zheng, W. Liang, M. Hada, M. Ehara, K. Toyota, R. Fukuda, J. Hasegawa, M. Ishida, T. Nakajima, Y. Honda, O. Kitao, H. Nakai, T. Vreven, K. Throssell, J. A. Montgomery, Jr., J. E. Peralta, F. Ogliaro, M. J. Bearpark, J. J. Heyd, E. N. Brothers, K. N. Kudin, V. N. Staroverov, T. A. Keith, R. Kobayashi, J. Normand, K. Raghavachari, A. P. Rendell, J. C. Burant, S. S. Iyengar, J. Tomasi, M. Cossi, J. M. Millam, M. Klene, C. Adamo, R. Cammi, J. W. Ochterski, R. L. Martin, K. Morokuma, O. Farkas, J. B. Foresman, D. J. Fox, Gaussian, Inc., Wallingford CT, **2016**.
- [5] J. Tomasi, B. Mennucci, R. Cammi, *Chem. Rev.* **2005**, *105*, 2999.
- [6] R. F. W. Bader, *Chem. Rev.* **1991**, *91*, 893.
- [7] T. Lu, F. Chen, *J. Comput. Chem.* **2012**, *33*, 580.
- [8] O. V. Shishkin, G. V. Palamarchuk, L. Gorb, J. Leszczynski, *J. Phys. Chem. B* **2006**, *110*, 4413.
- [9] I. Mata, I. Alkorta, E. Molins, E. Espinosa, *Chem. - A Eur. J.* **2010**, *16*, 2442.
- [10] I. Rozas, I. Alkorta, J. Elguero, *J. Am. Chem. Soc.* **2000**, *122*, 11154.
- [11] M. A. Spackman, *Chem. Phys. Lett.* **1999**, *301*, 425.
- [12] D. Flaig, M. Maurer, M. Hanni, K. Braunger, L. Kick, M. Thubauville and C. Ochsenfeld, *J. Chem. Theory Comput.*, **2014**, *10*, 572.